U.S. - JAPAN COORDINATED PROGRAM
FOR
MASONRY BUILDING RESEARCH

REPORT No. 3.2(a)

RESPONSE OF REINFORCED BLOCK MASONRY WALLS TO OUT-OF-PLANE STATIC LOADS

by

Ahmad A. Hamid
Bechara E. Abboud
Muris W. Farah
Michel K. Hatem
Harry G. Harris

September 1989

Sponsored by:

NATIONAL SCIENCE FOUNDATION
GRANT NO. ECE-8518699

Drexel University
Department of Civil and Architectural Engineering
Philadelphia, Pennsylvania 19104

ib

Contents

		Page
List of Tables		i
List of Illustrations		ii
Abstract		v
Acknowledgements		vii
1. INTRODUCTION		
1.1	General	1
1.2	Historical Development	2
1.3	Literature Review	3
1.4	Objectives and Scope	6
2. MATERIALS		
2.1	General	8
2.2	Concrete Masonry Units	8
2.3	Mortar	16
2.4	Grout	19
2.5	Reinforcement	23
2.6	Masonry Prisms	26
3. EXPERIMENTAL PROGRAM		
3.1	Scope	37
3.2	Test Specimens	37
3.3	Wall Panel Construction	40
3.4	Test Set-Up	43
3.5	Testing Equipment	48
3.6	Loading	50
3.7	Instrumentation	52

4. EXPERIMENTAL RESULTS AND DISCUSSION

4.1	Modes of Failure and Crack Patterns	56
4.2	Cracking Moment	67
4.3	Load-Deflection Curves	70
4.3.1	Monotonically Loaded Walls	70
4.3.2	Cyclically Loaded Walls	75
4.4	Flexural Strength	83
4.5	Displacement Ductility	88

5.CONCLUSIONS 91

REFERENCES 94

APPENDIX A : Sample Flexural Strength Calculations A-1

APPENDIX B : Tests of Reinforced Masonry Walls Built With Masonry Cement Mortar B-1

List of Tables

Table		Page
2.1	Dimensions and Properties of Concrete Masonry Units	13
2.2	Mortar Properties	22
2.3	Compressive Strength of Grout	25
2.4	Properties of Steel Reinforcement	29
2.5	Prism Compression Test Results	33
2.6	Bond Wrench Test Results	36
3.1	Wall Test Specimens	38
4.1	Experimental Results - Cracking Moments and and Maximum Tensile Stress at First Crack	68
4.2	Experimental and Analytical Results - Cracking, Moments and Maximum Moments	85
4.3	Experimental Results - Wall Displacements and Ductility	89

List of Illustrations

Figure		Page
2.1	Configuration of 6" Masonry Units	10
2.2	Configuration of 4.5" and 8" Masonry Units	11
2.3	Blocks at Bond Beam Locations	12
2.4	Axial Compression Test of Full Block	14
2.5	Strain Instrumentation for Compression Test of Half Unit	14
2.6	Typical Stress-Strain Curve for 6" Unit	15
2.7a	Splitting Test of Masonry Units: Test Setup	17
2.7b	Splitting Test of Masonry Units: Typical Failure Mode	17
2.8	Set-Up for Initial Rate of Absorption of Masonry Units	18
2.9a	Aggregate Grain Size Distribution for Mortar, Phase I: Unmodified	20
2.9b	Aggregate Grain Size Distribution for Mortar, Phase I: Modified	20
2.10	Aggregate Grain Size Distribution for Mortar, Phase II	21
2.11	Grout-Core Specimen	24
2.12	Tensile Testing of Reinforcement	27
2.13	Typical Failed Steel Specimens	27
2.14	Typical Stress-Strain Curves for Reinforcing Steel	28
2.15	Typical Compression Prism Configuration	30
2.16	Prism Instrumentation	30
2.17a	Typical Failure of Prisms Under Axial Compression: Hollow Prism	32
2.17b	Typical Failure of Prisms Under Axial Compression: Grouted Prism	32
2.18	Typical Flexural Prism Configuration	35
2.19	Flexural Tension Test Set-Up	35

3.1 Typical Wall Panel Dimensions 39
3.2a Locations of Vertical Reinforcement: Centrally Reinforced 41
3.2b Locations of Vertical Reinforcement: Staggered Reinforcement 41
3.3 Isometric View of a Wall Panel Showing Vertical and Horizontal Steel 42
3.4a Wall Panels Construction: Fully Grouted Walls 44
3.4b Wall Panels Construction: Partially Grouted Walls 44
3.5 Test Set-Up 45
3.6 Bottom Support Details 47
3.7 Top Support Details 49
3.8a Displacement Patterns for Cyclic Loading: Cyclic Pattern C1 51
3.8b Displacement Patterns for Cyclic Loading: Cyclic Pattern C2 51
3.9 Locations of the Wire Potentiometers for Deflection Measurements 53
3.10 Locations of the L.V.D.T's on the Wall Panels 55
4.1 Typical Flexural Cracking and Deflection of Reinforced Masonry Wall Under Flexure 57
4.2 Crack Patterns of Wall W1 58
4.3 Crack Patterns of Wall W4 58
4.4 Crack Patterns of Wall W6 59
4.5 Crack Patterns of Wall W8 59
4.6 Crack Patterns of Wall W10 60
4.7 Crack Patterns of Wall W12 60
4.8 Spalling of Faceshell 61
4.9 Bond Failure at Location of Vertical Rebars 62
4.10 Crack Patterns of Wall W2 63
4.11 Crack Patterns of Wall W3 63
4.12 Crack Patterns of Wall W5 64
4.13 Crack Patterns of Wall W7 64

4.14 Crack Patterns of Wall W9 65
4.15 Crack Patterns of Wall W11 65
4.16 Crack Patterns of Wall W13 66
4.17 Crack Patterns of Wall W14 66
4.18 Load-Deflection Curves for Wall W1 71
4.19 Load-Deflection Curves for Wall W4 71
4.20 Load-Deflection Curves for Wall W6 72
4.21 Load-Deflection Curves for Wall W8 72
4.22 Load-Deflection Curves for Wall W10 73
4.23 Load-Deflection Curves for Wall W12 73
4.24 Load-Deflection Curves for Wall W2 76
4.25 Load-Deflection Curves for Wall W3 76
4.26 Load-Deflection Curves for Wall W5 77
4.27 Load-Deflection Curves for Wall W7 77
4.28 Load-Deflection Curves for Wall W9 78
4.29 Load-Deflection Curves for Wall W11 78
4.30 Load-Deflection Curves for Wall W13 79
4.31 Load-Deflection Curves for Wall W14 79
4.32 Behavior of Cracked Section During Reversed Deformation 81
4.33 Proposed Idealized Envelope of the Hysteresis Loops of Flexural Walls 84

ABSTRACT

In order to develop a more appropriate limit states design methodology for reinforced masonry structures information about the inelastic behavior of reinforced walls is needed. The experimental study presented in this report, which is part of the U.S.- Japan Coordinated Program on Masonry Building Research (Task 3.1a), addresses the elastic and the inelastic behavior of vertically spanned reinforced block masonry walls under monotonic and cyclic out-of-plane lateral loads. Fourteen walls were tested to determine the effects of various parameters, such as percentage and location of vertical steel, block size, extent of grouting, and load pattern on wall behavior. The behavior included cracking patterns and cracking moment, load-deflection curves up to and beyond the peak load and displacement ductility. Two additional walls built with masonry cement mortar were tested under monotonic and cyclic loads to evaluate the effect of mortar type on wall flexural behavior.

The test results showed that the percentage and location (centrally located vs. staggered) of vertical steel had significant effect on wall load-deflection curve, strength and ductility. The extent of grouting (partially vs. fully grouted) affects the cracking load and consequently the flexural rigidity and deflection under service loads. The extent of grouting, however, did not show an adverse effect on the wall stability in the inelastic range.

The specified value of the modulus of rupture in the UBC-88 code is much lower than the experimental values of maximum tensile stress at first crack obtained for fully grouted walls. The theoretical analysis for the ultimate strength based on Whitney stress block method, which is included in the UBC-88 code , showed a good correlation with the experimental results.

The hysteretic behavior of the walls was obtained and documented in this study. The results showed a ductile behavior of the walls with a unique pinched shape of the loops for centrally reinforced walls, which departs considerably from the elasto-plastic curves commonly used for ductile materials. An idealized envelope of the hysteretic loops is proposed based on the experimental results. The wall with staggered reinforcement did not show the pinching phenomenon and, therefore, a higher energy absorption was achieved.

Displacement ductility ratios ranging from 1.79 for wall with 0.44 percent of vertical steel to 29.4 for wall with 0.15 percent of steel. As expected, the displacement ductility of the wall panels decreased as the percentage of vertical reinforcement increased. A steel ratio of 0.2 to 0.3 percent would result in adequate levels of displacement ductility. Partially grouted walls exhibited higher displacement ductility than fully grouted walls.

ACKNOWLEDGEMENTS

This report presents the results of a comprehensive test program conducted in the Structural Testing Laboratory, Department of Civil and Architectural Engineering, Drexel University to study the response of reinforced block masonry walls under out-of-plane monotonic and cyclic loads. The program was made possible through funding by the National Science Foundation under Grant No. ECE-8517019. Funding for the purchase of the two channel MTS structural loading system and a computer-based measurement and control system designed by Engineering Systems Inc., Belmont, Massachusetts, were made available through a matching equipment grant (No. ECE-8319178) from the National Science Foundation. Construction materials were made available by Concrete Masonry Association of California and Nevada. The Delaware Valley Masonry Institute, Inc., Narberth Pennsylvania, and D. M. Sabia and Company, masonry contractors, Conshohocken, Pennsylvania, provided the services of a mason for constructing the test specimens. Samuel Grossi and Sons, Bensalem, Pennsylvania, steel fabricators, provided materials and the fabrication of the test reaction frame. The Portland Cement Association, Skokie, Illinois provided partial support to test two additional walls built with masonry cement mortar.

1. INTRODUCTION

1.1 General

External concrete block walls in masonry buildings should be constructed to resist out-of-plane bending due to lateral wind loads. In seismic areas, both external and internal masonry walls are subject to out-of-plane bending due to inertia forces and due to in-plane motion of diaphragms. Even under gravity loads, out-of-plane bending is developed due to continuity of floor slabs and eccentricity of vertical loads.

For adequate performance under seismic loading, reinforced masonry should be ductile and capable of dissipating energy through elastic and inelastic response. Because strain energy transfer through elastic response is very small compared to inelastic response, it becomes much more efficient to rely on the inelastic response for energy dissipation (8,18).

Analytical procedures related to seismic failure analysis necessitate the establishment of the hysteretic response of reinforced masonry walls. The applicability of nonlinear analysis techniques hinges upon the nonlinear load-deflection characteristics. To be able to evaluate the adequacy of the seismic design provisions in the North American Masonry Codes (31,17), information about the inelastic response of masonry structures is needed (27).

1.2 Historical Development

Masonry, one of the oldest building materials, has been used by many early cultures in human history including the Egyptians, Greek and Roman (24). Over the years, the lack of information and understanding of the material properties of masonry and its structural behavior, has led to uneconomical design of masonry structures. More recently, through several research programs, a considerable amount of data on masonry properties and structural performance has been generated leading to the development of more sound production techniques and improved construction practices. This had led to the design of masonry structures based upon engineering principles rather than on empirical design.

The first method of masonry construction was to build massive structures from plain solid masonry to support gravity loads. In this method of construction, the stability of the structure against lateral loads due to wind or seismic action is achieved by the counteraction of gravity loads. A problem with this method of design is that the height of the structure is limited by economic constraints. A good example of this type of construction is the 16-story Monadnock Building, a brick bearing-wall structure built in Chicago in 1889-1891, which had a six foot thick unreinforced masonry wall at the base of the building. The need for more economical masonry structures led designers and builders to seek ways to reduce the thickness of the bearing walls without losing their structural stability.

In the 18th century, reinforced masonry structures were introduced into the construction field, where the reinforcement served the purpose of providing resistance on the tension side of the elements. As in reinforced concrete, the combination of

the masonry and reinforcing is a very compatible one. The masonry brings to the system a high degree of compressive resistance, weathering durability, fire protection, and stability, while the reinforcing steel provides the flexural tensile resistance and the ductility needed to resist lateral loads. This modern concept of engineered reinforced masonry combined with the multiple advantages of sound control, fire resistance, and low maintenance costs has expanded the application of masonry to all types of construction.

1.3 Literature Review

A literature review of previous research on vertically spanning block masonry walls under out-of-plane quasi-static lateral loading is presented below.

In the CMA-MRF test program (13), twenty feet (20') high panels were constructed of conventional 8 in. and 6 in. blocks and tested under out-of-plane loading. The lateral load was applied via an air bag system. All the wall panels were similar with only the spacing of the vertical steel varying. The objective of the test program was to determine the effect of the spacing of the vertical reinforcing on the flexural resistance of reinforced concrete block masonry walls and to establish the proper effective width available for design calculations. It was noted that eight-feet steel spacing in panels in running bond was as effective as two-feet spacing, that masonry deflects more without damage, and has greater earthquake damping characteristics than normally given credit. The walls with running bond exhibited a ductile failure. The walls with stack bond apparently did not reach yield before failure.

A total of 30 full-size masonry walls, 4-ft by 24-ft high with varying wall thickness were tested in the more recent SEASC-ACI (7) test program. The slender reinforced masonry walls were tested under combined axial load and monotonic quasi-static lateral loads. The main objective of the program was to investigate the applicability of the empirical limitation of height-to-thickness (h/t) ratio. The test results showed excellent behavior of all panels tested under the imposed load conditions, and most importantly, showed that the arbitrary and fixed limitation of height to thickness ratio by the codes is inappropriate and control should be based on strength and deflection considerations rather than on an arbitrary limits. These tests proved that thin masonry walls can resist all specified code loading for vertical and lateral forces with reserve deflection capacities far in excess of service requirements. The walls were deformed beyond the wall thickness dimension, indicating a ductile behavior. Displacement ductility ratios(ratio of mid-span displacement at maximum moment to displacement at yield moment) were limited to 2-3 for the walls that were tested to failure. Inelastic deformations beyond peak load and corresponding displacement ductilities were not considered in this study.

Fereig and Hamid (14) studied the effect of different parameters on the flexural strength of reinforced block masonry members. A correlation study of the experimental strength with the strength predicted by the Uniform Building Code 1985 was obtained. A total of eighteen wall elements 8 blocks long and 1 1/2 blocks wide were tested in flexure to investigate the effects of different parameters including block size and strength, mortar type, steel distribution across the wall element and steel percentage on the ultimate moment capacity. The results showed a very good agreement between the wall

flexural strength as predicted by the code and the strength obtained experimentally.

A study on 1/4-scale concrete block masonry walls was conducted at Drexel University (1). A total of thirteen reinforced concrete blocks masonry walls were constructed and tested under out-of-plane monotonic and cyclic loading with and without axial load. The primary objective was to examine and evaluate the applicability and feasibility of 1/4-scale direct modeling techniques in predicting the behavioral characteristics of reinforced concrete block masonry walls. The results indicated that walls reinforced with normal steel ratios (ranging from 0.15 to 0.25 percent) would exhibit large inelastic deformations with high displacement ductility ratios.

In other programs reported in the literature (12,20), the prime objective was to develop P-M interaction diagrams for different material combinations and to study the strength capacity under combined axial force and bending moment. Post-yield behavior was not considered. In others (6,9,10,11) the main objective was to verify the applicability of reinforced concrete ultimate strength design approach and the yield line theory to masonry walls. The effects of horizontal and vertical reinforcement on the lateral resistance of block masonry wall panels supported on two sides, three sides and four sides were studied. The applied load was monotonic and the post yield behavior was not included.

In New Zealand, Scrivener (23) tested thin reinforced brick walls under out-of-plane cyclic loading. The lateral pressure was applied by an air bag system and cycled by changing the air bag from one side to the other. The test results, which are more applicable to brick masonry, showed that the walls

exhibited a ductile behavior characterized by large inelastic deformations. A unique pinched shape of the envelope of the hysteresis loops was obtained for centrally reinforced brick masonry walls. Review of masonry literature on flexural masonry walls indicates that no data is available regarding the post peak behavior and displacement ductility under cyclic loading.

The U.S. Coordinated Program for Masonry Building Research, which was initiated and sponsored by the National Science Foundation, aims at providing adequate test data for the seismic behavior of reinforced masonry buildings (19). As part of this program, Task 3.2(a) of the Technical Coordinating Committee on Masonry Building Research (TCCMAR) addresses the response of reinforced masonry walls to out-of-plane static loading. This report describes the test program conducted at Drexel University for grouted block masonry walls. A similar program for grouted clay masonry walls was conducted by Computech Engineering Services (25).

1.4 Objectives and Scope

The objective of this program is to study the behavior of vertically spanning reinforced block masonry walls under out-of-plane monotonic and cyclic loadings. The effects of different parameters on the deflection, flexural strength, ductility and failure modes were investigated with emphasis on the post-peak behavior which is more related to seismic areas.

A total of 14 concrete block masonry wall panels of varying parameters were constructed in the Structural Testing Laboratory of the Department of Civil and Architectural Engineering, Drexel University. The parameters studied include: percentage and location of vertical steel, block size, mortar type, extent of

grouting and load pattern.

Two additional walls built with type S masonry cement mortar were tested for the Portland Cement Association under monotonic and cyclic loadings.The objective was to study the effect of mortar type on the flexural behavior of partially grouted reinforced masonry walls. The results of tests on these walls are presented in Appendix B.

2. MATERIALS

2.1 General

The materials used in the construction of the fourteen reinforced concrete block masonry wall test panels are commercially available and are typical of those used in reinforced masonry building construction in North America. Selected materials used in this experimental study comply with the current Technical Coordinating Committee on Masonry Building Research (TCCMAR) Program.

In the test program, the wall test panels were constructed in two time intervals. Mortar, grout and control specimens are classified in this report as Phase I or Phase II to reflect the wall construction time. The physical and mechanical characteristics of the individual material components (concrete block, mortar, grout, reinforcing bars) used in constructing the wall test panels and their control specimens were investigated and are documented in this section.

2.2 Concrete Masonry Units

Three different size blocks 4.5", 6", and 8" nominal, were used in this program. The 6" blocks were considered the standard reference size from which the majority of the walls were built. The blocks complied with ASTM Standard C90-75 (5), grade N blocks. The blocks were manufactured by Blocklite in Fresno, California. Two types of 6 inches hollow two-core

masonry units were used in the construction of the wall test panels (Figure 2.1). One was full double corner block with nominal dimension of 6 inches by 8 inches by 16 inches and the other was sash block with nominal dimension of 6 inches by 8 inches by 8 inches. Average dimensions of the 4.5" and 8" blocks are shown in Figure 2.2. Blocks at bond beam locations were cut from full blocks (Figure 2.3) and were used to facilitate the placement of the horizontal rebars in the wall panels.

The physical and mechanical properties of the blocks were obtained in accordance with ASTM Standards. Average block properties and average dimensions are summarized in Table 2.1. The compressive strengths of the full blocks were determined using a Tinius-Olsen 300 kips testing machine and a Tinius-Olsen 120 kips Universal testing machine for the half block both available in the Department of Civil and Architectural Engineering, Drexel University. The tests were conducted in accordance with ASTM C140-75 (5) procedures. The blocks were capped at top and bottom with Hydrostone to achieve uniform load on the bearing surfaces during the test. A typical axial compression test is shown in Figure 2.4. The stress - strain relationships under uniaxial compression were obtained using only half block as shown in Figure 2.5. Strain readings were obtained using Linear Variable Differential Transformer's -L.V.D.T 's- (see Figure 2.5). A typical stress-strain curve for 6" masonry units is shown in Figure 2.6.

Splitting tests were also conducted on half blocks according to ASTM Standards C1006-84 (5).The splitting tensile stress was developed by applying two line loads at the center of the bearing surfaces.The loads were applied through steel rods 3/4 in. diameter. The set-up and a typical splitting failure

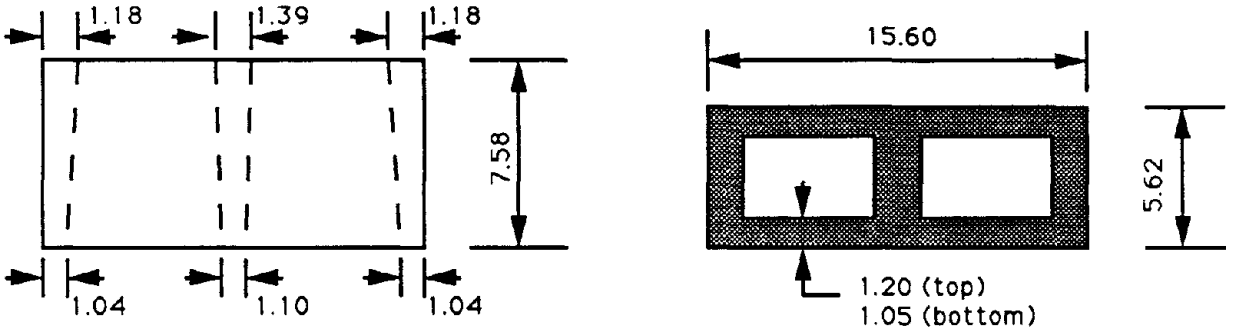

(a) Typical elevation and cross-section of the 6 in. full double corner block

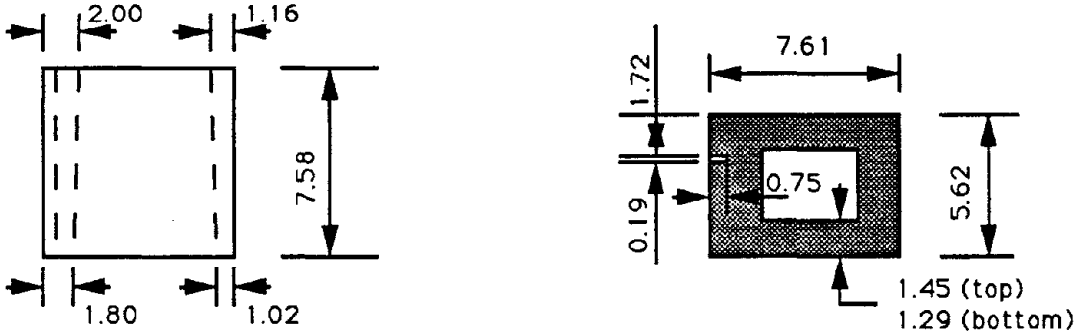

(b) Typical elevation and cross-section of the 6 in. half sash block

(all dimensions in inches)

Figure 2.1 Configurations of 6" Masonry Units

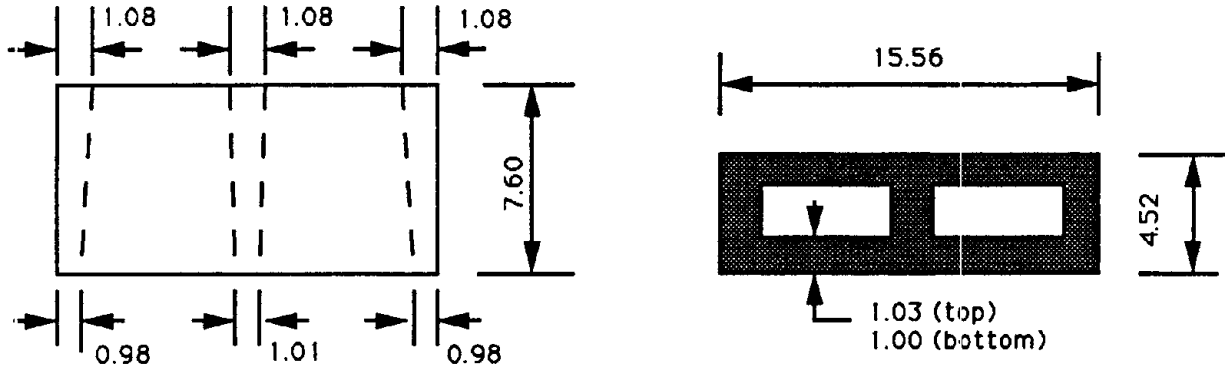

(a) Typical elevation (b) Typical cross-section

Configuration of 4.5 in. Concrete Masonry Units

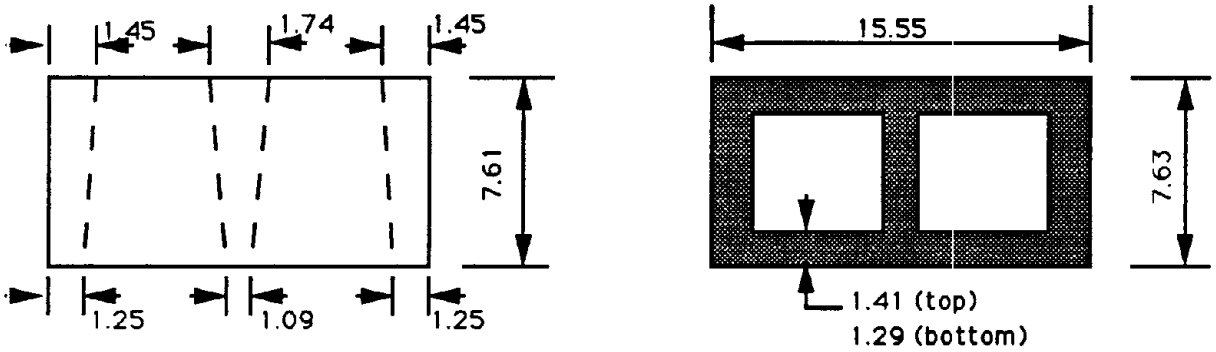

(a) Typical elevation (b) Typical cross-section

Configuration of 8 in. Concrete Masonry Units

(All dimensions are in inches)

Figure 2.2 Configurations of 4.5" and 8" Masonry Units

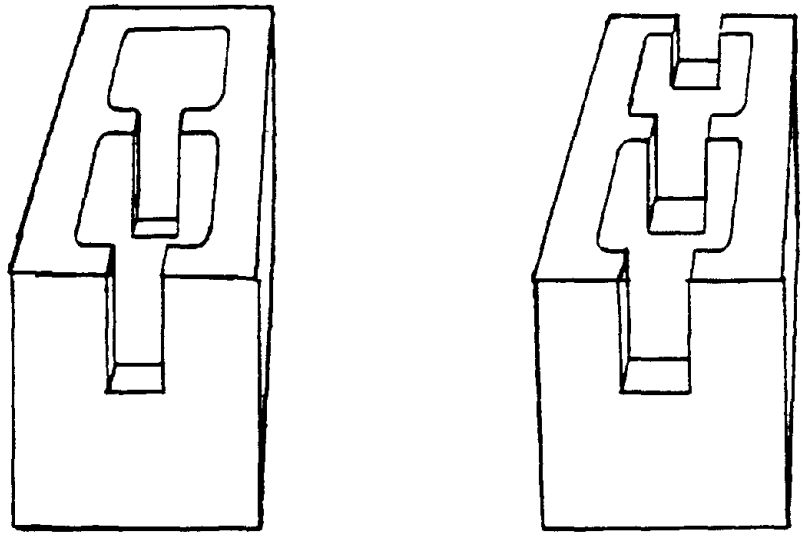

(a) End Bond Beam Block (b) Middle Bond Beam Block

Figure 2.3 Blocks at Bond Beam Locations

Table 2.1 - Dimensions and Properties of Concrete Masonry Units[a]

Description	ASTM standard	Block Size: 6 in.[b] full block	6 in.[b] half block	4.5 in.	8 in.[c]
width, in.	C140-87	5.62	5.64	4.52	7.63
height, in.	C140-87	7.58	7.58	7.60	7.61
length, in.	C140-87	15.60	7.61	15.56	15.55
min. face shell thick, in.	C140-87				
at top		1.20	1.45	1.03	1.405
at bottom		1.05	1.29	1.00	1.291
min. end web thick, in.	C140-87				
at top		1.39		1.08	1.737
at bottom		1.10		1.01	1.093
min. end web thick, in.	C140-87				
at top		1.18	2.00,1.16[d]	1.08	1.454
at bottom		1.04	1.80,1.02[d]	0.98	1.247
cross area, $in.^2$	C140-87	87.50	42.90	70.29	118.65
net area, $in.^2$	C140-87				
at top		49.70	30.50	41.33	62.4[e]
at bottom		43.00	27.40	39.41	
percent solid	C140-87				
at top		56.90	71.10	58.80	52.6[e]
at bottom		49.20	63.90	56.10	
density, pcf	C140-87	102.0		99.70	104.5
absorption, pcf	C140-87	11.00		12.76	11.56
%		10.80		12.79	11.18
moisture content, %	C140-87	3.83		6.27	7.10
initial rate of absorption, gm/min/30 in^2	C67-87	43.9		60.34	53.3
saturation coefficient	C67-87	0.72		0.73	0.73
axial compressive strength, psi	C140-87				
for net area		2920		2430	2810
for cross area		1550		1390	1480
splitting tensile strength, psi	C1006-87	280			

a. Average of three units
b. from Ref.11
c. from Ref.15
d. See Figure 2.1
e. Average value between top and bottom

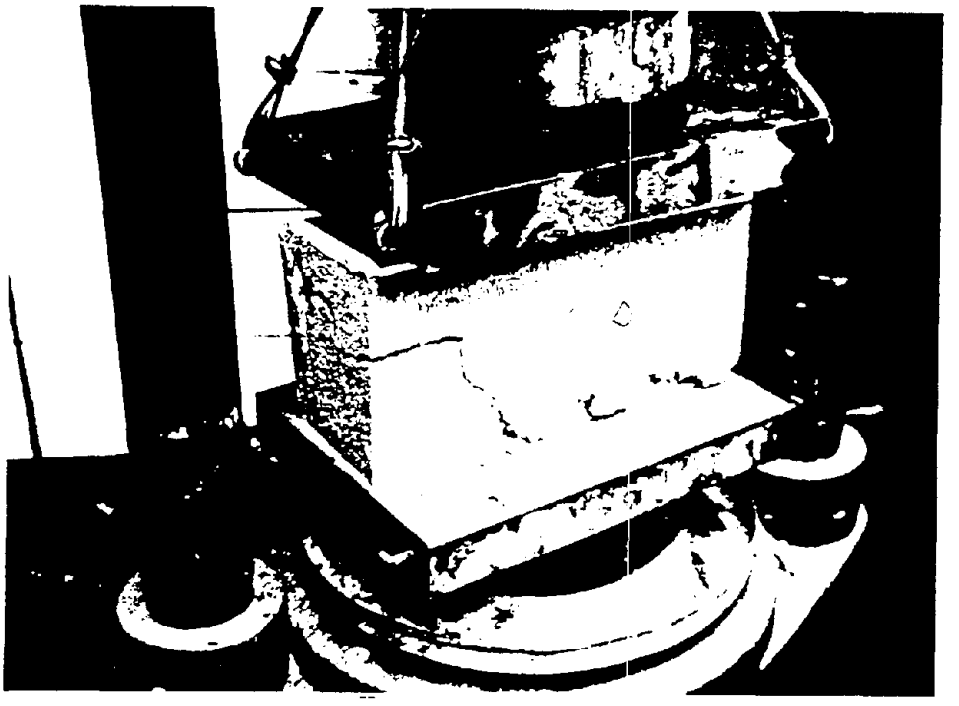

Figure 2.4 Axial Compression Test of Full Block

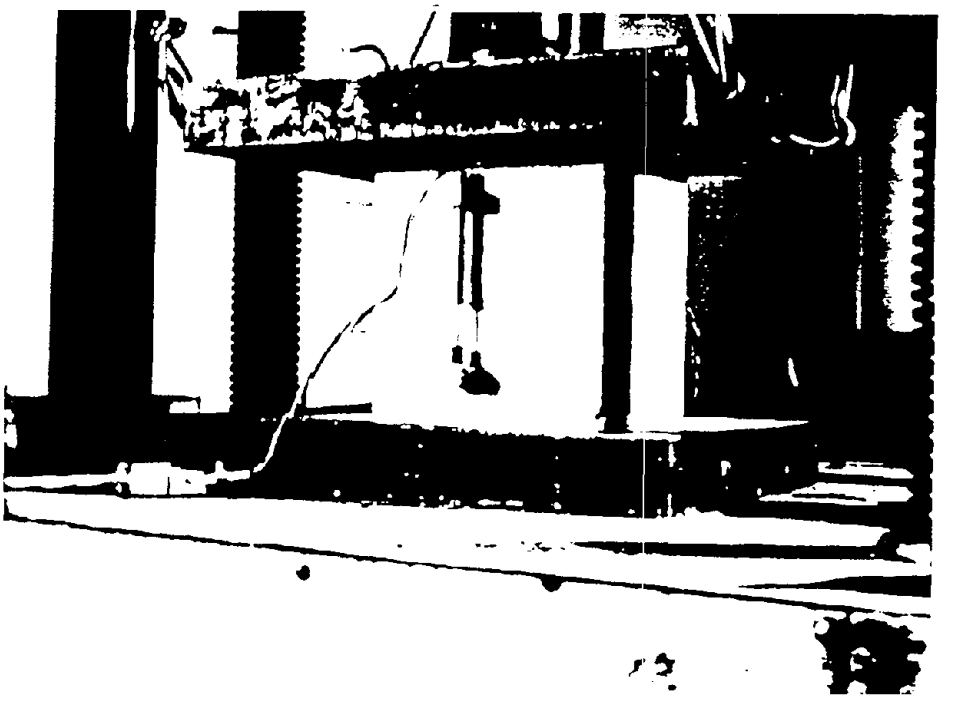

Figure 2.5 Strain Instrumentation for Compression Test of Half Unit

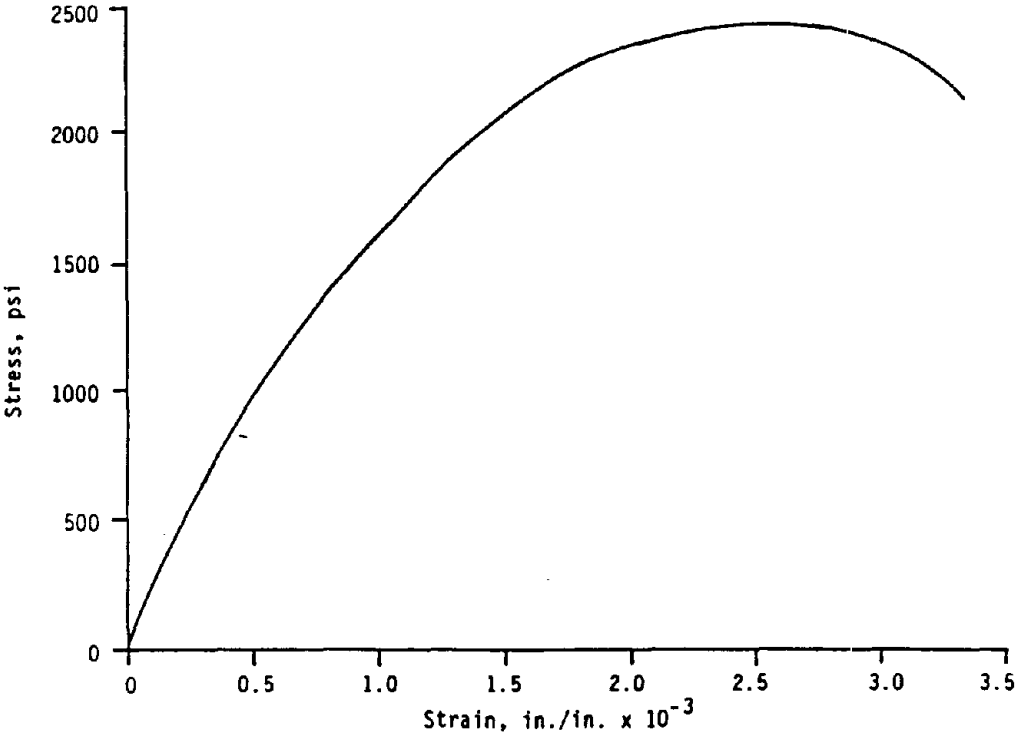

Note: stress is based on net area of the unit

Figure 2.6 Typical Stress-Strain Curve for 6" Units

are shown in Figure 2.7(a) and Figure 2.7(b), respectively. The test was conducted on two types of blocks. One was sash block and the other was half a block cut from full block.

Initial Rate of Absorption and Saturation coefficients were determined in accordance with ASTM Standard C67-83 (5). The Initial Rate of Absorption was determined using the top section of the full block. An apparatus with a tray size of 560 square inches was fabricated to determine the Initial Rate of Absorption (Figure 2.8). This tray size is a proportioned modification of the minimum tray size used for testing a standard brick specimen with a cross-sectional area of 30 square inches. The test results are shown in Table 2.1.

Other properties such as moisture content and absorption were determined only for full blocks in accordance with ASTM Standard C140-75 and are presented in Table 2.1.

2.3 Mortar

Type S mortar was used in the construction of the fourteen wall panels. The mortar mix consisted of 1 part of Type II Portland cement, 1/2 part of hydrated lime (Super Limoid, air entrained), and 4 1/2 parts of masonry sand by volume conforming to the proportions requirement for type S mortar described in ASTM C270-82 (5). For better control, the mortar mix proportions were measured by weight rather than by volume. The proportions by weight were 1 part Type II Portland cement, 0.213 parts hydrated lime and 3.83 parts sand. The sand was dried and sieved to meet the aggregate requirement of ASTM Standard C144-81(5). In Phase I of wall construction, 20% of

(a) Test Setup

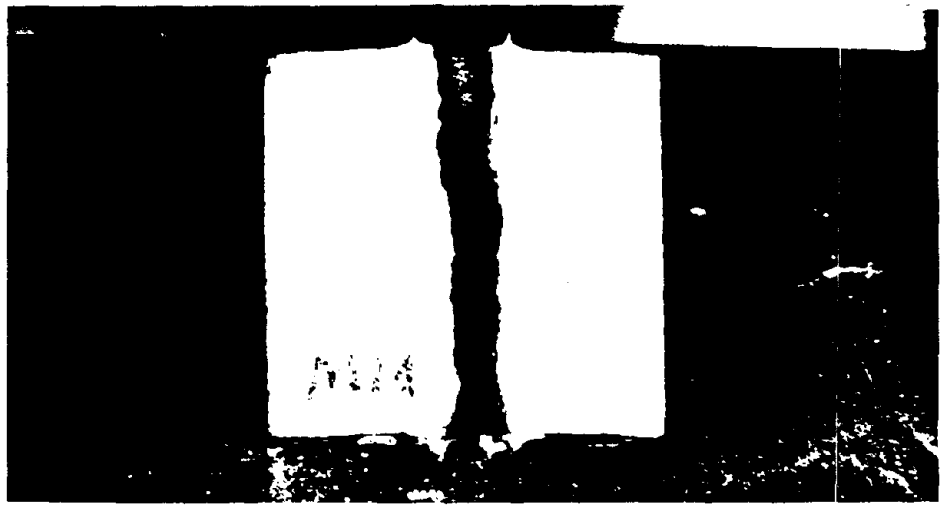

(b) Typical Failure Mode

Figure 2.7 Splitting Test of Masonry Units

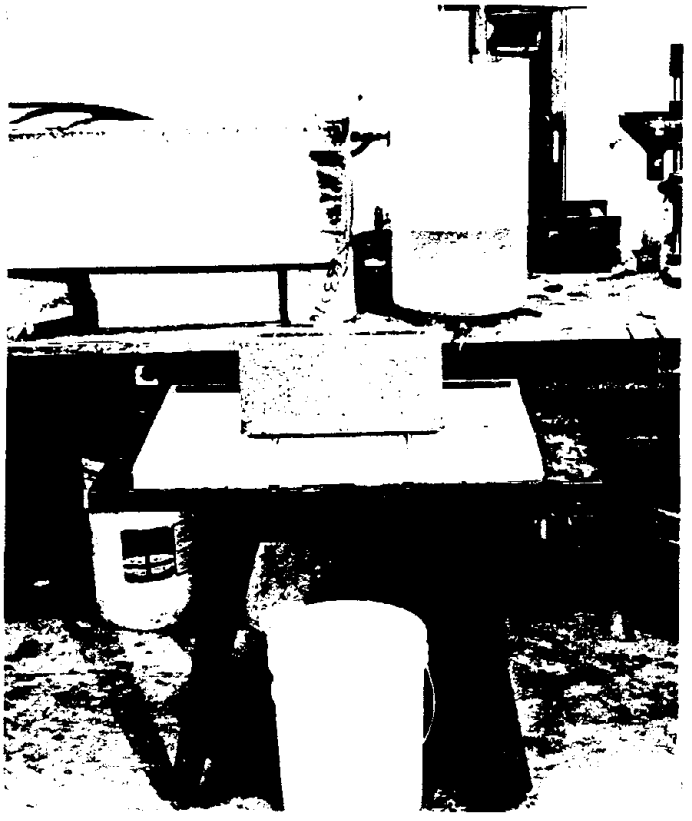

Figure 2.8 Set-Up for Initial Rate of Absorption of Masonry Units.

sand passing sieve No. 4 and retained on sieve No. 30 was added to the total amount of sand to reduce the percentage of fines and to meet the requirements of ASTM Standard C144-81 (5). The particle size distribution curves for the sand in Phase I and Phase II are shown in Figure 2.9 and Figure 2.10, respectively . It is to be noted that the sand was within the ASTM requirements. An average water/cement ratio of 0.88 for Phase I and 0.97 for Phase II was used to achieve initial flow of 115-120 percent. Table 2.2 shows the w/c ratio and initial flow for each mix used in the construction of the wall panels.

Two types of control specimens were used to determine the compressive strength of the mortar. Cylinders 2-in. in diameter by 4-in. high and two inches cubes were used. The cylinders were obtained following procedures similar to those described in ASTM Standard C109-80 (5) for 2-in cubes. The specimens were kept in a water-lime solution for 28-days until 24 hours before the test. Prior to testing , the cylinders were capped on both sides with sulfur to achieve uniform load distribution during the test. The test results for the control specimens are shown in Table 2.2.

2.4. Grout

Normal strength coarse grout was used in the construction of the wall test panels. The grout mix consisted of one part of Type II Portland cement, 3 parts of fine aggregates (sand) and 2 parts of coarse aggregate (3/8 in pea gravel) by weight conforming to ASTM Standard C476-83 (5). The mix proportions were measured by weight. The coarse grout was pre-mixed at a local concrete batch plant with a slump of 4 inches. A small amount of water was added gradually at the laboratory site to

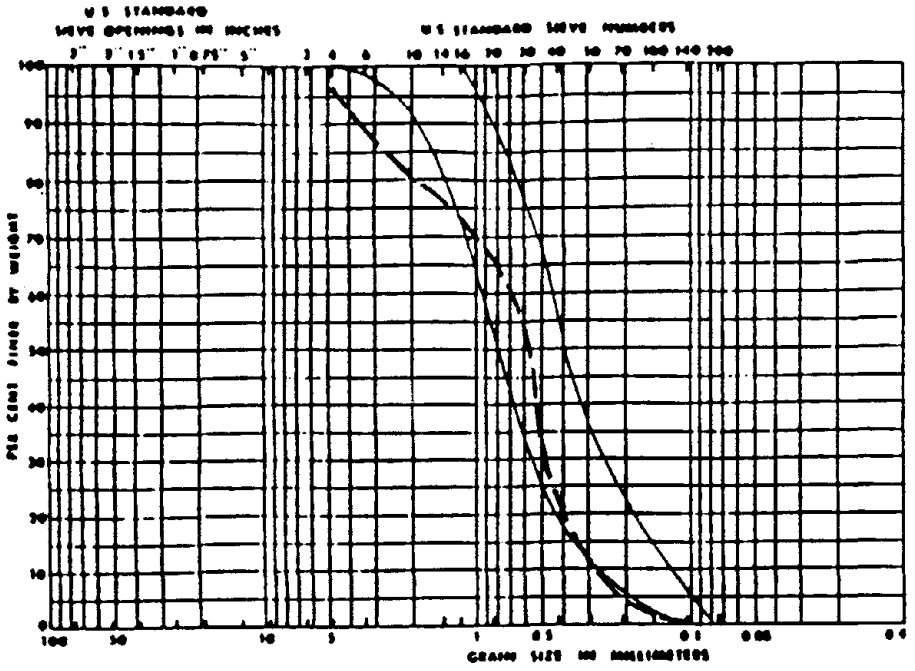

(a) Unmodified

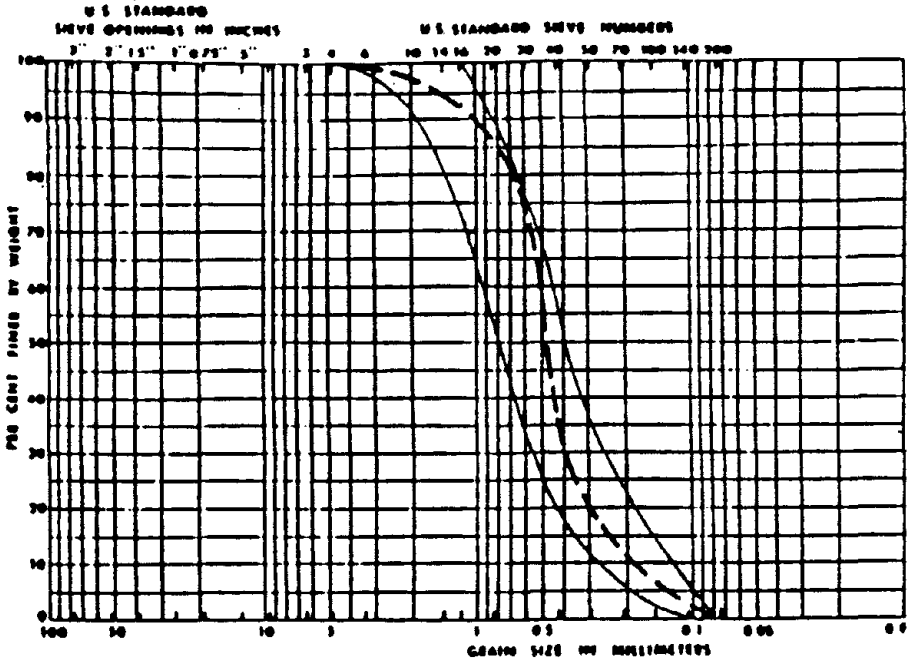

(b) Modified

_____ Limits of ASTM range

----- Gradation used for mortar

Figure 2.9 Aggregate Grain Size Distribution for Mortar, Phase I.

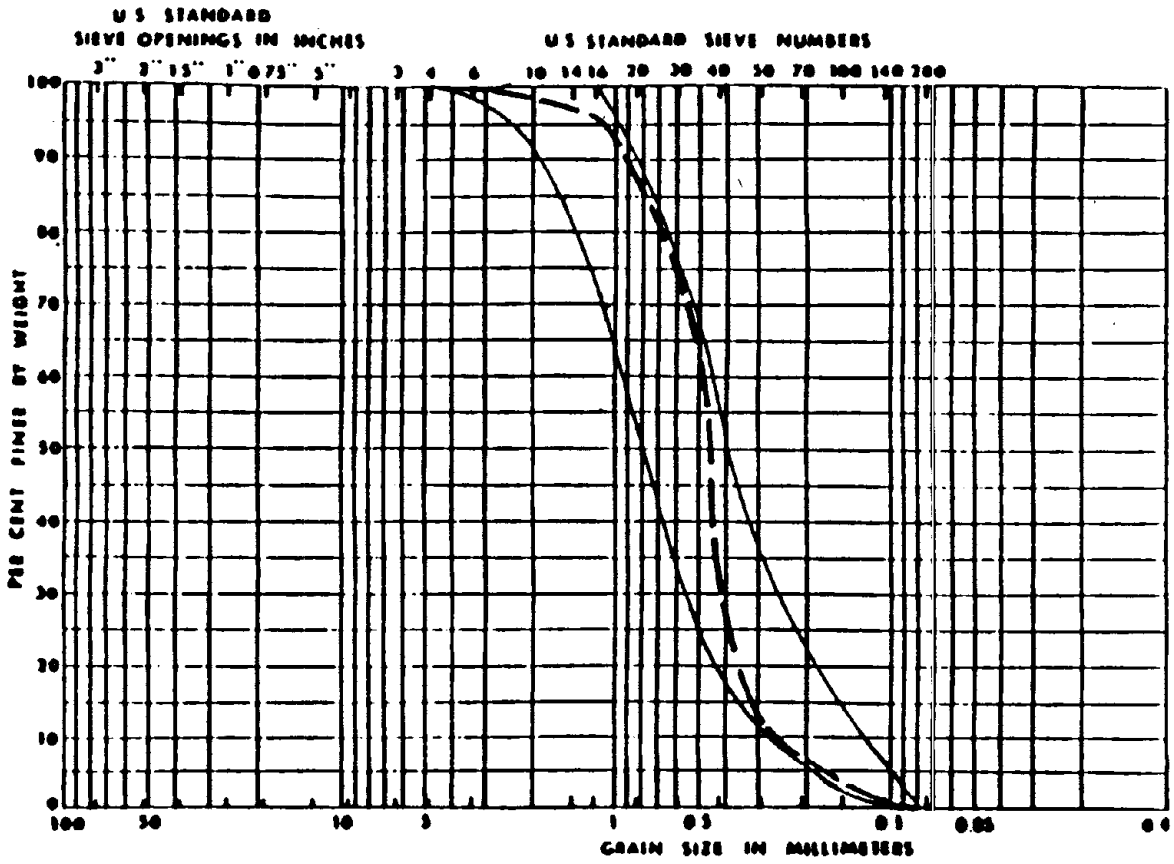

____ Limits of ASTM range.

----- Gradation used for mortar.

Figure 2.10 Aggregate Grain Size Distribution for Mortar, Phase II.

Table 2.2 - Mortar Properties

Wall No.	Wall Designation	Phase	% Flow	W/C Ratio	Compressive Strength 2"x4" Cylinders (psi)	Strength 2"x2" Cubes (psi)
W1	6PLFG5M	I	119	0.88	5590	5520
W2	6PLFG5C1	I	118	0.9	4880	4940
W3	6PLFG5C2	I	120	0.88	5310	5250
W4	6PLFG4M	I	101	0.88	4130	5420
W5	6PLFG4C1	II	122	0.98	4880	____
W6	6PLFG7M	II	119	0.97	4590	____
W7	6PLFG7C1	II	116	0.98	4820	4470
W8	6PLFG3M	II	121	0.99	____	5370
W9	6PLFG3C1	I	105	0.88	4670	____
W10	6PLPG5M	II	115	0.97	4900	____
W11	6PLPG5C1	I	115	0.88	4660	____
W12	4.5PLFG4M	II	118	0.97	3600	____
W13	4.5PLFG4C1	II	117	0.97	3100	3670
W14	8PLFG6C1	II	119	0.97	3050	3510

the mix to achieve a slump of 10-11 inches. Grout Aid , Type II (Sika Mix 119/120, manufactured by Sika Corporation) was added to the grout mix to provide workability to the mix and to prevent shrinkage which leads to the separation of the grout from the block wall. The grout aid was pre-mixed in the water that was added to the mix prior to grouting. The proportion of the Grout Aid used was as specified by the manufacturer and was 1 lb for every 94 lb of Type II Portland cement.

Three types of control specimens were used to determine the compressive strength of the grout; cylinders 2 in. by 4 in. and 3 in. by 6 in., block-molded prisms having 3 in. x 3 in. cross section and 6 in. height (as per ASTM 1019-84) and 1.7 in. by 3.4 in. grout-core specimens. The grout-core specimens were taken from the center of the cells (Figure 2.11). All specimens were air cured under the same condition as the wall test panels. The specimens were capped and tested under axial compression at the same age as the wall test panels. The test results of the control specimens are shown in Table 2.3. The 3 in. by 6 in. nonabsorbent cylinders revealed the lowest strength because of their high water/cement ratio.

2.5 Reinforcement

The wall test panels were reinforced vertically and horizontally with grade 60 steel. Vertical steel consisted of No. 4, No. 5, and No. 7 rebars, while horizontal steel consisted of No. 3 rebars. All the reinforcement rebars conformed to ASTM Standard A615-84a (4).

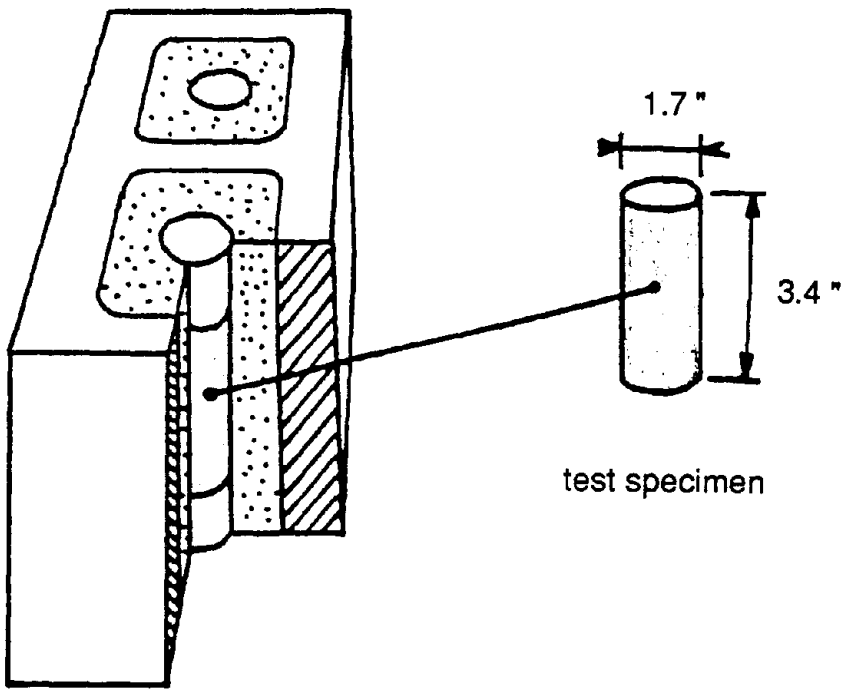

Figure 2.11 Grout-Core Specimen

Table 2.3 - Compressive Strength of Grout

Phase	Cylinders 3"X 6"			Core Drilled Cylinders[a] 1.7"X 3.4"			Block Molding 3"X 3"X6"		
	indiv. (psi)	mean (psi)	C.O.V.	indiv. (psi)	mean (psi)	C.O.V.	indiv. (psi)	mean (psi)	C.O.V.
Phase I	2820 2650 2910 2930 3000 2830 3170	2900	5.7	3820 3930 3490 3610 3760 4330 3530 4110 3600 3640 3740 3760	3780	6.5	----	----	----
Phase II	2450 2360 3060	2620	14.4	3400 3150 3510 3230 2800 3120 3010 2880 3010	3130	7.4	3630 3970 4140 3600 4060 4170 3580 4230	3920	7.0

a. See Figure 2.11

The steel reinforcement was delivered in lenghts of 20 feet. The bars were cut at 8 ft 8 in. from each end leaving a center piece of 2 ft-8 in. long. The two 8 ft 8 in. pieces were used for the vertical reinforcement of the wall panels while the 2 ft-8 in. pieces was used to determine the tensile properties of the steel rebar used in the wall test panels.

The tensile test was conducted according to ASTM Standard A370 (4) using a Tinius-Olsen 120 Kips Universal testing machine (Figure 2.12) equipped with a Tinius- Olsen S-1000 extensiometer to obtain the stress-strain characteristics. Typical failures of the test specimens are shown in Figure 2.13. Typical stress-strain curves for the steel rebars are shown in Figure 2.14. The properties of the rebars are summarized in Table 2.4.

2.6 Masonry Prisms

A total of 21 prisms were built along with the walls and were air cured in the laboratory under the same conditions as the wall panels. Two types of prisms were used to determine the maximum compressive stress of masonry, f'_{mt} , and the maximum flexural tensile stress normal to the bed joints (modulus of rupture).

The maximum compressive stress of masonry was determined using three course prisms. A total of 14 prisms were constructed in running bond with faceshell mortar bedding and flush joints. Figure 2.15 shows typical prism configurations. Eleven of the fourteen prisms were grouted with the same grout used in the wall panels. The remaining three prisms were left ungrouted. The prisms bearing surfaces were capped with gypsum cement and tested under axial compression normal to bed joints. The load

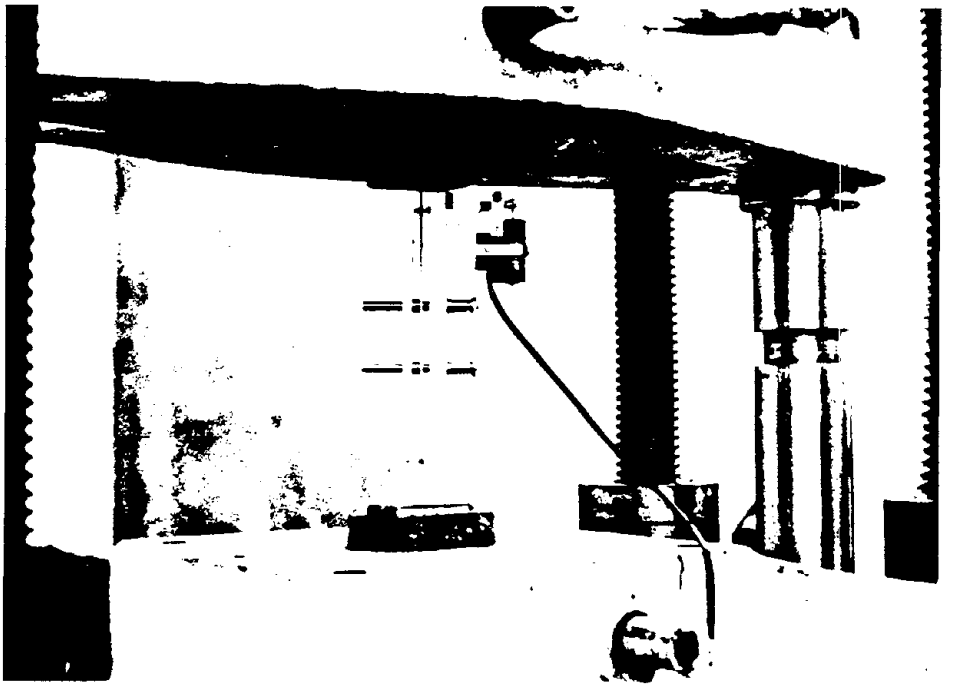

Figure 2.12 Tensile Testing of Reinforcement

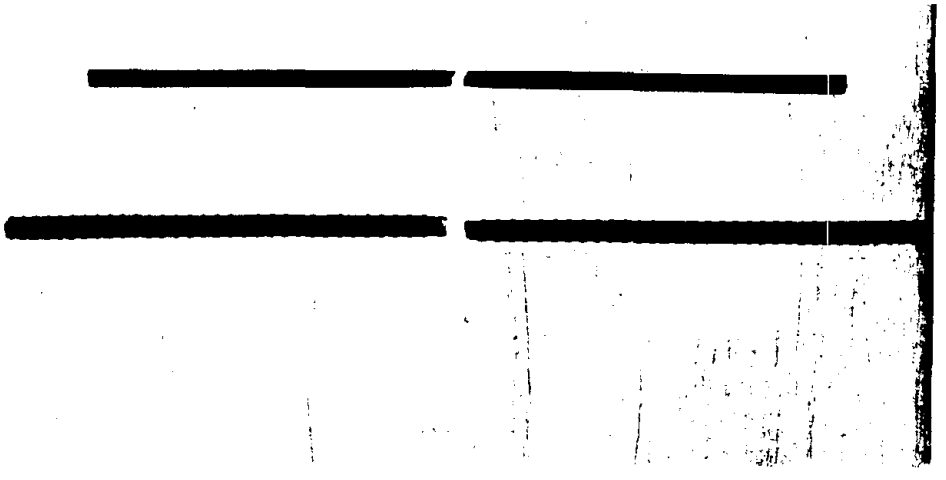

Figure 2.13 Typical Failed Steel Specimens

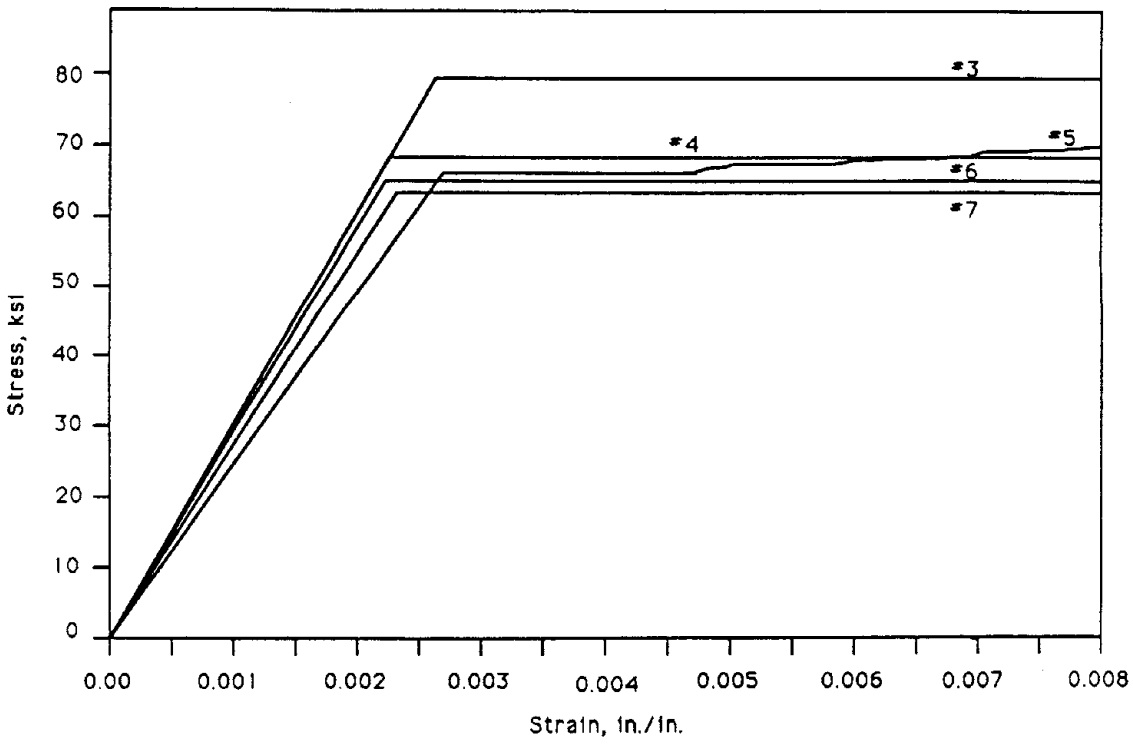

Figure 2.14 Typical Stress-Strain Curves for Reinforcing Steel

Table 2.4 - Properties of Steel Reinforcement

Vertical Reinforcement	Wall No.	Yield stress (ksi)	Ultimate stress (ksi)	Modulus of Elasticity (ksi)	Yield strain (in./in.)	Elongation (%)
#5	W1	66.8	110	25220	0.00265	12.5
#5	W2	65.5	110	24170	0.00271	10.9
#5	W3	70.0	113	26540	0.00264	13.3
#4	W4	65.0	100	26190	0.00210	7.3
#4	W5	69.4	105	26520	0.00224	14.0
#7	W6	63.2	94	27480	0.00230	8.5
#7	W7	62.2	94	27520	0.00226	18.7
#3	W8	79.6	121	31850	0.00250	14.0
#3	W9	78.2	119	30450	0.00257	12.8
#5	W10	68.1	110	24770	0.00275	5.2
#5	W11	66.4	111	25530	0.00260	10.9
#4	W12	70.0	106	26550	0.00226	11.7
#4	W13	68.8	105	26490	0.00222	16.4
#6	W14	64.8	105	25260	0.00217	18.0
Horizontal Reinforcement (#3 bars) for all walls		79.4	120	30083	0.00264	11.7

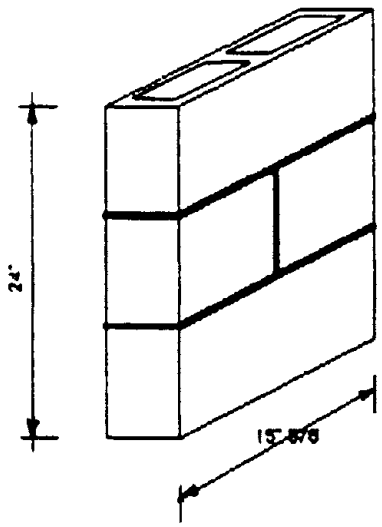

Figure 2.15 Typical Compression Prism Configuration

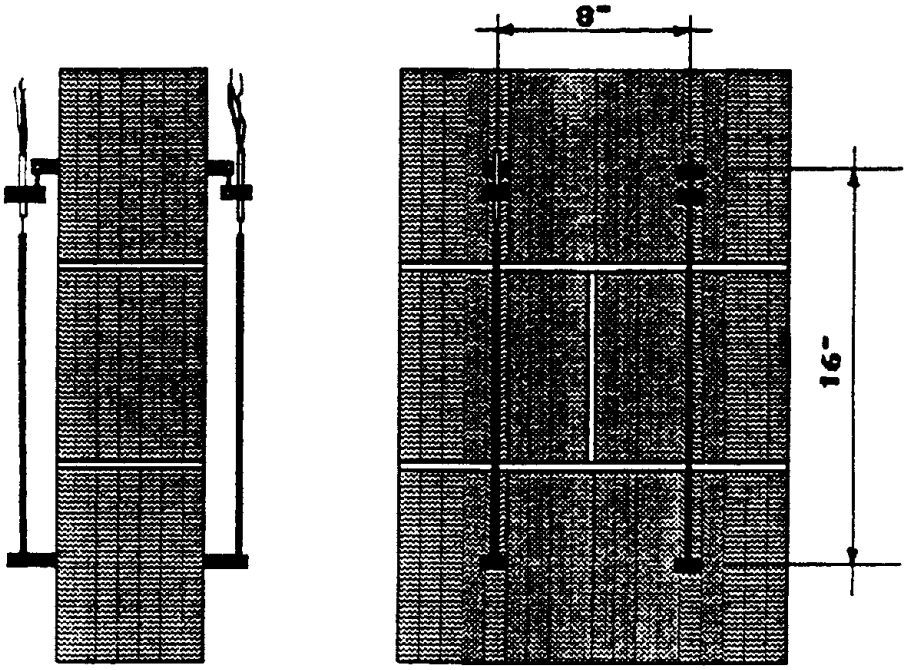

Figure 2.16 Prism Instrumentation

was applied at the net area of ungrouted prisms and the gross area of grouted prisms using an MTS servo-control system coupled with a 328 Kips hydraulic actuator. The axial deformations were measured with four + 0.25 in. L.V.D.T.'s (Linear Variable Differential Transformers).The gage length was 16 inches. Figure 2.16 shows a typical prism setup for axial compression testing.

The mode of failure observed in the ungrouted prisms tested under axial compression was a typical vertical splitting, which developed in the middle unit and spread into the other units as the load increased. Cracking in the joints was observed also on the wide face of the prism. For the grouted prisms, a mode of failure similar to that observed in the ungrouted prisms occurred followed by a separation of the faceshells from the grout cores. The splitting of the face-shells was caused by the high bilateral tensile stresses produced. Some of the grouted prisms exhibited a compression-shear mode of failure observed by the diagonal cracks developed at the narrow face of the prism. Typical modes of failure of prisms are shown in Figure 2.17.

The prism test results under axial compression are summarized in Table 2.5. The maximum compressive stress of the grouted prisms for Phase I was 21 percent higher compared to that of Phase II. The difference in maximum stress is attributed to the different grout strengths used, see Table 2.3. The average maximum compressive stress of both Phase I and II grouted prisms was 2050 psi (based on the gross area). For the ungrouted prisms, the average maximum compressive stress was 1560 psi (based on the net area), which is 24 percent less compared to that of the grouted prisms. The average masonry strain recorded at the peak load was 0.0018 in/in for the grouted prisms and 0.0013 in/in for the ungrouted prisms of

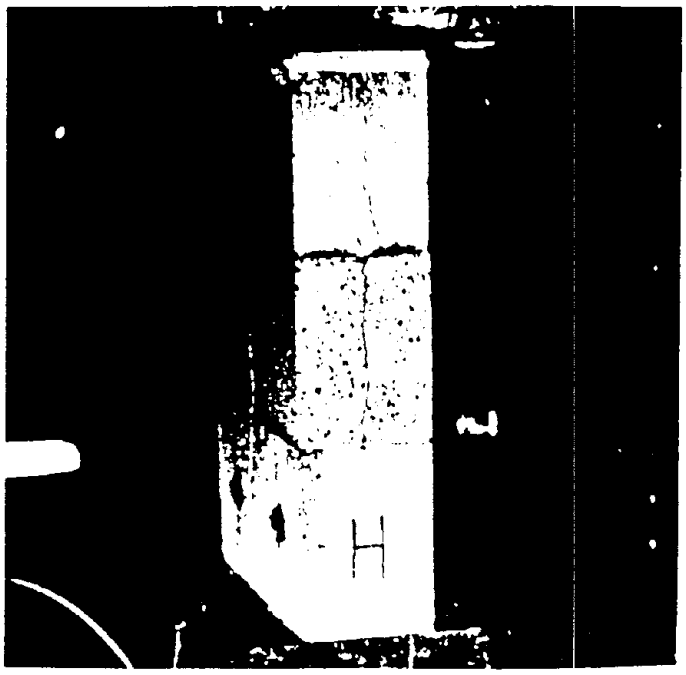

(a) Hollow Prism

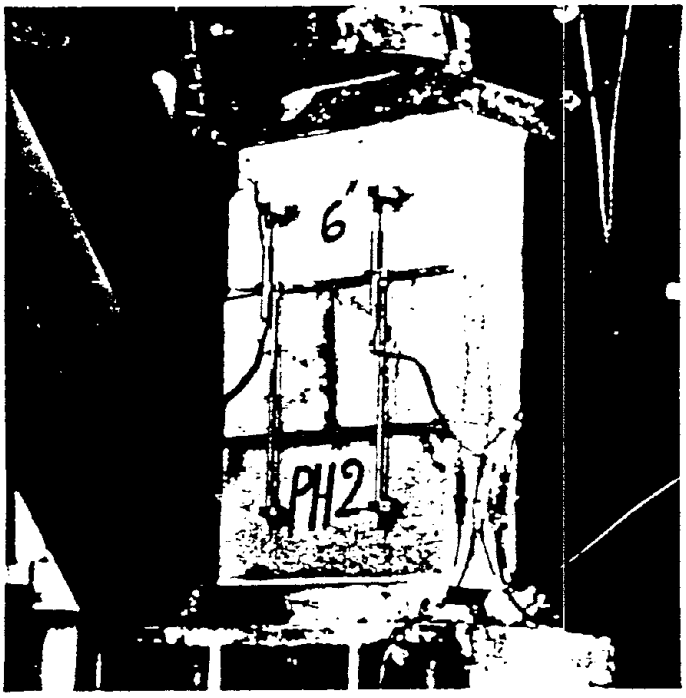

(b) Grouted Prism

Figure 2.17 Typical Failure of Prisms Under Axial Compression

Table 2.5 - Prism Compression Test Results

Phase	Nominal thickness (in.)	Grouting	Max. Comp. stress (psi)		Strain at Max. stress		Modulus of Elasticity[a], (ksi)	
			indiv.	mean	indiv.	mean	indiv.	mean
I	6	Hollow	1740 1410 1530	1560	0.0017 0.0009 0.0013	0.0013	1110 1210 1160	1160
I II II	6	Fully grouted	2320 1950 1880	2050	0.0018 0.0016 0.0017	0.0017	2080 1930 1820	1940
II	4.5	Fully grouted	1830 1470 1270	1520	0.0016 0.0013 0.0016	0.0015	1280 1750 1290	1440
II	8	Fully grouted	2000 2110 1890	2000	0.0014 0.0015 0.0015	0.0015	2720 2200 1960	2290

a) Calculated at 1/3 maximum stress.

Phase I. For Phase II, the average compressive strain was 0.00165 for the grouted prisms. The Em was calculated as secant average modulus at one third of the maximum prism compressive stress.

The modulus of rupture was determine by testing a total of 4 prisms. The prisms were constructed in stack bond. The prisms were one unit long (16 in.) and four courses high (32 in.). Two courses were full blocks and the other two courses were two half blocks each cut from full block (Figure 2.18). The prisms were tested under flexural tension normal to the bed joints. A special Bond Wrench set-up was constructed in the Structural Testing Laboratory of Drexel University to accomplish this test. Figure 2.19 shows the detail of the test set-up. The load was applied through a double acting hydraulic jack having a 21000 lb.load cell to measure the applied load. The load cell reading was measured electronically. The load was applied in equal increments until failure of the bed joint took place.

The results of the prisms tested under flexural tension are summarized in Table 2.6. The average maximum flexural tensile stress for Phase I was 280 psi which was 4 percent less than that of Phase II (295 psi). The mode of failure observed for the grouted prisms tested under flexural tension (bending parallel to the bed joints) was cracking at the mortar-block interface followed by tension failure of the grout cores. Figure 2.19 shows typical mode of failure of the grouted prisms.

The modulus of rupture as a function of the square root of the maximum prism compressive stress, f'_{mt}, is also presented in Table 2.6. As it can be seen, a k value of 6.2 to 6.5 was obtained for grouted prisms which is much higher than the 2.5 value specified in the UBC-88 (16) Code design provisions.

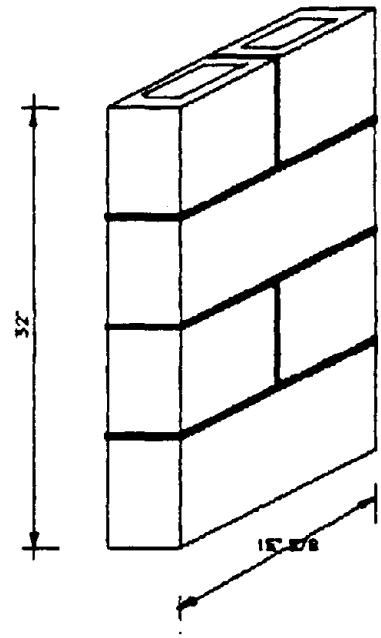

Figure 2.18 Typical Flexural Prism Configuration

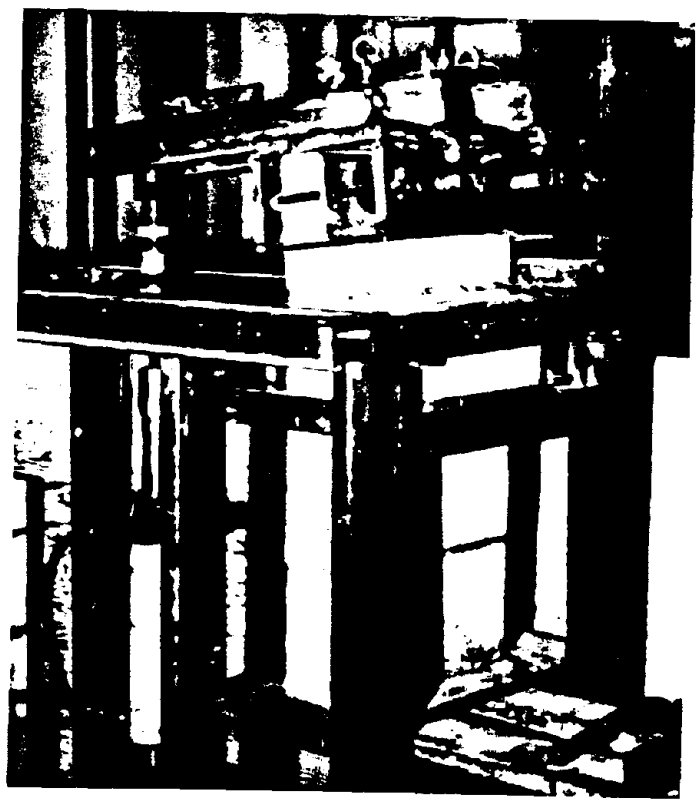

Figure 2.19 Flexural Tension Test Set-Up

Table 2.6 Bond Wrench Test Results

Phase	Nominal thickness (in.)	Prism No.	Joint[a]	Load (lb)	Moment (lb*in)	Flexural tension, f_t, psi indiv.	mean	K[b]
I	6	P1	T	1040	23400	265	270	6.0
			M	1000	22590	255		
			B	1160	26010	300		
I	6	P2	T	1100	24750	280	290	6.4
			M	1170	26280	300		
			B	1140	25650	290		
II	6	P3	T	1220	27450	310	310	6.8
			M	1240	27900	320		
			B	1170	26280	300		
II	6	P4	T	980	22050	250	280	6.2
			M	1200	27000	310		
			B	1100	24750	280		
II	8	P5	T	2100	51450	310	340	7.5
			M	2340	57330	350		
			B	2376	58210	355		
II	8	P6	T	2128	52140	320	280	6.2
			M	1800	44100	270		
			B	1700	41650	255		
II	4.5	P7	T	480	9996	175	240	5.3
			M	610	12850	230		
			B	840	17560	315		

a) T = top joint M = middle joint B = bottom joint

b) $K = ft/\sqrt{f'_{mt}}$ The average values of f'_{mt} listed in Table 2.5 are used.

3. EXPERIMENTAL PROGRAM

3.1 Scope

In this program, a total of 14 full-scale reinforced concrete block masonry walls were constructed and tested under out-of-plane monotonic and cyclic loads. The parameters considered were percentage and location of the vertical reinforcement,extent of grouting (fully grouted versus partially grouted) and block size (wall thickness). The test matrix is presented in Table 3.1. Two additional walls (W15 & W16), whose test results are presented in Appendix B, were tested for the Portland Cement Association to evaluate the effect of mortar type (Portland cement vs. masonry cement) on wall flexural behavior.

3.2 Test Specimens

Reinforced concrete block masonry walls 4 ft wide by 8 ft high were adopted in this experimental program. The wall test panel was made up from three units long (48 in.) by 13 courses high (104 in.). It was felt that this size was large enough to mimic the actual construction details of residential masonry walls. The masonry wall panels were constructed in running bond with faceshell mortar bedding and concaved tooled joints. Typical masonry wall panel dimensions are shown in Figure 3.1.

The amount of steel reinforcement used in the wall panels was generally based on the guidelines presented in the UBC code (16) and the ACI 530/ASCE 5 Code(3), which specify the minimum amount of reinforcement in either the vertical or horizontal direction to be 0.07 percent of the respective

Table 3.1 Wall Test Specimens

Wall No.	Wall Designation	Phase	Extent of grout[1]	Block Size (in.)	Reinforcement rebars	Location[2]	% [3]	Loading[4]
W1	6PLFG5M	I	F	6	2#5	C	0.23	M
W2	6PLFG5C1	I	F	6	2#5	C	0.23	C1
W3	6PLFG5C2	I	F	6	2#5	C	0.23	C2
W4	6PLFG4M	I	F	6	2#4	C	0.15	M
W5	6PLFG4C1	II	F	6	2#4	C	0.15	C1
W6	6PLFG7M	II	F	6	2#7	C	0.44	M
W7	6PLFG7C1	II	F	6	2#7	C	0.44	C1
W8	6PLFG3M	II	F	6	6#3	S	0.24	M
W9	6PLFG3C1	II	F	8	6#3	S	0.24	C1
W10	6PLPG5M	II	P	6	2#5	C	0.23	M
W11	6PLPG5C1	I	P	6	2#5	C	0.23	C1
W12	4.5LFG4M	II	F	4.5	2#4	C	0.19	M
W13	4.5PLFG4C1	II	F	4.5	2#4	C	0.19	C1
W14	8PLFG6C1	II	F	8	2#6	C	0.24	M

1 F=Fully grouted P=Partially grouted

2 C=Centrally located S=Staggered

3 Percentage of vertical steel=Area of steel/gross wall area

4 M=Monotonic loading C1=Cyclic pattern 1 C2=Cyclic pattern 2

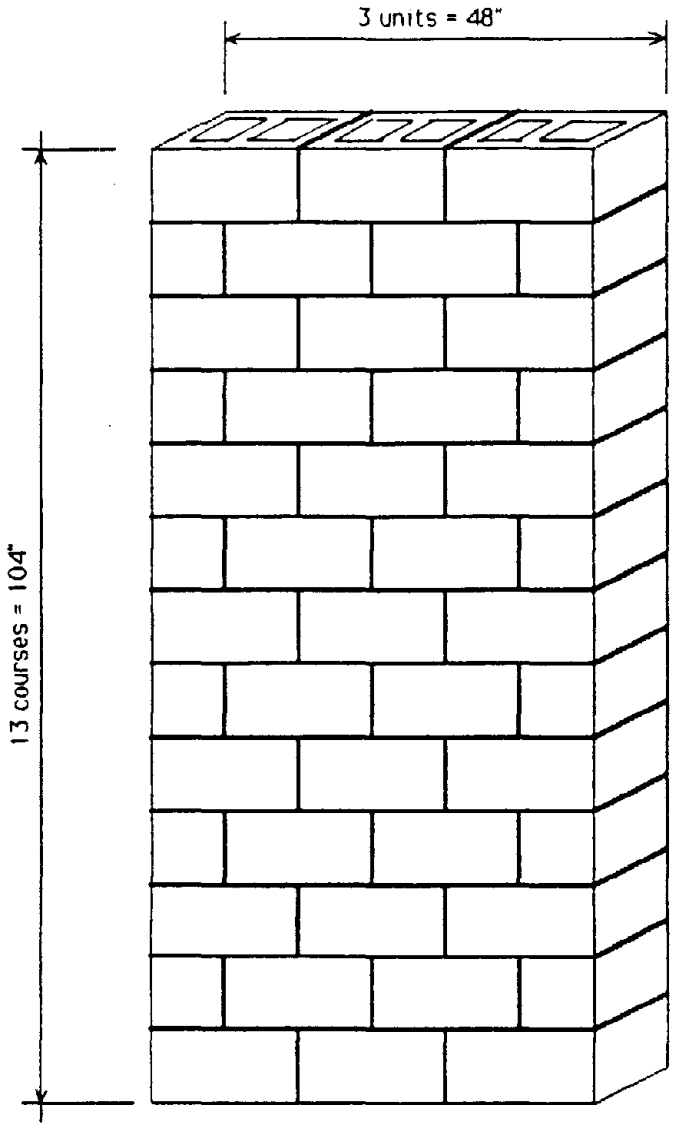

Figure 3.1 Typical Wall Panel Dimensions

gross - sectional area of the wall. In addition, the sum of the percentages of the vertical and horizontal reinforcement is specified to be at least 0.20 percent. The percentage of the vertical reinforcement varied from 0.15% to 0.44%. The vertical reinforcement for all the wall panels was provided by two rebars placed at a distance of 24" o.c. , see Figure 3.2. The spacing of the vertical reinforcement was kept constant throughout the program. In the horizontal direction, No. 3 rebars were used every third course to provide the minimum horizontal reinforcement (0.07%) specified by the code.

All the walls, except wall W8, had two vertical rebars centrally located as shown in Figure 3.2(a).Wall W8 had staggered reinforcement shown in Figure 3.2(b). Comparing the results of wall W2 (centrally reinforced) with those of wall W8 would provide information regarding the effect of rebar location on the cyclic response of the walls.

3.3 Wall Panel Construction

The masonry wall panels were constructed in the Structural Testing Laboratory of Drexel University by an experienced and qualified mason. A total of 14 walls were constructed, 12 of them were fully grouted and the other two were partially grouted (only the cells which contain the steel rebars were grouted). A steel frame was constructed to aid in the construction of the wall panels and to stabilize the walls against any lateral movement during and after the construction.

The walls were built on steel channels to facilitate the movement of the walls to the test set-up (Figure 3.3). To control the location of the vertical rebars at the bottom of the wall, two holes were drilled in each channel at the center

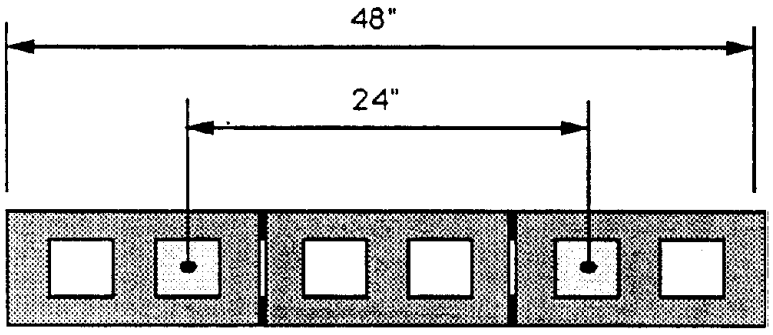

(a) Centrally Reinforced

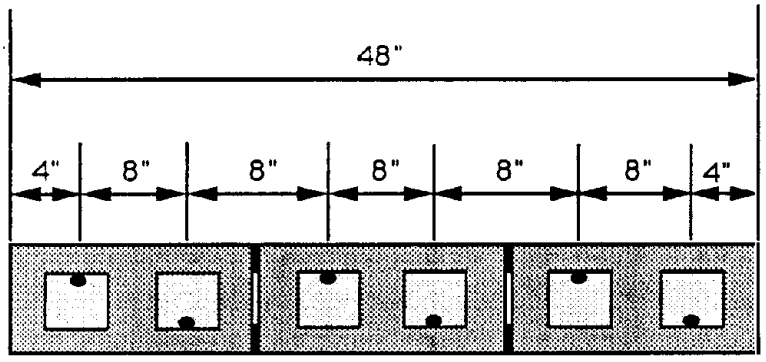

(b) Staggered reinforcement

Figure 3.2 Locations of Vertical Reinforcement

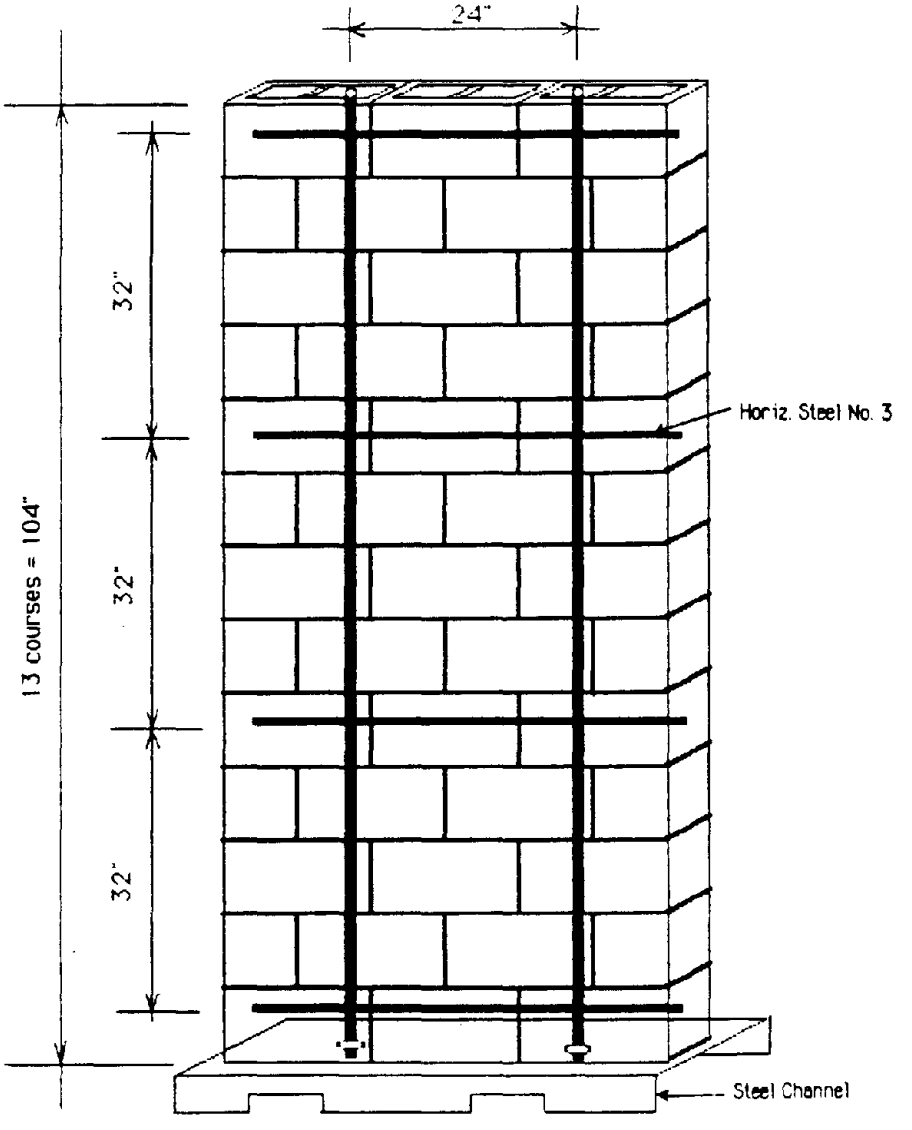

Figure 3.3 Isometric View of a Wall Panel Showing Vertical and Horizontal Steel

of the block. The masonry walls were constructed in running bond with a face shell mortar bedding. No mortar was placed on the webs except those at the ends to prevent the grout from flowing out, see Figure 3.4a. To prevent the flow of the grout to the other cells in the partially grouted wall panel, a fine wire mech was used to plug the opening at the location of the horizontal reinforcement, see Figure 3.3b. For the partially grouted wall panels, the mortar was placed also at the webs of the grouted cells to prevent the grout from flowing out to the other cells, see Figure 3.4b. All the joints were tooled on both sides for further compaction of the mortar joints.

Grouting of the walls took place a week after constructing the walls. The grout was pre-mixed at a local concrete batch plant and was grouted in the walls by the aid of a high-lift grout pump. All the walls were cast in plywood forms stiffened with wood battens. After the grout was placed, it was consolidated using a 3/4 in. electrical vibrator. The wall panels were air-cured in the laboratory under an average temperature of 75° F and an average relative humidity of 70 percent.

3.4 Test Set-Up

The walls were tested as simply supported elements under out-of-plane bending. Two equal line loads were applied to the face of the wall panels at the third points to provide a middle pure bending zone. A typical test arrangement used for the walls is shown schematically in Figure 3.5. The test set-up consisted

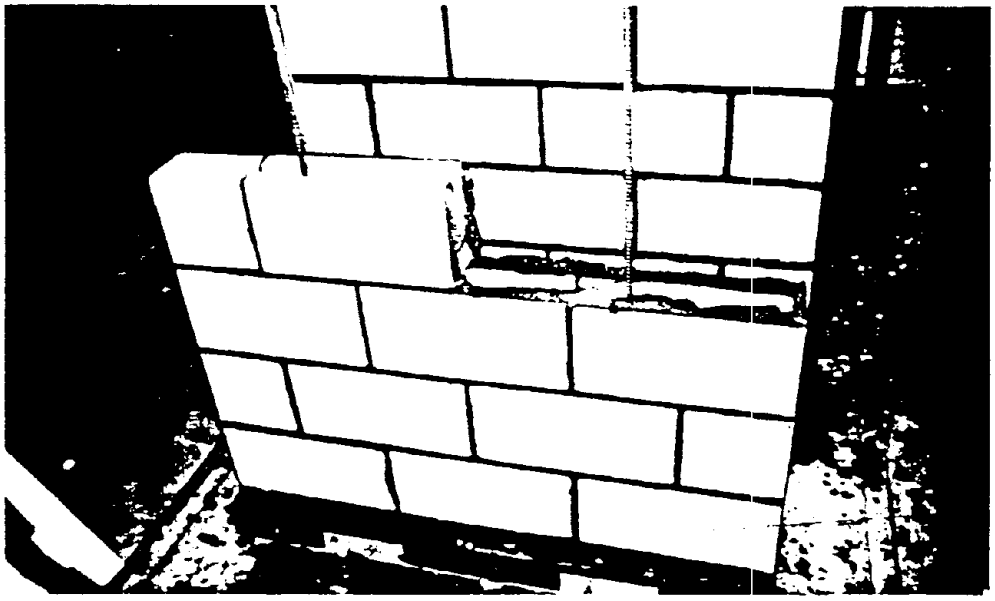

(a) Fully Grouted Walls

(b) Partially Grouted Walls

Figure 3.4 Wall Panels Construction

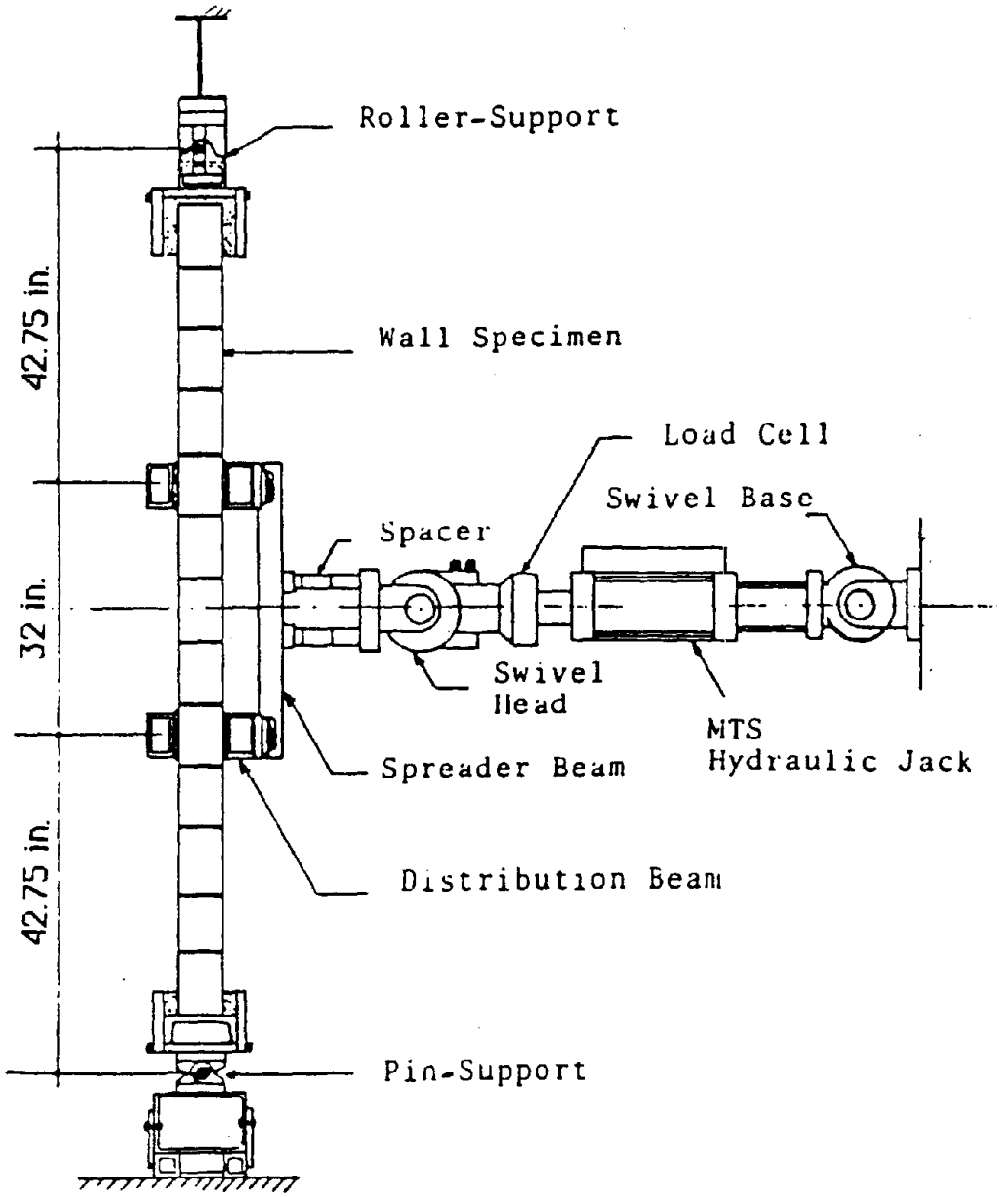

Figure 3.5 Test Set-Up

of three parts: the loading frame, the bottom support and the top support.

For the loading frame, two steel tubes, 3 in. by 6 in., were clamped to the wall at the location of the applied loads. Clamping of the tubes was accomplished through one inch diameter threaded rods provided at each side of the wall. A space of less than 1/2 in. was maintained between the tubes and the wall. The space was filled with Hydrostone to provide an even bearing. The two line loads were provided to the steel tubes through a steel push-pull spreader beam as shown in Figure 3.5. The spreader beam was roller supported on the tubes. The center of the spreader beam was connected to a load cell through a swivel head. The swivel head permitted rotation in all directions to accommodate any movement without introducing bending in the load cell. The load cell was connected to an MTS hydraulic actuator bolted firmly to an existing reaction frame.

The bottom support was designed as a hinge that permitted only angular movement. Figure 3.6 shows the details of the bottom support. The steel channel at the bottom of the wall sat directly on a horizontal steel plate connected to a roller assemblage. The roller assemblage was bolted to a tube fixed firmly to the floor as shown in Figure 3.6. On each side of the horizontal steel plate , two vertical steel plates with the same horizontal dimensions were connected to it to prevent the wall from sliding outside the set-up during the test. The space between the wall and the vertical steel was filled with Hydrostone to prevent the lateral movement of the wall at that location. This space was especially designed to accommodate the different thickness of the wall panels used in this project.

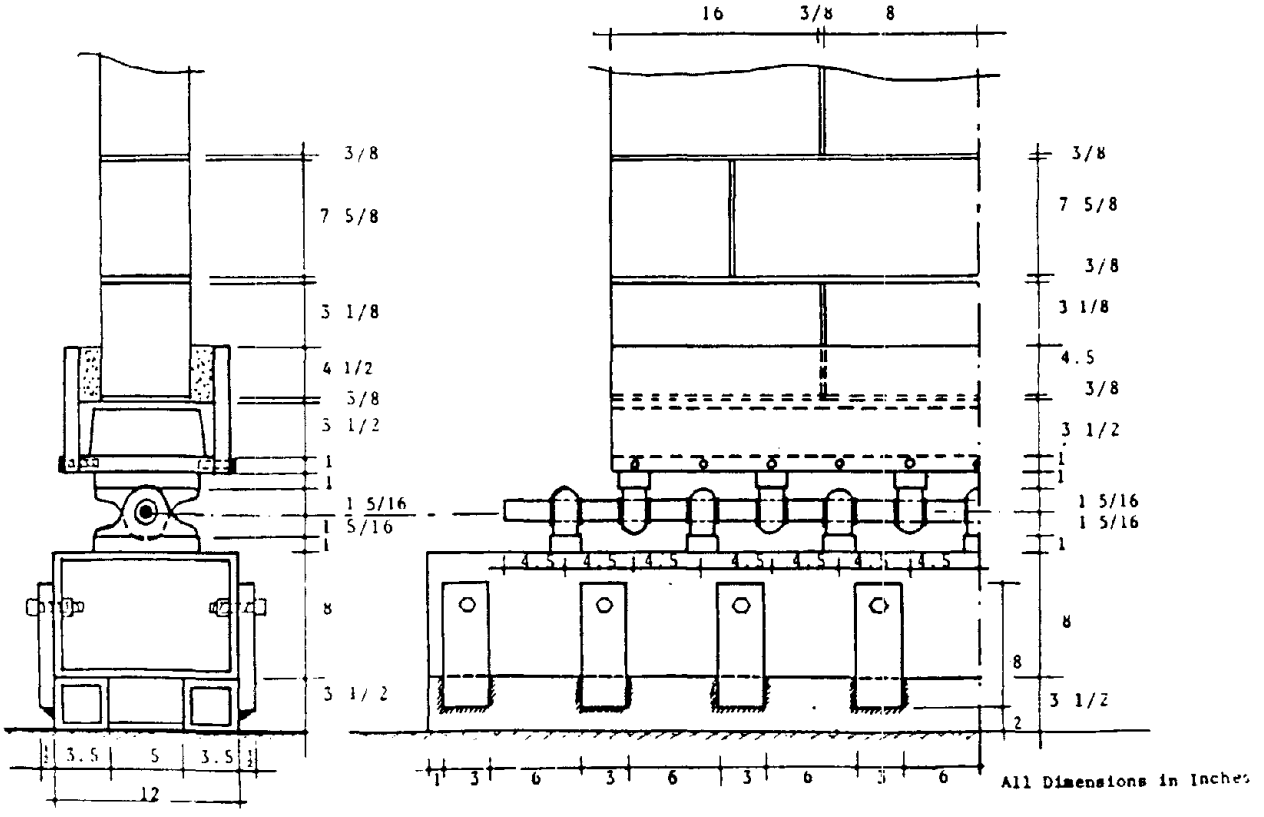

Figure 3.6 Bottom Support Details

The top support was designed as a roller that permitted vertical and angular movement. The details of the top support are shown in Figure 3.7. The top support consisted of a fixed part and a movable part. The fixed part consisted of a pair of 2 in. by 6 in. vertical steel plates spaced 4 in. on center. The vertical steel plate were connected to an I-beam which in turn, was connected to an existing reaction frame. The movable part was sliding in between the pair of vertical steel plates through a roller assemblage. The roller assemblage was connected to a horizontal steel plate through 4 in. by 6 in. steel tubes spaced 4 in. on center. The horizontal steel plate was placed directly on the top of the wall. Two vertical steel plates were bolted on either side of the wall to the horizontal steel plate. The gap between the interconnected steel plates and the wall was filled with gypsum in order to distribute the load and prevent slippage between the top support and the wall.

3.5. Testing Equipment

An MTS double acting hydraulic jack with push pull capacity of 55 kips was used to provide the lateral load to the wall panels. The MTS hydraulic jack was operated under displacement control at a constant rate through an MTS computer control station,which has been developed at the Structural Testing Laboratory of Drexel University. The MTS control station consists of: a computer control system, data acquisition equipment, plotter and printer. Data acquisition is carried out using a dedicated computer system. Displacement and the corresponding load are recorded automatically and continuously at equal time increments up to and beyond failure. Through a specially developed software (STRUCT-1) the acquired data is mathematically manipulated and displayed in a graphical form.

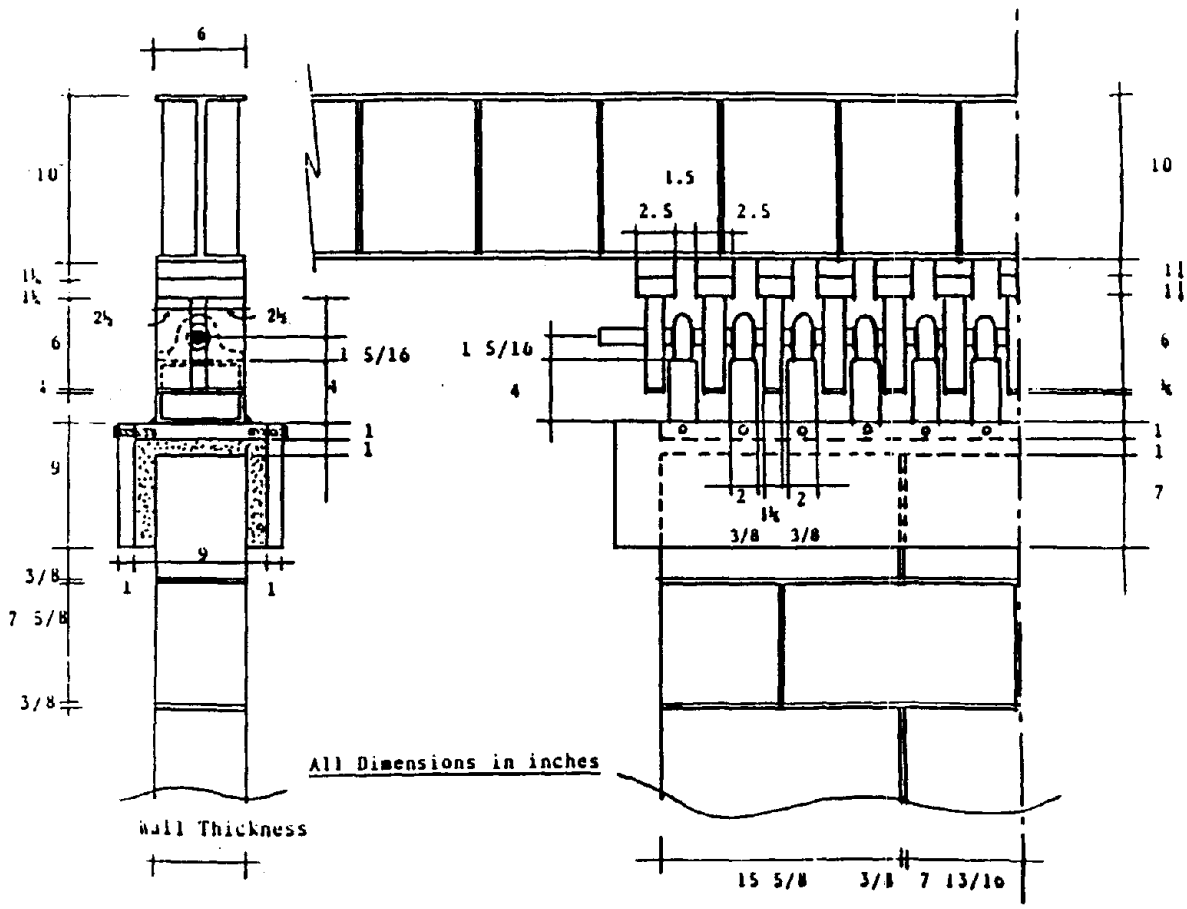

Figure 3.7 Top Support Details

3.6. Loading

Walls were tested under monotonic and cyclic loads. For monotonic loading a displacement ramp was specified and the test was continued post the peak to about 50 percent reduction of load carrying capacity. Two patterns of cyclically reversed out-of-plane loadings were used to test the vertically spanned reinforced concrete block masonry walls; 1) the sequential phase cyclic loading as recommended by TCCMAR (pattern C1) and 2) another pattern (pattern C2) which was selected to represent an earthquake of a large initial peak to drive the wall into a high level of inelastic deformation in an early stage of loading. Figures 3.8 shows the two cyclic displacement patterns C1 and C2.

The cyclic displacement pattern C1 consisted of five stages of cycles. The first three stages of cycles of three repeating cycles each, (at the same displacement amplitude) the displacement amplitude was 75,50, and 25 percent of the predicted yield displacement. The fifth stage of cycles was stablizing cycles of three repeating cycles at the maximum displacement amplitude of stage of cycle four. Stages of cycles four and five were repeated at maximum displacement amplitude of 200, 300, 400, and 500 percent of predicted yield displacement. It is to be noted that the displacement amplitude was limited by the maximum extension of the stroke of the hydraulic actuator.

In the cyclic displacement pattern C2, three stages of cycles were used. The first stage of cycles was three repeating cycles of 25 percent of the predicated yield displacement. The second stage of cycles was a series of four cycles starting with

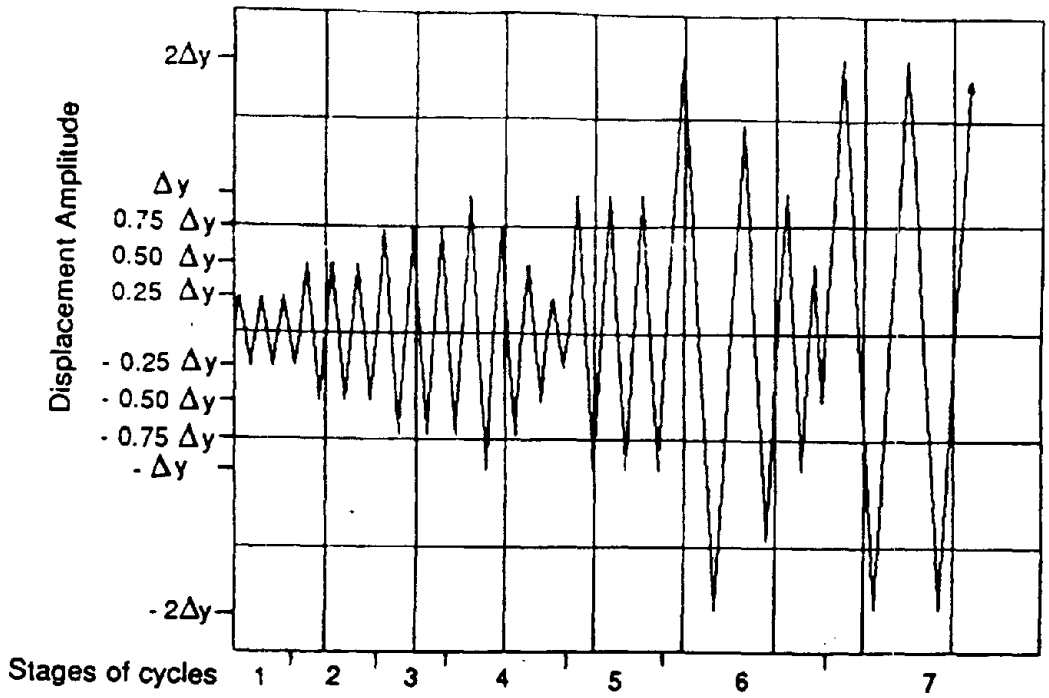

(a) Cyclic Pattern C1

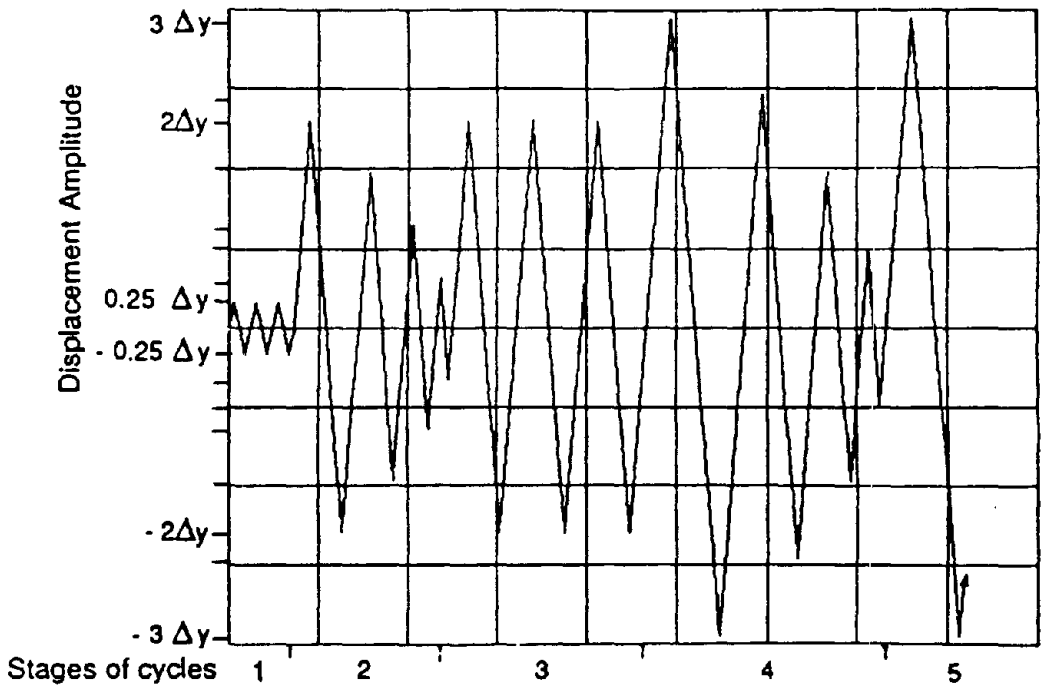

(b) Cyclic Pattern C2

Figure 3.8 Displacement Patterns for Cyclic Loading

twice the predicated yield displacement and three decaying cycles of 75, 50, and 25 percent of twice the predicated yield displacement, respectively. The third stage of cycles was stablizing cycles of three repeating cycles at the maximum displacement amplitude of stage of cycles two. Stages of cycles two and three were repeated at maximum displacement amplitude of 300 and 400 percent of the predicated yield displacement or up to the maximum stroke of actuator. Wall panel W3 (6PLFG5C2) was tested using cyclic displacement load pattern C2, whereas all the other wall panels were tested using cyclic displacement pattern C1. For the purpose of defining the displacement pattern described above the yield displacement of the cyclic walls was taken equals to the displacement at calculated yield load(see Appendix A) of similar monotonic walls, which were tested first in the program.

3.7. Instrumentation

The out-of-plane deflection of the wall panels was measured by using L.V.D.T's (Linear Variable Differential Transformers) and wire potentiometers. One L.V.D.T of ±5 in. stroke was used to measure the mid-height deflection of the wall panel. The deflection at that point was also measured by the load cell L.V.D.T connected to the jack. Two potentiometers of 10 inches in length were used to measure the deflection at the location of the applied loads. Another two potentiometers of 20 in. length were used to measure the deflection at the mid-span between the applied loads and the center of the supports. Figure 3.9 shows the location of the potentiometers on the wall panel. Four L.V.D.T's were placed on each side of the wall panel to measure the masonry strain on the compression side and the crack opening on the tension side. The L.V.D.T's were placed parallel to the wall length at the four joints which are located

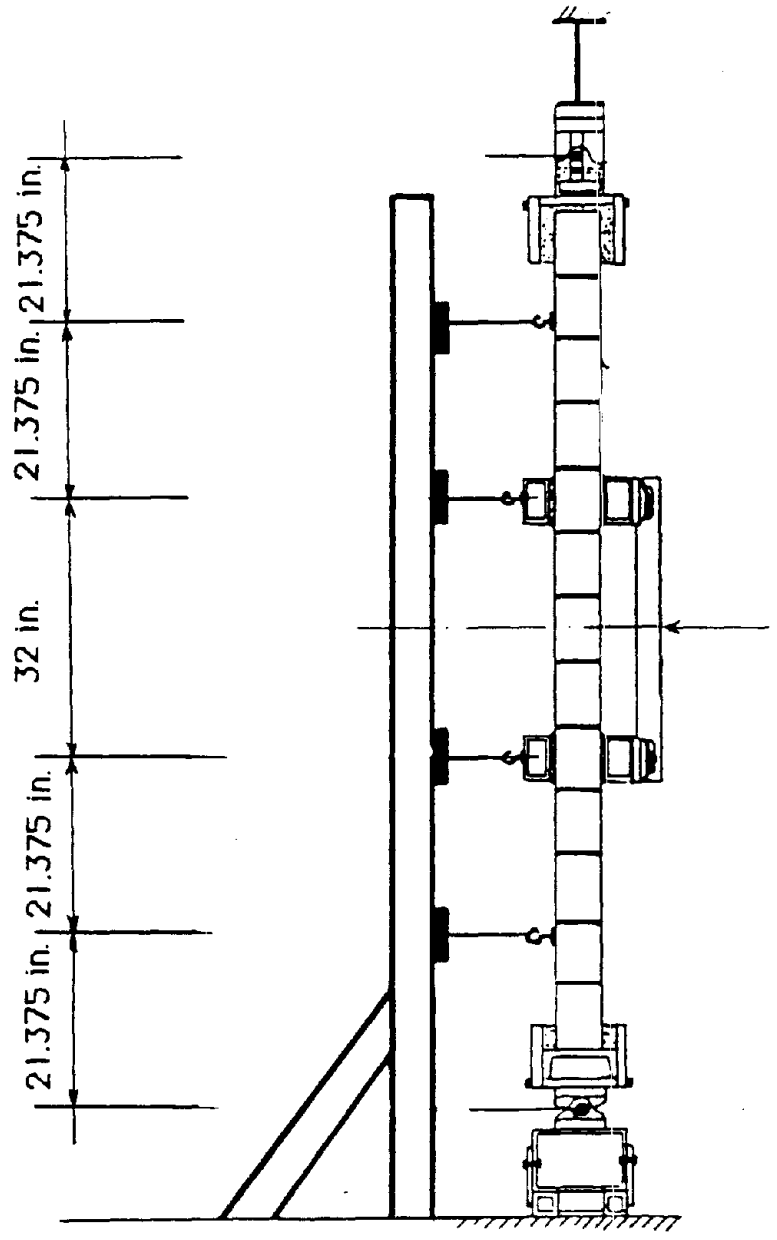

Figure 3.9 Locations of the Wire Potentiometers for Deflection Measurements

between the applied loads. The strain measurements were calculated from the shortening of the precision L.V.D.T's. The distribution and location of the L.V.D.T's on the wall panel is shown in Figure 3.10. Strain data from the reinforcing rebars was obtained through electrical strain gages. Four strain gages were fixed to one of the rebars at the location of the four joints between the applied loads. The strain gages were bonded and water proofed before grouting the walls.

All these instruments were connected to a computerized control station and data aquisition system.

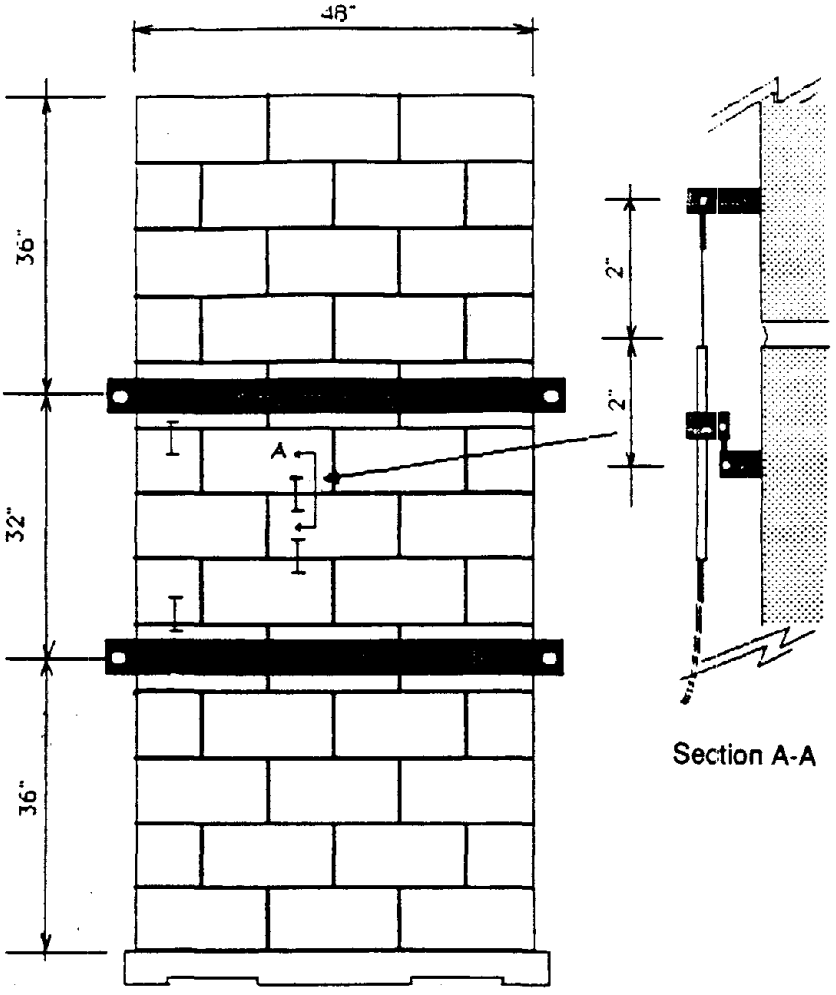

Figure 3.10 Locations of the L.V.D.T's on the Wall Panels

4. EXPERIMENTAL RESULTS AND DISCUSSION

4.1 Modes of Failure and Crack Patterns

The vertically spanned reinforced concrete block masonry walls responded in a flexural ductile mode, where flexural cracks were initiated in the pure moment region, see Figure 4.1. Cracking patterns of the six wall panels tested under monotonically increasing out-of-plane bending are shown in Figures 4.2-4.7. The numbers alongside the cracks indicate the chronological order in which the cracks appeared. The first flexural crack was initiated at the block-mortar interface in the pure moment region. With the increase of load beyond the cracking load, further flexural cracks were developed and flexural-shear cracks outside the pure moment region also were generated at a later stage of loading. All the cracks were essentially at the bed joints at the mortar-block interfaces as shown in the figures.

Wall W4 (Figure 4.3) with the least amount of reinforcement and wall W7 (Figure 4.7) with the highest amount of reinforcement showed fewer cracks compared to wall W1 with moderate amount of reinforcement (Figure 4.2).

Most of the flexural cracks widened and extended slowly toward the compression face in a straight line as the load was increased to a level that caused yielding of the reinforcing bars. The onset of wall maximum capacity was observed when one of the flexural cracks opened more than the others, causing spalling of the mortar joint on the compression side near the ultimate load. Spalling of faceshell was observed in some of the walls (Figure 4.8).

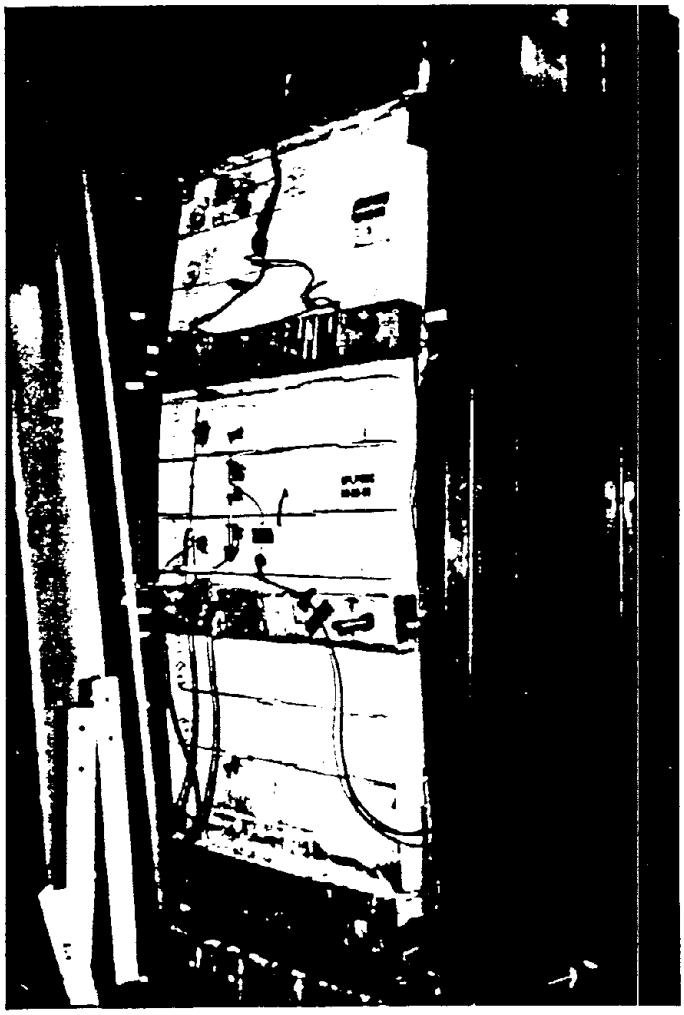

Figure 4.1 Typical Flexural Cracking and Deflection of Reinforced Masonry Wall Under Flexure

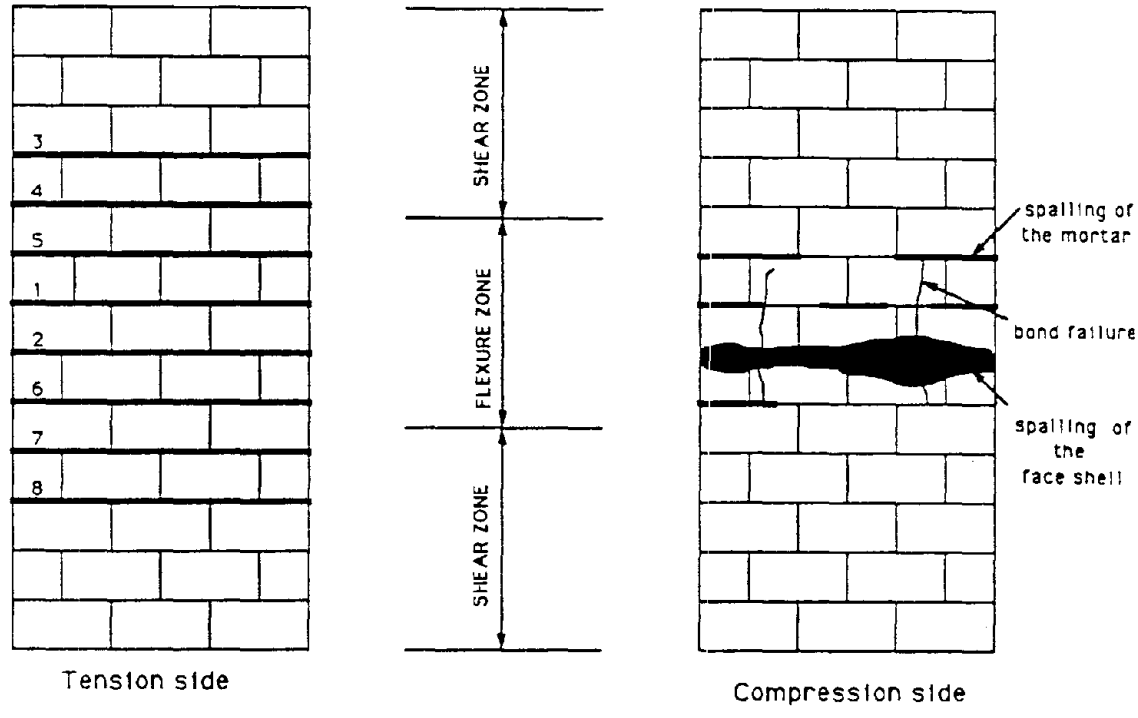

Figure 4.2 Crack Patterns of Wall W1

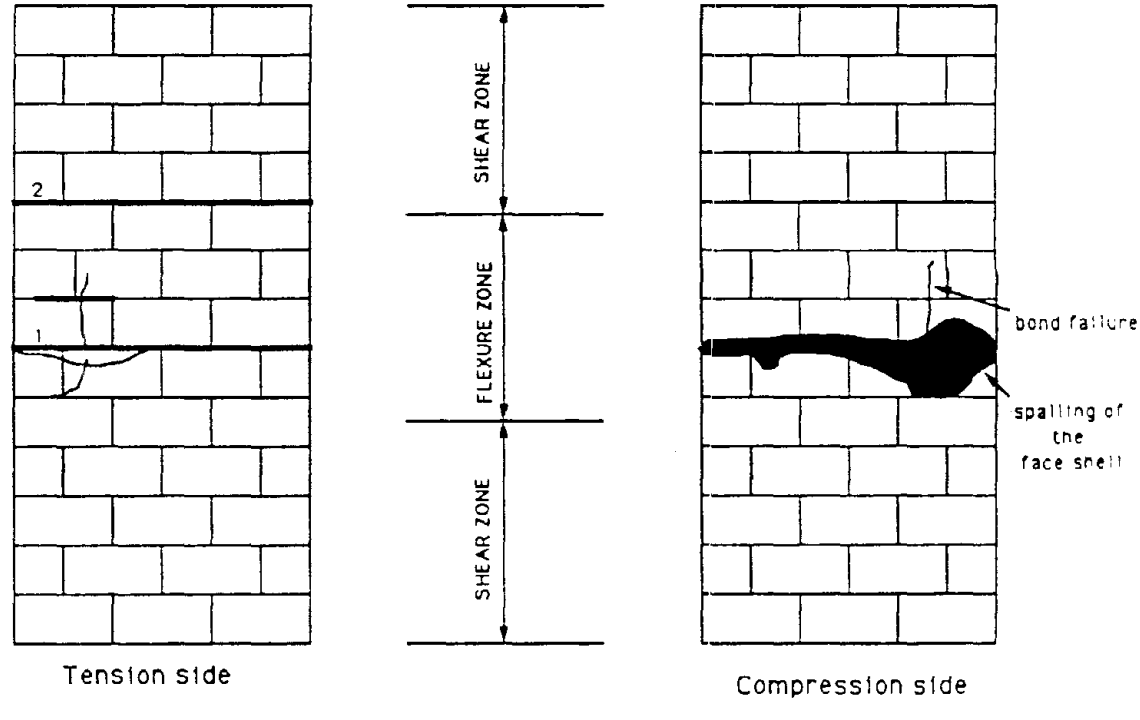

Figure 4.3 Crack Patterns of Wall W4

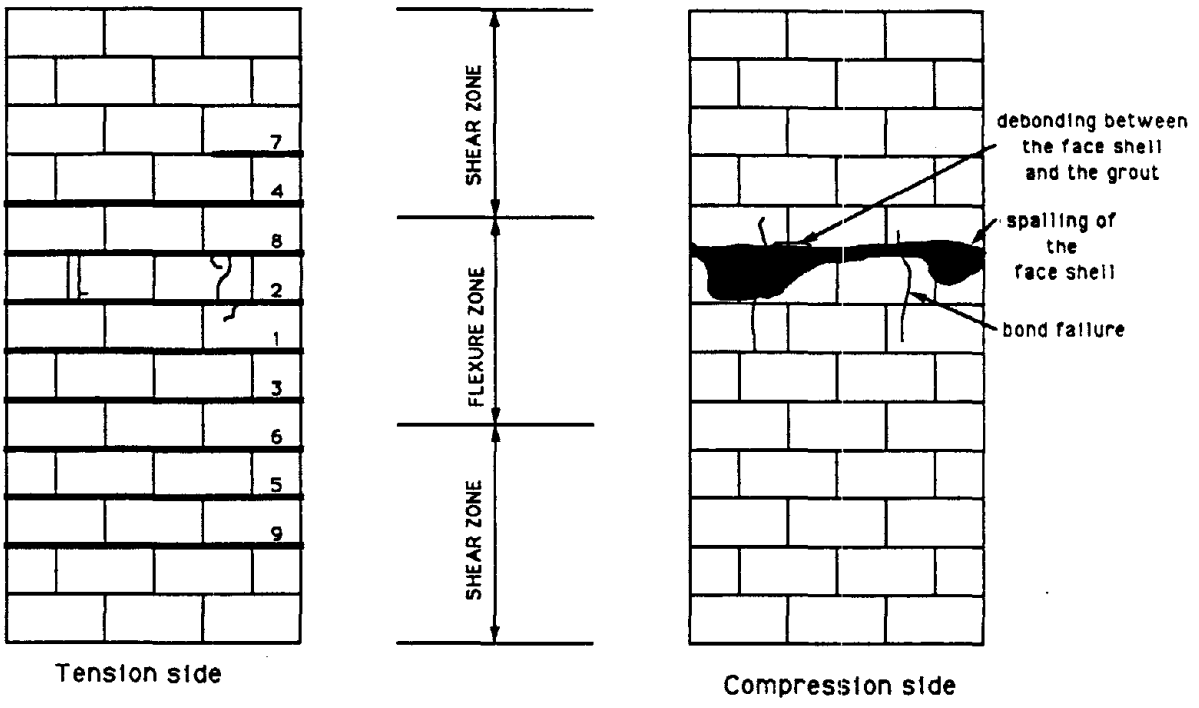

Figure 4.4 Crack Patterns of Wall W6

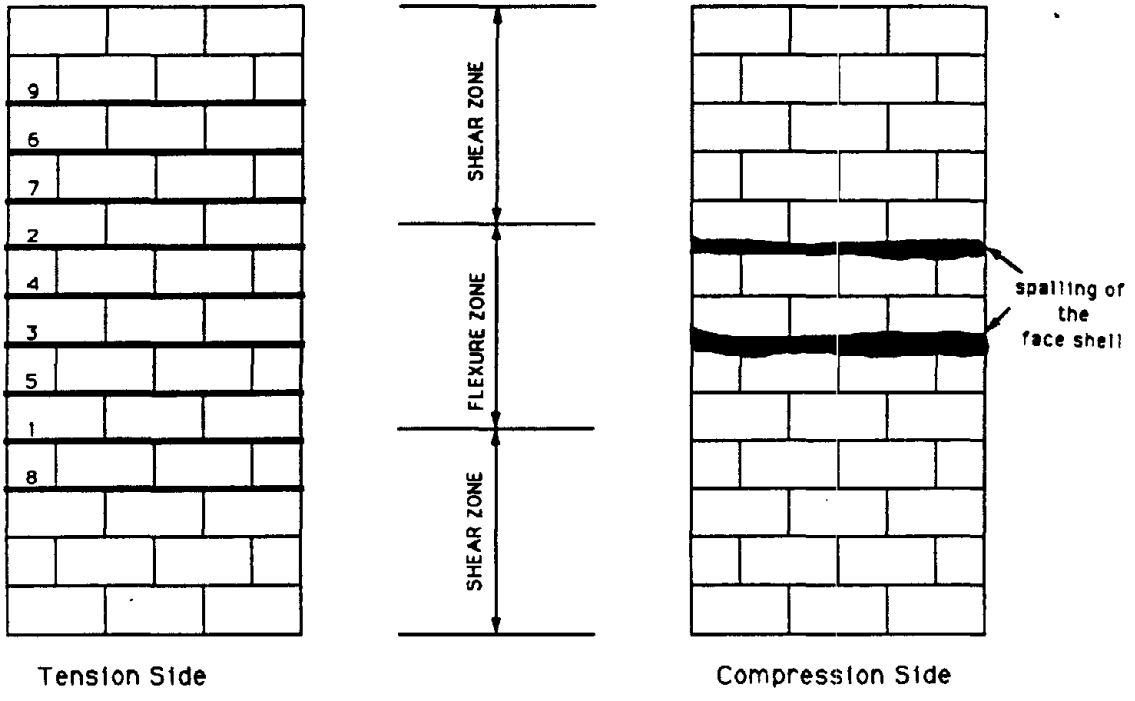

Figure 4.5 Crack Patterns of Wall W8

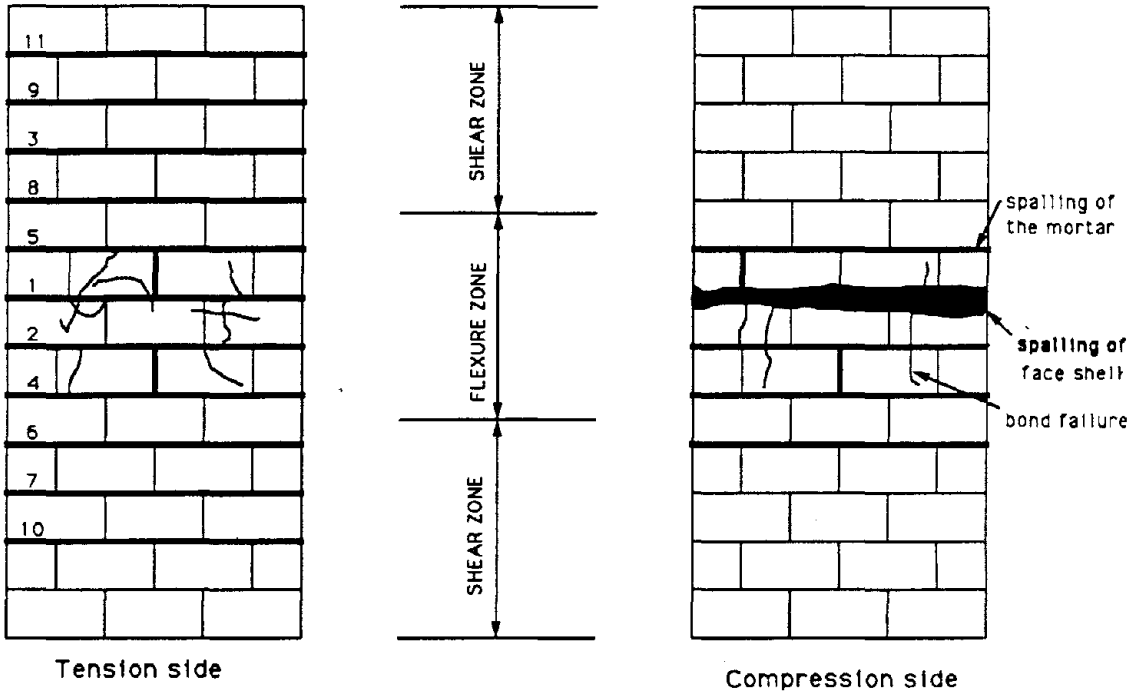

Figure 4.6 Crack Patterns of Wall W10

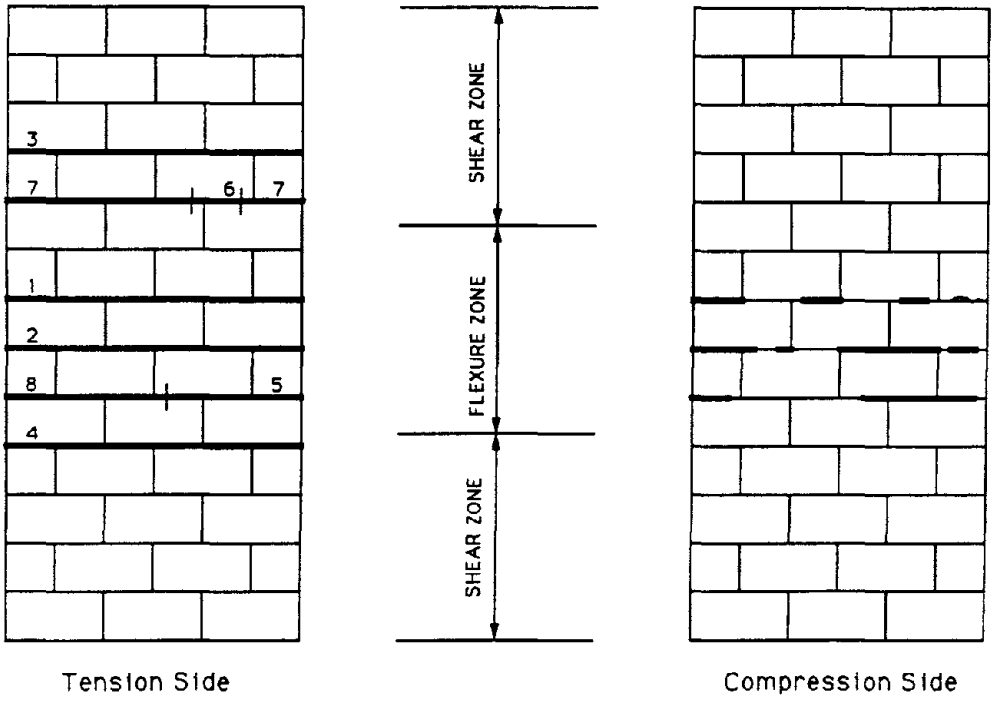

Figure 4.7 Crack Patterns of Wall W12

Figure 4.8 Spalling of Faceshell

Figure 4.9 Bond Failure at Location of Vertical Rebars

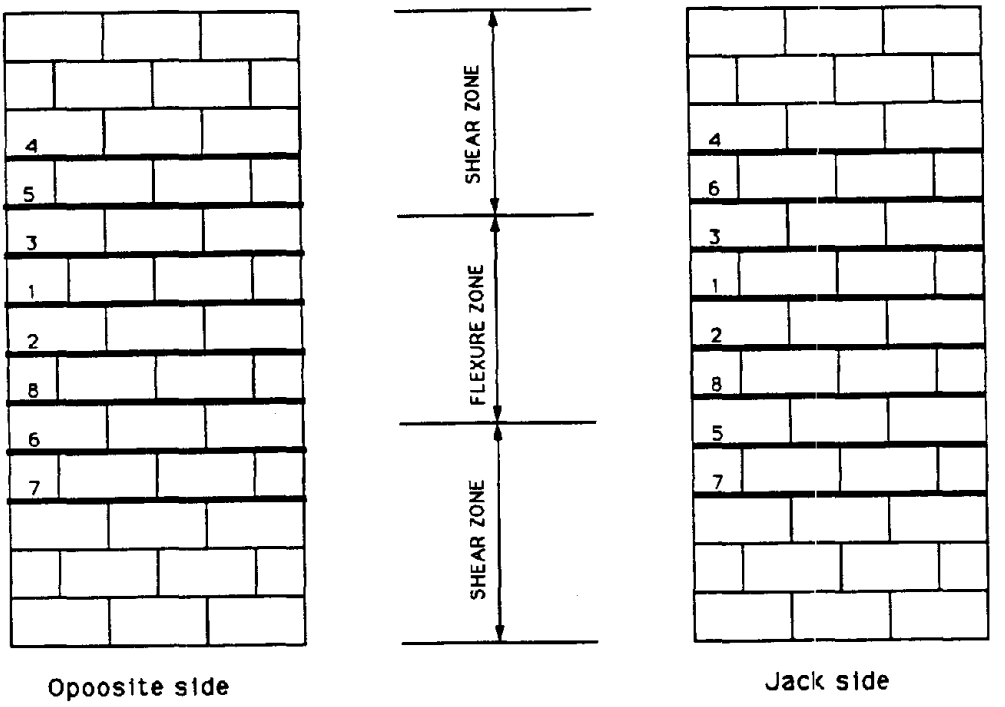

Figure 4.10 Crack Patterns of Wall W2

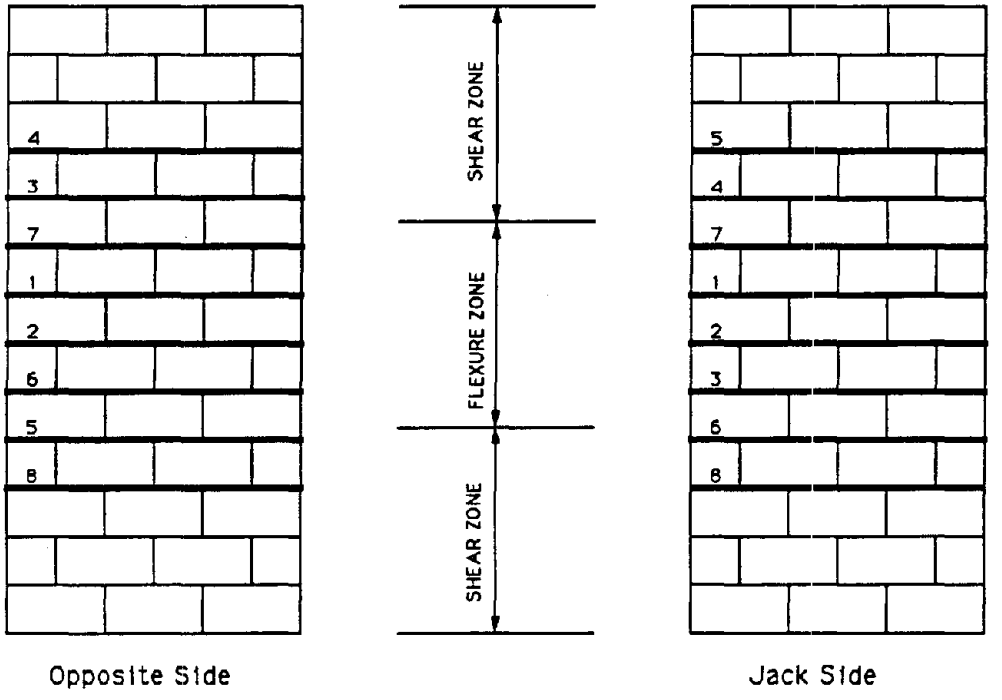

Figure 4.11 Crack Patterns of Wall W3

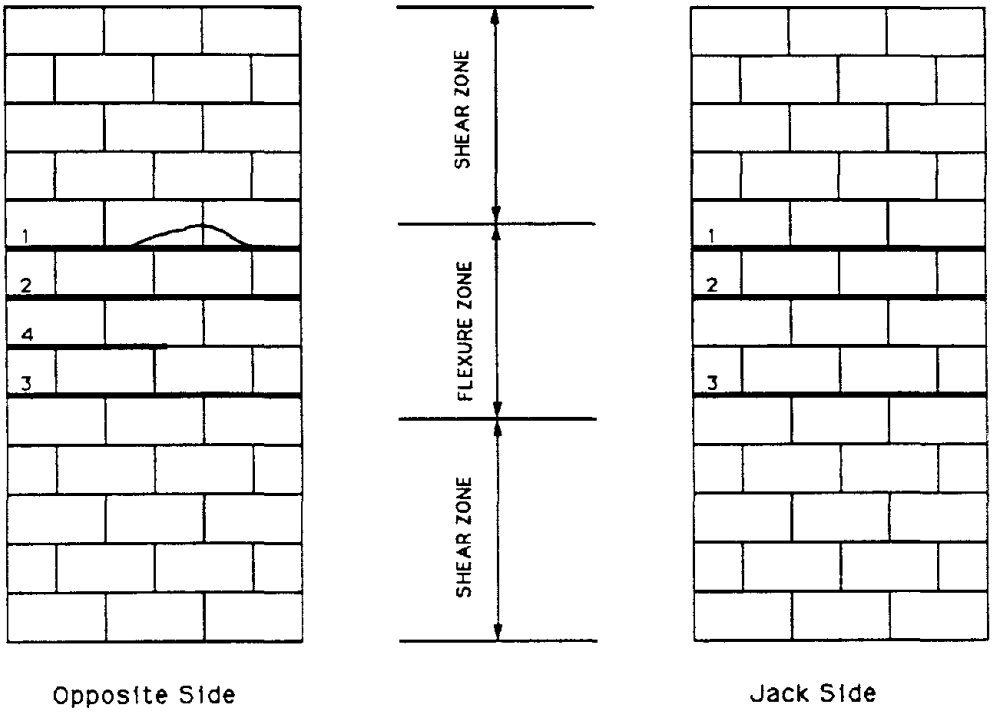

Figure 4.12 Crack Patterns of Wall W5

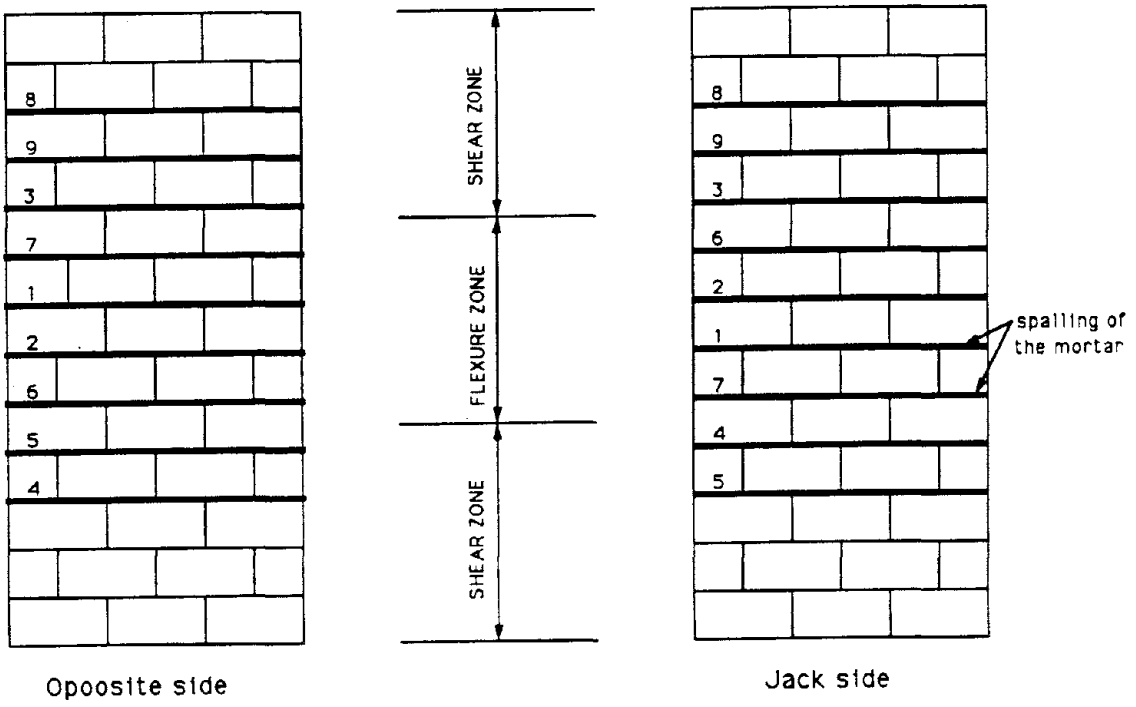

Figure 4.13 Crack Patterns of Wall W7

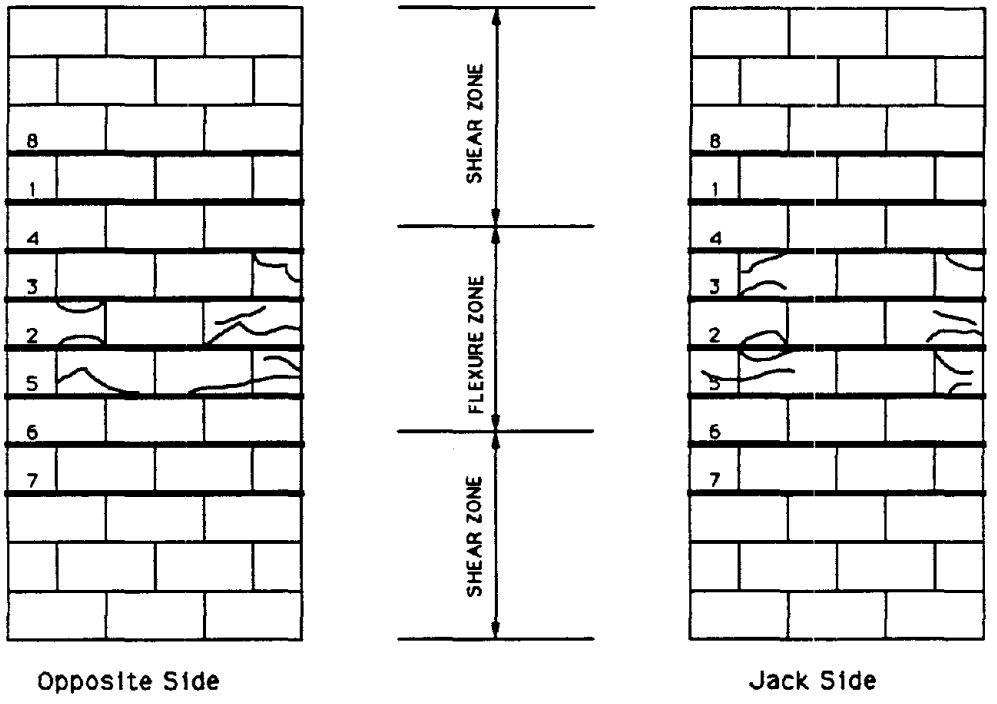

Figure 4.14 Crack Patterns of Wall W9

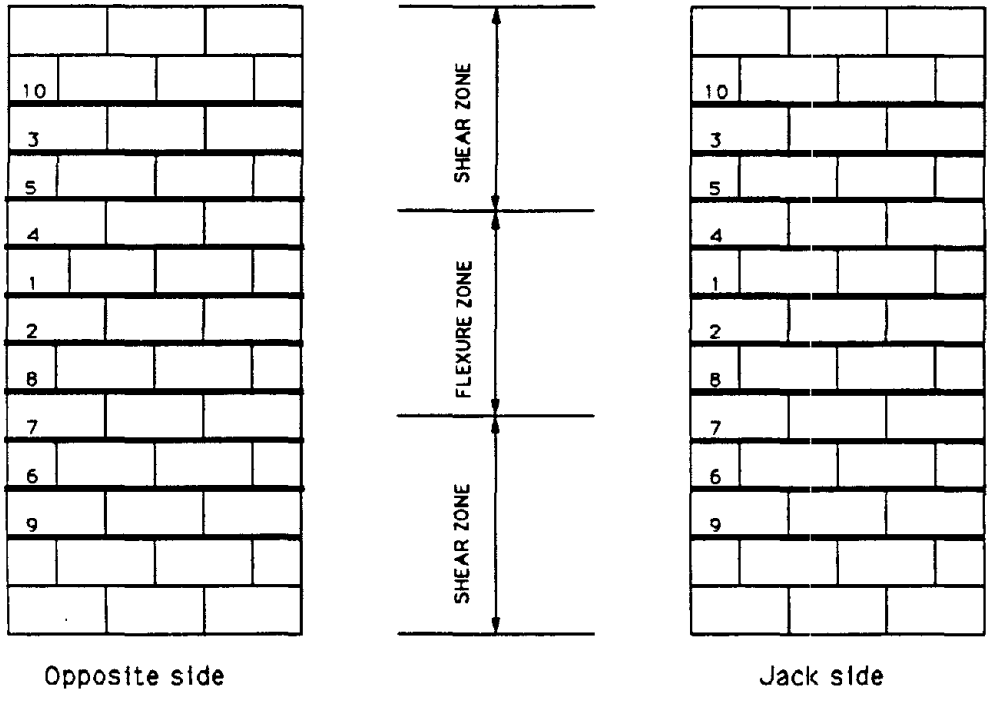

Figure 4.15 Crack Patterns of Wall W11

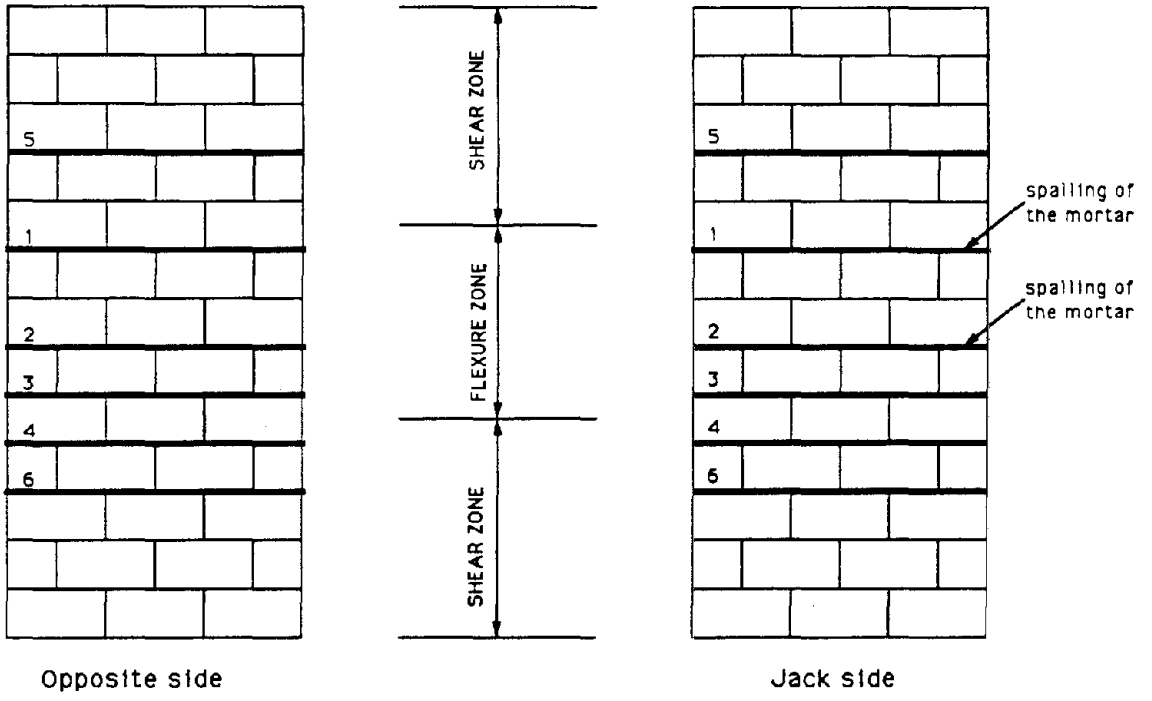

Figure 4.16 Crack Patterns of Wall W13

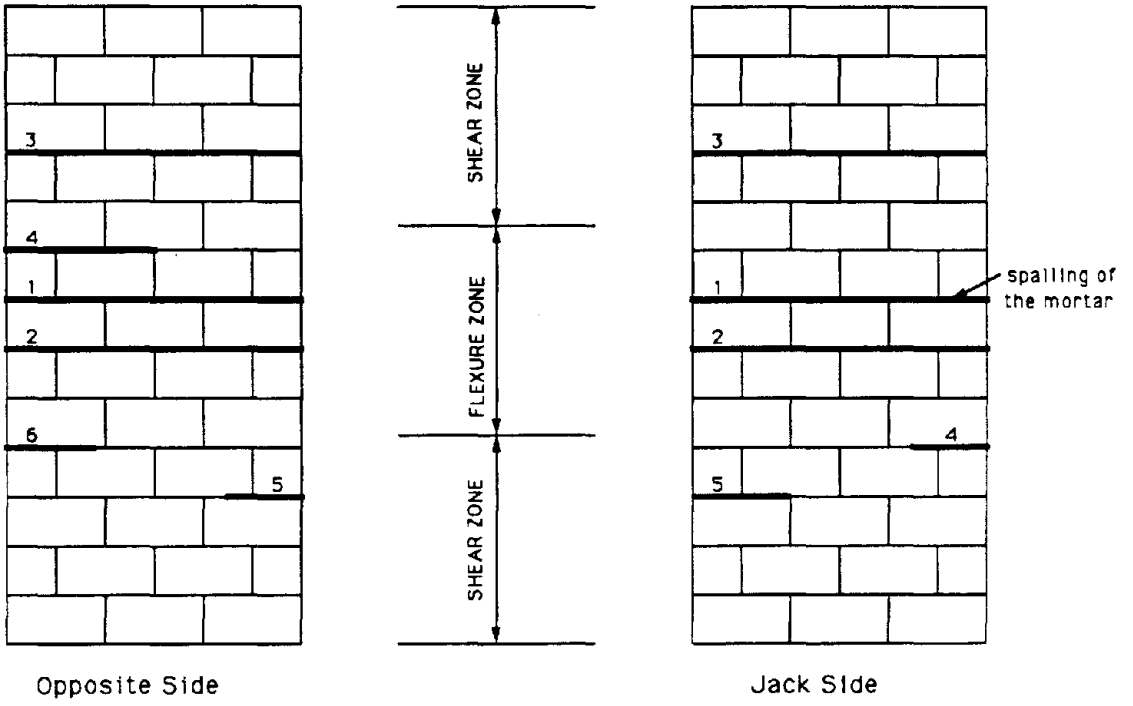

Figure 4.17 Crack Patterns of Wall W14

A comparison of the observed crack patterns for the wall panels tested monotonically and their counterpart panels tested cyclically showed that the type of loading imposed on the walls had practically no effect on the number of cracks. Similarly, the unit size had no effect on the number and distribution of cracks.

4.2 Cracking Moment

The initial cracking loads, P_{cr}, and corresponding cracking moments, M_{cr}, and maximum fiber tensile stress at first crack, f'_t, for the wall panels are summarized in Table 4.1. The initial cracking loads correspond to the first visible crack in the wall panels . As can be seen, cracking load was significantly effected by the extent of grouting (fully grouted versus partially grouted). Grouting the six core spaces in walls W1 and W2 resulted in a greater cracking moment than grouting only two core spaces at the steel locations in walls W10 and W11. This is attributed to the high tensile capacity of grout in comparison to the weak mortar bond strength (16) and to the increase in grout net cross-sectional area. However, it is to be noted that fully grouting lightly reinforced vertically spanned walls (satisfying minimum code requirements for reinforcement) could result in a cracking moment much higher than the yield moment. The wall would hinge at one crack without generating further cracks (See Figures 4.4 & 4.5).

The maximum fiber tensile stress at first crack, f'_t, was calculated using the following relationship:

$$f'_t = \frac{M_{cr} \cdot t}{2\, I_g} + \frac{W}{A}$$

Table 4.1 Experimental Results - Cracking Moments, and Maximum Tensile Stress at First Crack

Wall No.	P_{cr} (lb)	M_{cr} (lb-in)	f'_t (psi)	f'_{mt} (psi)	K[b]
W1	1830	78,200	319	2050	7.0
W2	1650	70,600	277	2050	6.1
W3	1670	71,400	281	2050	6.2
W4	1850	79,100	314	2050	6.9
W5	2300	98,300	384	2050	8.5
W6	1630	69,800	285	2050	6.3
W7	1290	55,255	220	2050	4.9
W8	1330	56,900	234	2050	5.2
W9	1170	50,000	199	2050	4.5
W10	670	28,800	141	1800[a]	3.3
W11	600	25,700	127	1800[a]	3.0
W12	1040	44,500	278	1520	7.1
W13	900	38,500	244	1520	6.3
W14	3280	140,130	308	2000	6.9

a- Average compressive strength of ungrouted and grouted prisms

b- $K = f'_t/\sqrt{f'_{mt}}$

M_{cr} = cracking moment

t = wall thickness

I_g = moment of inertia of the gross cross-section (ignoring the contribution of the transformed area of reinforcement)

W = weight of wall above the initial crack

A = gross cross-sectional area

The values of maximum fiber tensile stress at first crack, f'_t, are presented in Table 4.1 for the 14 walls. The results show that the block size has no significant effect on f'_t values. Additionally, reinforcement ratio had no effect because the transformed cross-section area of steel was very small and would not alter neither the distance from neutral axis to the extreme fiber in tension nor the moment of inertia of the section. The f'_t values of fully grouted wall panels tested under monotonic load ranged from k=5.2 to k=7.1 times the square root of the maximum compressive stress of grouted masonry prisms (f'_{mt}), with an average of $6.5\sqrt{f'_{mt}}$. In the case of partially grouted wall panels, the f'_t value was k=3.3 times the square root of the average maximum compressive stress of grouted and ungrouted masonry prisms (f'_{mt}*). On the other hand, the f'_t values ranged from $4.5\sqrt{f'_{mt}}$ to $8.5\sqrt{f'_{mt}}$ for fully grouted wall panels tested under cyclic loads, with an average of $6.2\sqrt{f'_{mt}}$. This value was $3.0\sqrt{f'_{mt}}$* for partially grouted wall panels tested under cyclic loads. This indicate that the type of loading had no effect on the k value (approximately 5 percent), whereas grouting (fully grouted versus partially grouted) has a significant effect on the k value.

Comparing the f'_t values and the k values obtained from the tested wall panels to that obtained from the bond wrench test (Table 2.6) indicates that the two approaches reveal similar results and that the bond wrench test technique is an appropriate method to determine the modulus of rupture of grouted masonry.

The k values for fully grouted masonry construction obtained from the experimental test results of the wall panels or the bond wrench are much higher than the k=2.5 value specified in the UBC-88 code (16). It is to be noted, however, that the k values for partially grouted wall panels are close to the UBC specified value of 2.5. A distinction should be made in the code design provisions between the modulus of rupture of partially grouted and fully grouted masonry.

4.3 Load-Deflection Curves

4.3.1 Montonically Loaded Walls

The load-deflection relationships for masonry wall panels tested under monotonic loading are presented in Figures 4.18 through 4.23. The load-deflection-relationship of wall W12 (Figure 4.23) is not the complete curve. Due to testing equipment failure and the disruption of the data acquisition system, the peak load and ultimate displacement could not be recorded. The load- deflection curve in Figure 4.23 is, however, sufficient for comparison and analytical evaluation.

The load-deflection curves of the walls showed a distinct response to cracking of the bed joints. At the initiation of each crack (especially in the constant bending region), the load carrying capacity of the wall dropped at a fast rate to approximately 90 to 95 percent of the attained load level as can

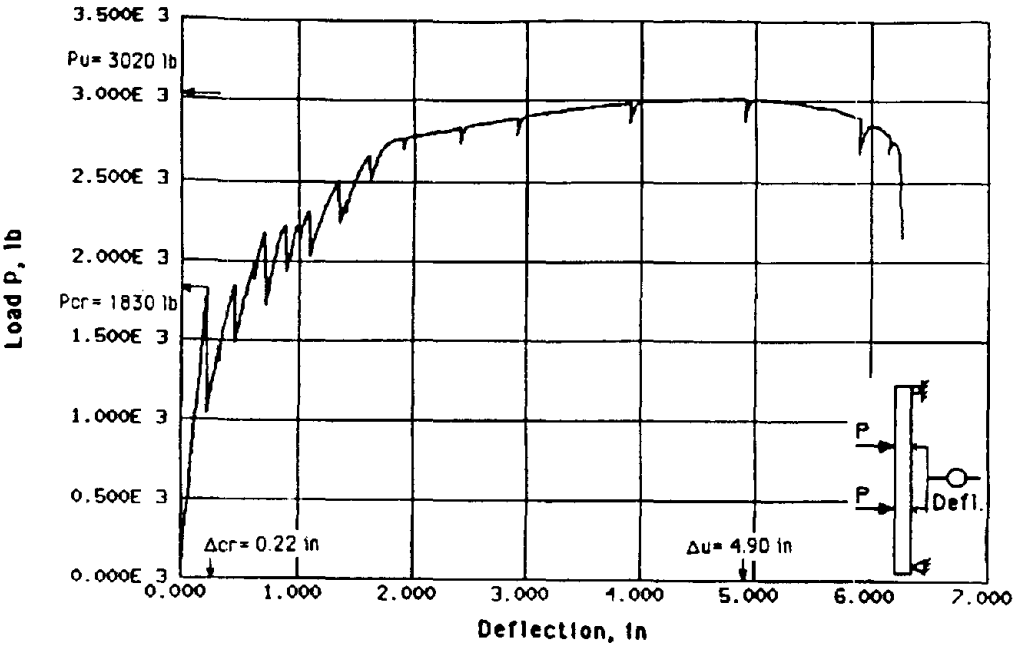

Figure 4.18 Load-Deflection Curve for Wall W1

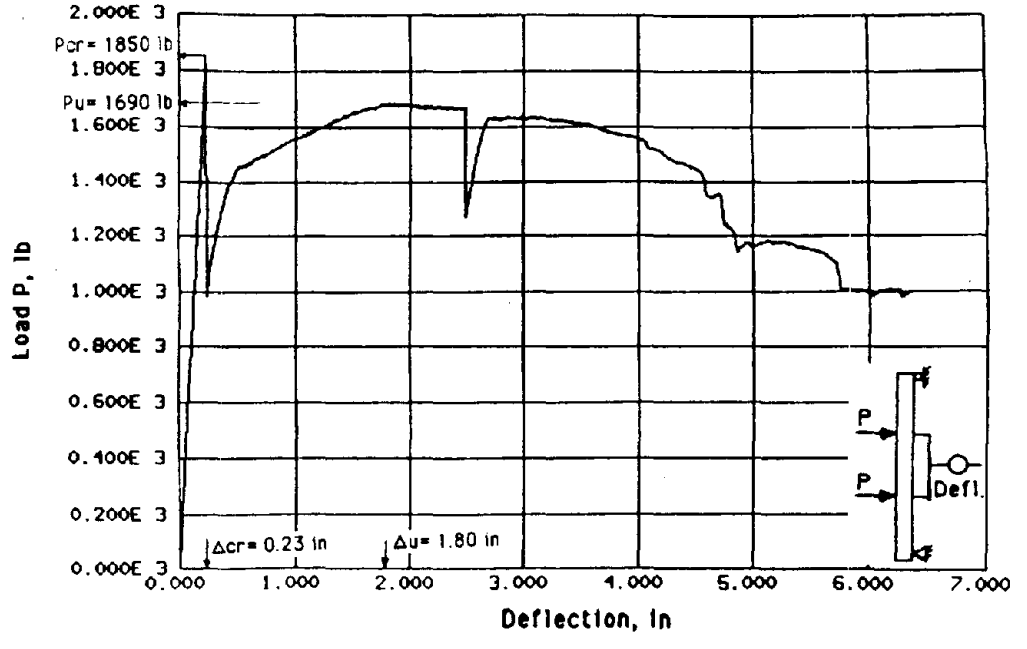

Figure 4.19 Load-Deflection Curve for Wall W4

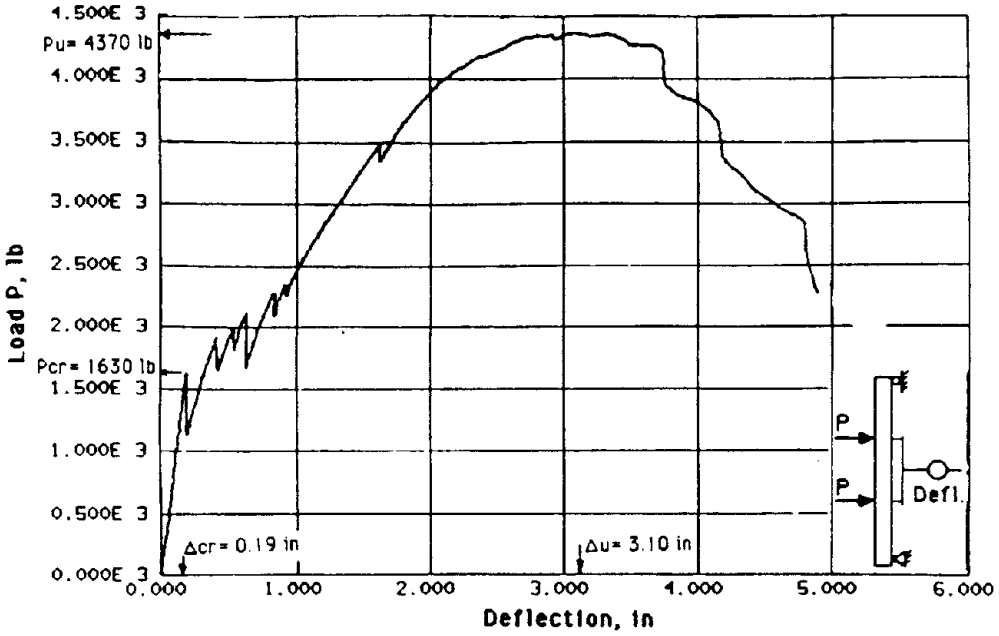

Figure 4.20 Load-Deflection Curve for Wall W6

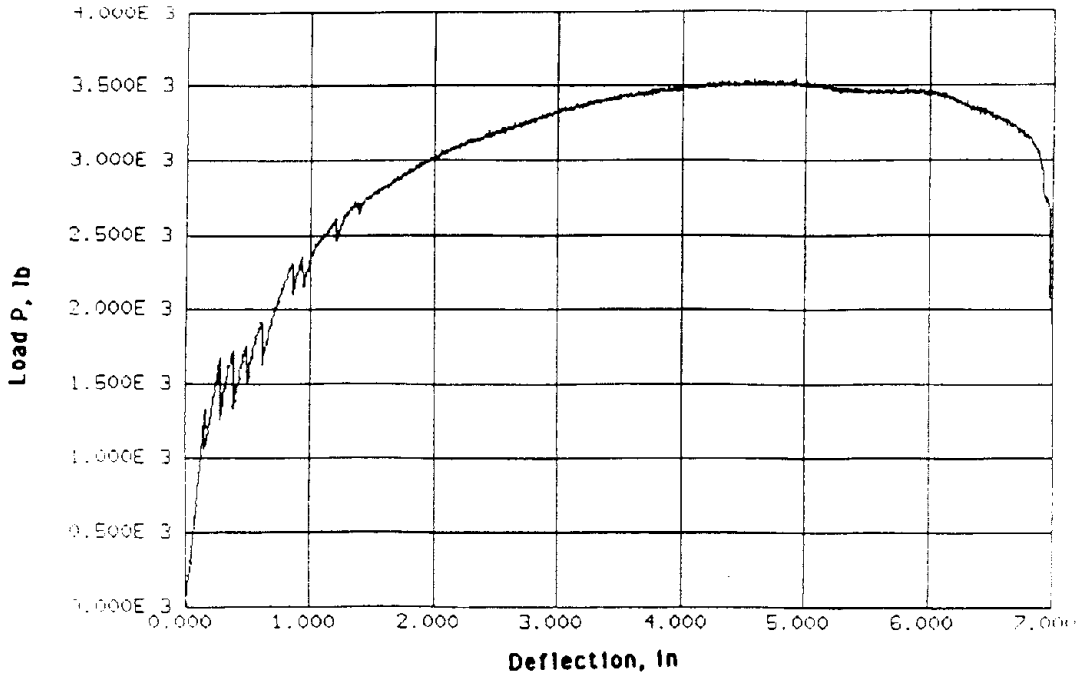

Figure 4.21 Load-Deflection Curve for Wall W8

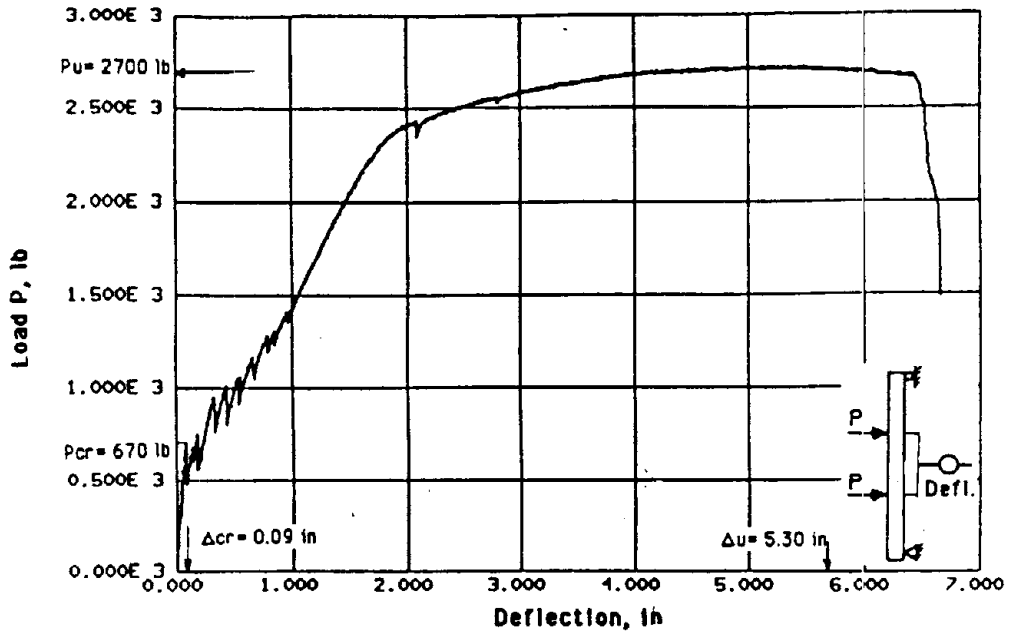

Figure 4.22 Load-Deflection Curve for Wall W10

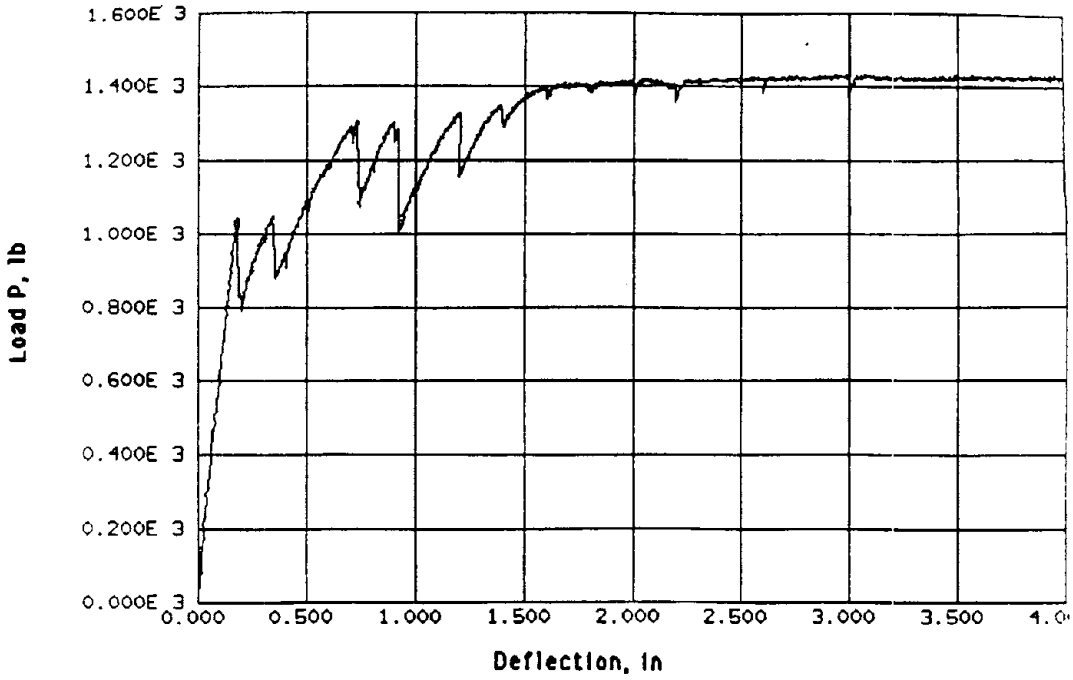

Figure 4.23 Load-Deflection Curve for Wall W12

be seen in the figures . The load capacity then started to increase to a level equals to or greater than the previous attained load level but with a reduced stiffness (slope of the curve). The drop in the load-deflection curves at the initiation of each crack is mainly attributed to the occurrence of the cracks at defined planes (block-mortar interface) and to the brittle nature of the debonding failure at the bed joints where a sudden release of energy took place (1). This sharp drop in the load-deflection curve had a dramtic impact on the response of the wall. The stiffness of the wall approached the crack section at a much faster rate with the initiation of each cracks. It is to be noted that there was a consistency between the onset of cracking and the drop in the load deflection curve.

The general shape of the load-deflection curve for the vertically spanned reinforced concrete block masonry walls was affected by the vertical reinforcement ratio, the extent of grouting (fully grouted versus partially grouted), and the location of vertical steel (centerally located versus staggered).

In comparison, the shape of the load-deflection curve for walls W1 and W4 (Figures 4.18 & 4.19) with vertical reinforcement ratio of 0.15% and 0.23%, respectively showed more inelastic deformation beyond the peak load than wall panel W6 (Figure 4.20) with higher reinforcement ratio of 0.44%. This is expected due to the fact that the lower the percentage of steel the higher is the sectional ductility of under-reinforced sections.

Comparing the load-deflection curve of the fully grouted wall W1 (Figure 4.17) with that for the partially grouted wall W10 (Figure 4.21) indicates the effect of the extent of grouting on cracked stiffness. The partially grouted wall showed earlier cracking and lower post-cracking flexural stiffness.

The wall with staggered reinforcement (W8) showed less load drop at the onset of cracking whic is attributed to the smaller cover of the reinforcement compared to centrally reinforced walls. Wall W8 showed considerable inelastic deformations (Figure 4.20) and deflection continued to increase with gradual reduction in the peak load indicating a stable behavior.

The load at yielding of the reinforcing bars and the corresponding displacement of the wall panels could not be identified directly from the shape of the load-deflection curves. The load at yielding of the reinforcing bars for the wall panels was observed from the strain measurement of the reinforcing bars. The yield load and the corresponding yield displacement are indicated in Figures 4.17 through 4.22.

4.3.2 Cyclically Loaded Walls

The hysteresis load-deflection relationships for centrally reinforced wall panels W2, W3, W5, W7, W9, W11, W13 and W14 are shown in Figures 4.23 through 4.30. As can be seen, generally, first cracking of the bed joints occurred during the up-load half (positive loading) of the first cycle in the first stage of cycles. This crack caused the load to drop and produced a decrease in the slope of the load deflection curve during unloading. In the down-load half (negative loading) of the same cycle, the load was less than the load at first crack, and the slope of the load-deflection curve was a function of the cracked section. The remaining two cycles in the first stage of cycles had essentially the same slope after cracking and they overlapped each other. This overlapping indicates a relatively stable behavior of the wall. In the subsequent stages of cycles, the

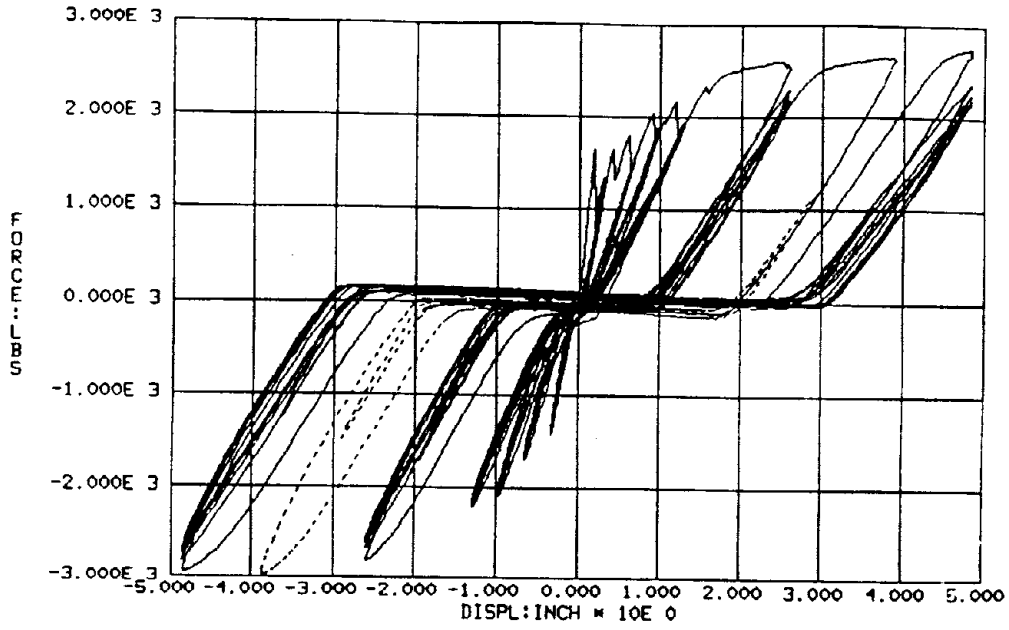

Figure 4.24 Load-Deflection Curves for Wall W2

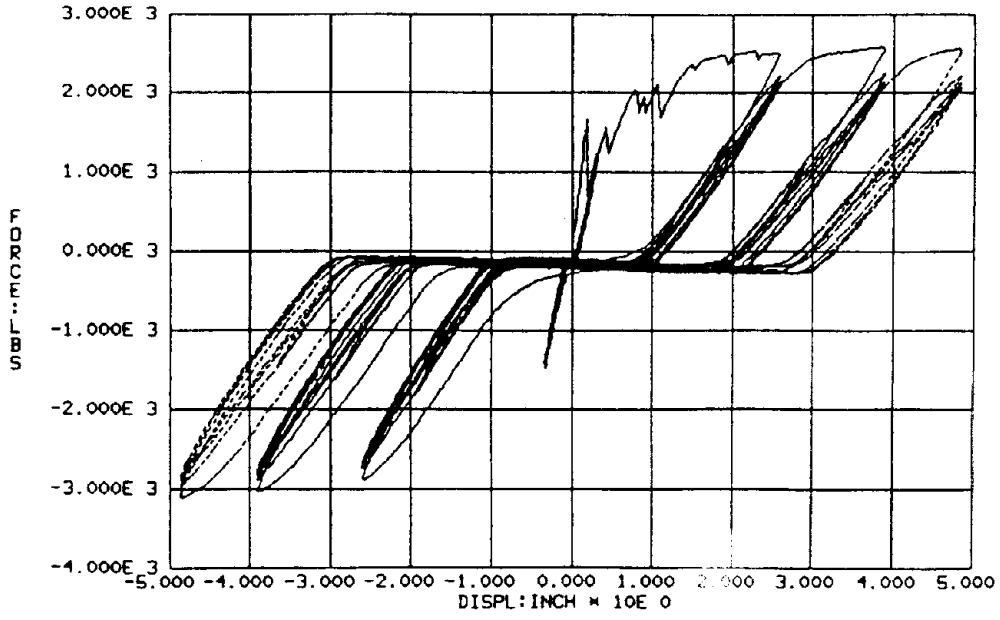

Figure 4.25 Load-Deflection Curves for Wall W3

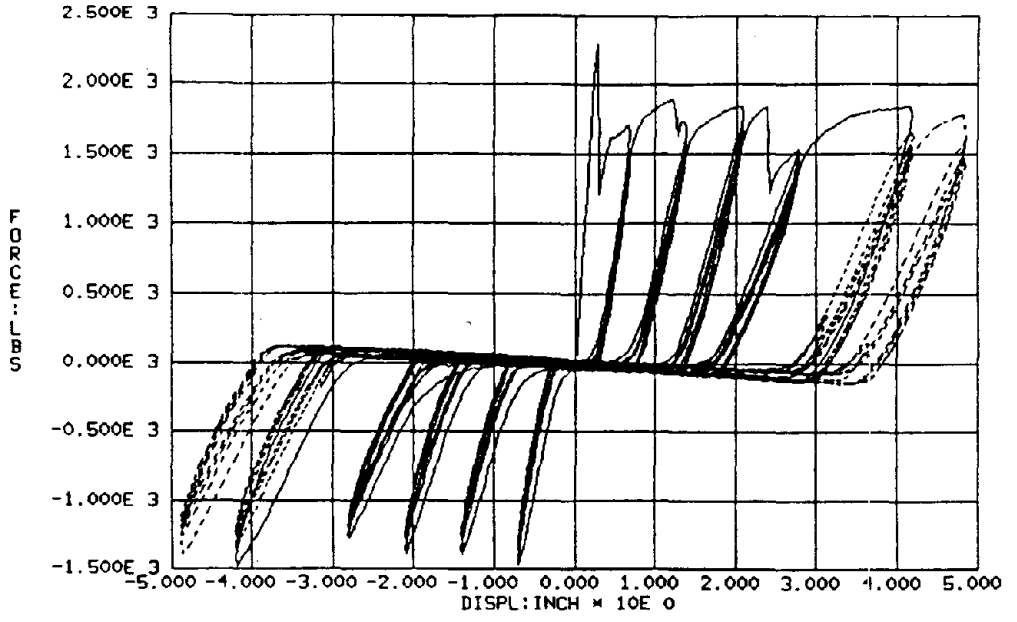

Figure 4.26 Load-Deflection Curves for W5

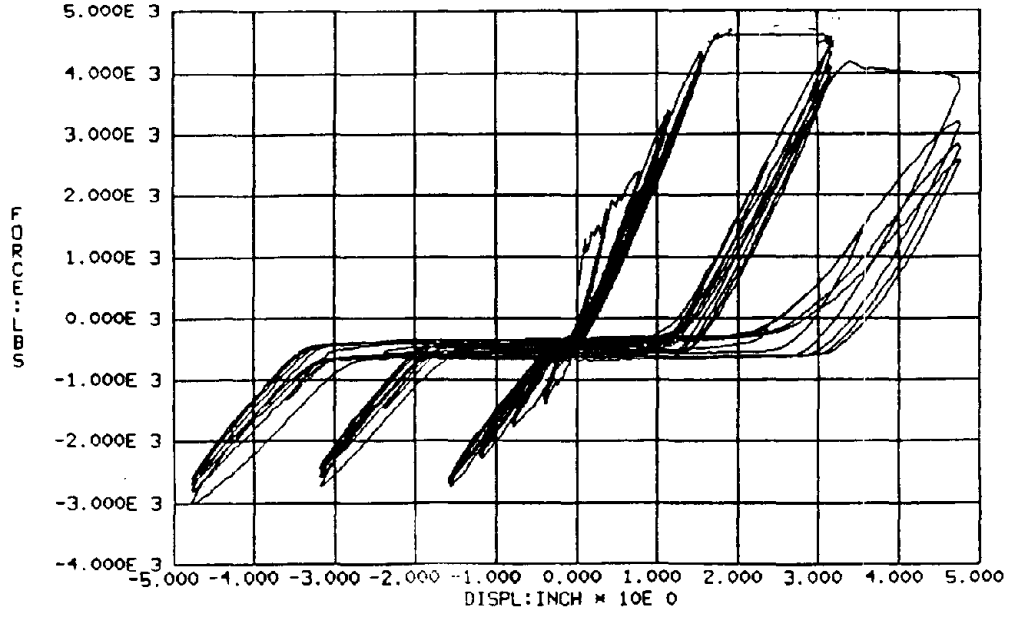

Figure 4.27 Load-Deflection Curves for Wall W7

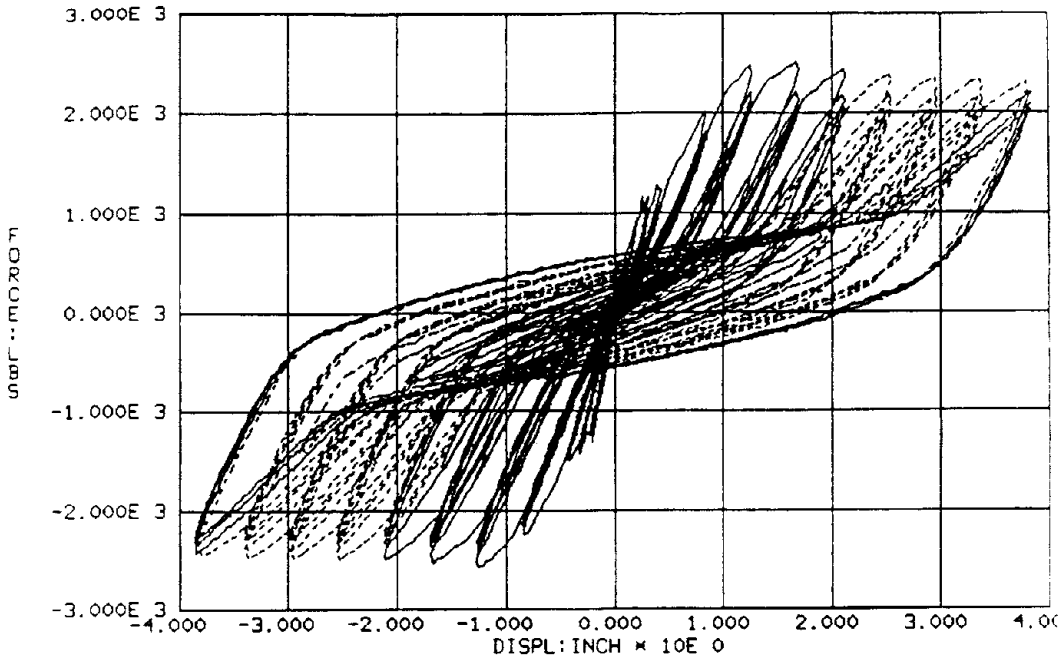

Figure 4.28 Load-Deflection Curves for Wall W9

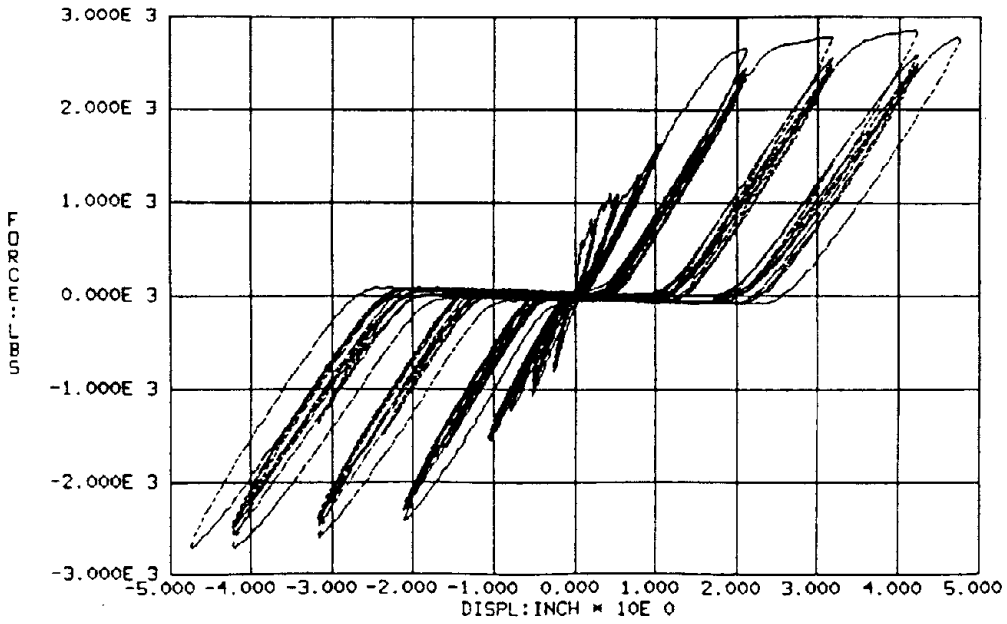

Figure 4.29 Load-Deflection Curves for Wall W11

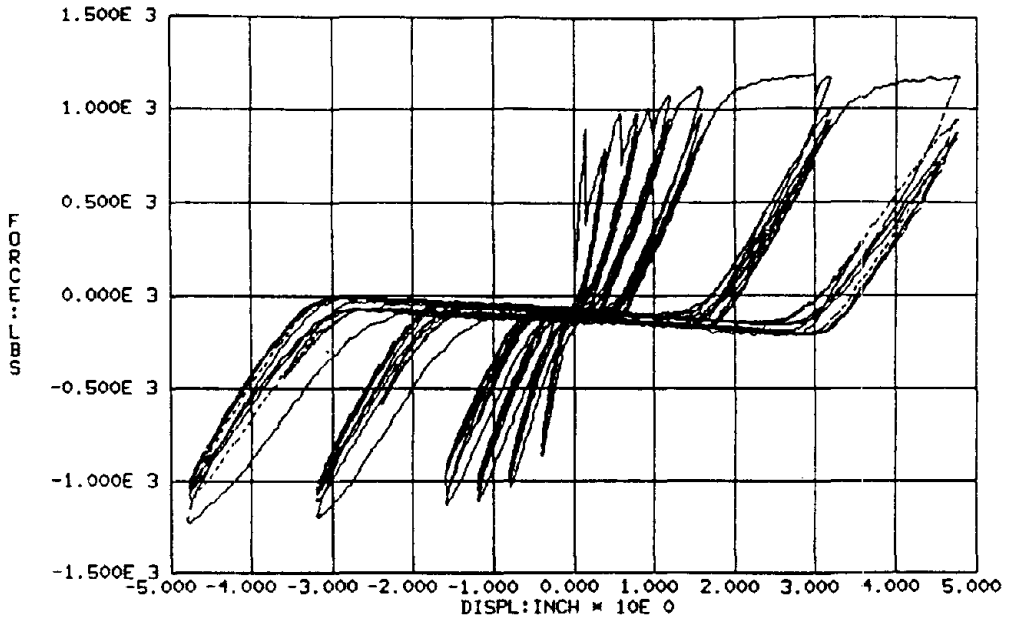

Figure 4.30 Load-Deflection Curves for Wall W13

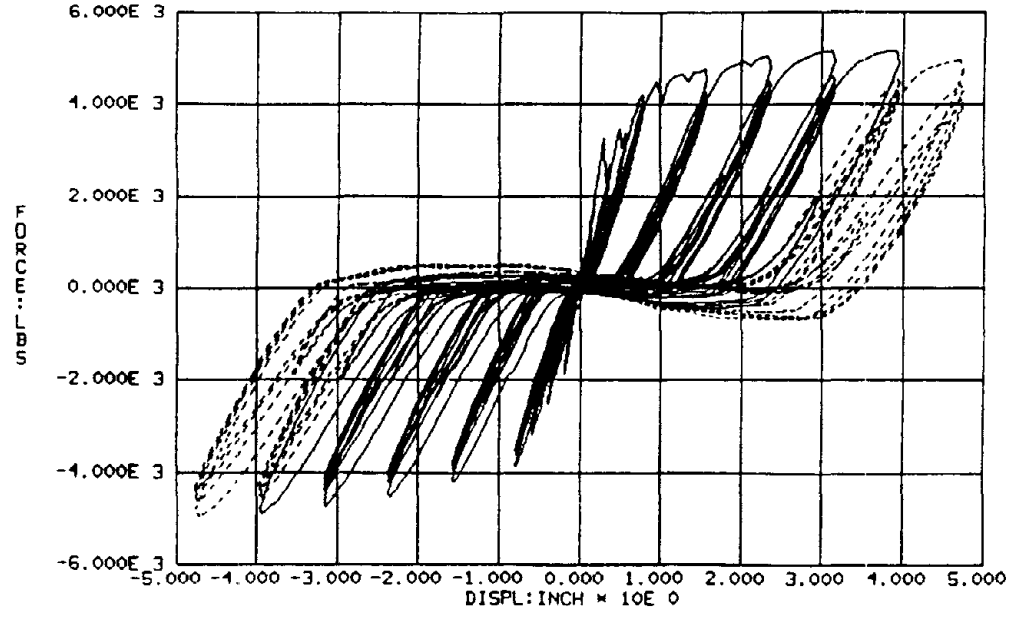

Figure 4.31 Load-Deflection Curves for Wall W14

load continued to increase and the slope of the load-deflection curve continued to change as cracking continue to occur. The load consistently dropped after the completion of the first cycles in each succeeding stage of cycles of three repeated cycles, following the initial cracking of the wall. This drop is primarily due to the widening of the crack as the displacement amplitude increased, causing the crack to extend toward the other face of the wall. It is to be noted that, due to the limited extension of the stroke of the hydraulic actuator, the ultimate load carrying capacity of the wall panels was not achieved after a successive number of stages of cycles. However, the ultimate load of wall panel W7, having a higher percentage of vertical steel, was attained after the 5th stage of cycles. Beyond the achieved peak load, the load carrying capacity of the wall panel started to decrease with each succeeding stage of cycles, See Figure 4.27.

The hysteresis loops of the load-deflection curves for all walls except wall W9 show a large narrow region of zero stiffness in the stages of cycles beyond yielding of the reinforcement. Continued loading of the wall beyond the yield point caused the reinforcing bars to elongate plastically and to produce a residual plastic deformation in the bars. Upon load reversal, a "slack" in the hysteresis loops resulted as shown by the narrow region of zero stiffness, until the cracks in the opposite face closed and the masonry assemblage was in compression with the bars again in tension. Figure 4.32 shows schematically the behavior of a cracked section during reversed deformation. With cycling at displacement levels higher than the yield displacement, large residual plastic deformation develops in the rebars and the crack opening becomes successively large. This "pinching" of the hysteresis loop has been shown to be a characteristic behavior of cenerally reinforced sections

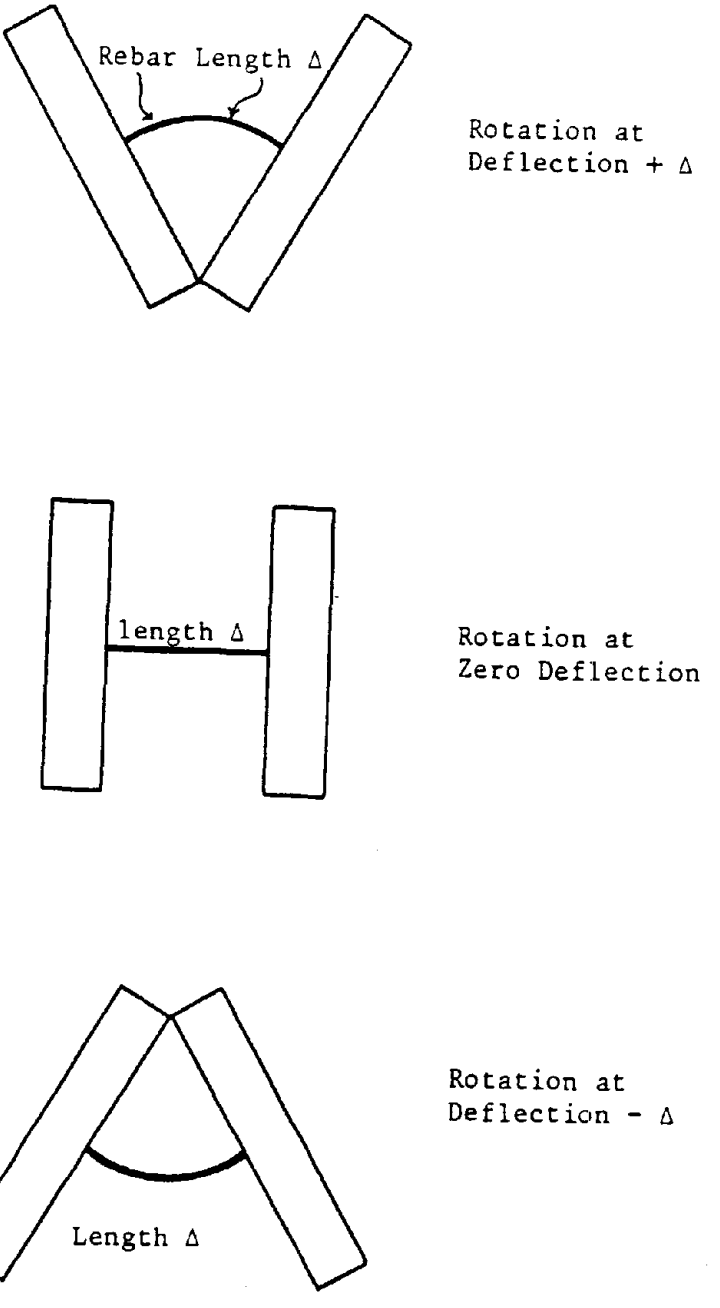

Figure 4.32 Behavior of Cracked Section During Reversed Deformation

(1,23,25). The envelope of the hysteresis loops departs considerably from the idealized parallelogram shape normally assumed for elasto-plastic bending. Loading to yield in each direction almost produces the sharp cornered shape. Nonlinear behavior of masonry in compression is the major cause for departure from straight lines. In subsequent, cycles the nonlinear behavior of steel subjected to reversed application of inelastic strain (the Bauschinger effect) is a major cause for round-off of the sharp corners. The hysteresis loops were generally symmetrical in both directions of loading. However, in the last stage of cycles beyond the yield point the hysteresis loops no longer retained a symmetry. This behavior is attributed to the crushing and spalling of the mortar at the bed joints and to the excessive elongation of the rebars. It is to note that wall panel W7 showed no symmetry in both direction of loading. This may be attributed to an error in placing the vertical rebar in the center of the section during construction, resulting in the dissimilarity of the tensile stress in the rebar as the load direction changed.

Comparing the hysteresis loops of load-deflection curves of wall panel W2 and wall panel W3, Figures 4.24 and 4.25, respectively, indicates that the loading pattern did not have a significant effect on wall strength and displacement. However, the location of vertical steel showed a dramtic effect on the hysteresis loops. Figure 4.28 shows the hysteresis loops for wall panel W9 with staggered reinforcing rebars. As can be seen, the hysteresis loops did not show the "pinching" phenomenon. The shape of the envelope of the load-deflection curves was similar to a parrallelogram shape. This indicated a higher energy absorption capability in comprasion to the centrally reinforced masonry wall panels.

From the foregoing descriptions of the hysteretic behavior an idealized envelope for analysis of walls under cyclic loads,

can be established by defining the cracking load and yield load and their corresponding displacements. A propcsed envelope of the load-deflection curves of centerally reinforced masonry walls, similar to that proposed earlier by Abboud (1) and more recently by Sveinson, et.al.(25) is shown in Figure 4.32. The limit of the maximum displacement is dictated by the expected displacement ductility ratio.

4.4 Flexural Strength

The maximum moment capacities of the wall panels are summarized in Table 4.2. The maximum moment(flexural strength) of wall W3 with the high percentage of steel (0.44%) was 45 percent higher, compared to wall W1 with the moderate percentage of steel (0.23%), while the ultimate moment of wall W2 with the low percentage of steel (0.15%) was 45 percent less. The maximum moment of the fully grouted wall panels increased as the amount of the vertical reinforcement increased which is expected for under-reinforced sections. The same conclusion was drawn by Fereig and Hamid (13) on a similar study. The flexural strength also increased with grouting. The maximum moment of the fully grouted wall panel W1 was 11 percent higher, compared to the partially grouted wall panel W4 with the same percentage of reinforcement.

Comparing the results of walls W1, W2 and W3 tested under different types of displacements indicates that type of loading (monotonic vs. cyclic) had no significant effect on the moment carrying capacity of the wall.

The theoretical values of maximum moments obtained from calculation based on the Whitney stress block method, developed for reinforced concrete flexural members, which is described in the UBC-88 Code (17) for reinforced masonry walls spanning vertically, are given in Table 4.3. The theoretical ultimate

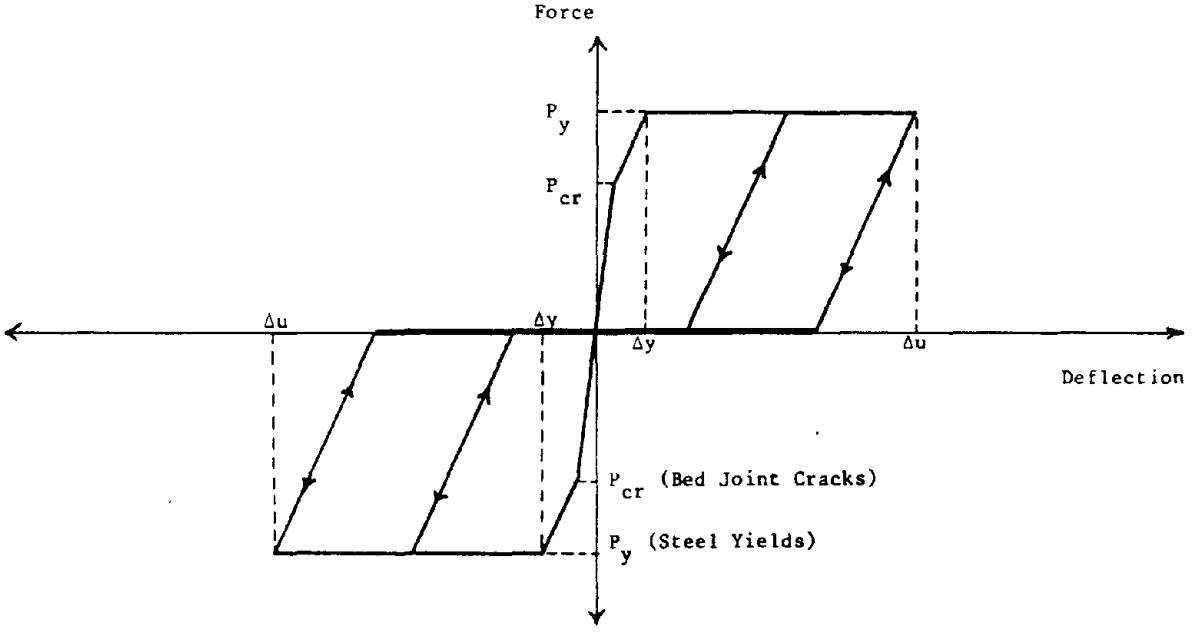

Figure 4.33 Proposed Idealized Envelope of the Hysteresis Loops of Flexural Walls

Table 4.2 Experimental and Analytical Results - Cracking Moments and Maximum Moments

Wall No.	M_{cr}[a]	M_u[b]	M_u / M_{cr}	Mu[c]	Mu (Test) / Mu (Cal)
W1	78.3	129.2	1.64	113.5	1.14
W2	70.6	125.9	1.79	105.6	1.19
W3	71.5	132.9	1.85	111.7	1.19
W4	79.2	72.3	0.92	71.0	1.02
W5	98.4	93.2	0.94	80.5	1.16
W6	69.8	187.0	2.70	185.8	1.01
W7	55.2	____[d]	____	217.8	____
W8	56.9	151.9	2.70	131.3	1.16
W9	50.1	107.4	2.13	129.3	0.83
W10	28.7	116.5	4.00	109.5	1.06
W11	25.7	123.8	4.76	103.8	1.19
W12	44.5	____[d]	____	57.0	____
W13	38.5	68.4	1.79	59.1	1.15
W14	140.4	221.4	1.59	203.7	1.09

a- Moment at first visible crack, in kip-in.

b- Maximum attained moment, in kip-in.

c- Based on Whitney stress block distribution for all walls except walls W6 $ W7 where strain compatibility analysis was used.

d- Walls were not tested to failure

moment capacity of wall W3 was not obtained by the Whitney stress block approach due to the fact that the wall is over reinforced and the Whitney stress block approach is not applicable to over reinforced members. The wall panel W3 considered over-reinforced because the percentage of vertical reinforcement ($p=A_s/bd$) is greater than the balanced ratio (p_b) calculated based on the formula specified for reinforced concrete members. The flexural strength of wall W3 was determined from analysis based on the actual stress - strain curve of masonry obtained from prisms tested under compression (14) and on strain compatibility. Sample calculations of the theoretical flexural strengths for walls W1, W4 and W6, having different percentage of steel, are contained in Appendix B. The depth of vertical steel used in the calculation was determined by actual measure of the location of the bars after the wall was tested.

The ratio of the experimental to theoretical maximum moments of the fully grouted wall panels ranged from 0.83 to 1.18. The method contained in the UBC-88 code provides a conservative approach for estimating the maximum moment capacity of the partially and fully grouted masonry walls. The only exception is wall W9 which resulted in a strength lower than predicted theoretically.This may be attributed to an error in determining the location of the reinforcing bars.

4.5 Displacement Ductility

Ductility is an important design parameter especially in high seismic areas where the structure should be capable of dissipating energy through inelastic deformations. It is important to ensure that the structure will behave in a ductile manner and is capable of sustaining large deformations at near-maximum load carrying capacity to avoid catastrophic collapse.

Ductility is commonly defined by the ratio of the displacement at maximum load to the displacement at first yielding of reinforcement. Because of the difficulty in determining the first yield of reinforcing bars, the method recommended by Priestley and Park (21) for reinforced concrete members was used in this study and is illustrated in Figure 4.34. The yield displacement(at first yielding of reinforcing bars) was determined by extrapolating a straight line extending from the origin through the load-deflection point at 75 percent of the theoretical yield load (see Appendix A), to the actual experimental maximum load.

The displacement dutility ratios (μ) determined for the wall panels are presented in Table 4.3. Because of the limited stroke of the actuator, the displacement at maximum load was not attained during the cyclic loading. Walls W2, W3, W5, W11 and W13 were pushed monotonically after the cyclic tests to attain displacement at maximum capacity. The displacement ductilities obtained experimentally for walls W5, W11 and W13 are lower bound values because these walls were not pushed monotonically after the cyclic loads to maximum capacity. The displacement dutility ratio (μ) for the 14 walls ranged from 1.79 for the wall with the highest percentage of steel to 29.4 for the wall with the lowest percentage of steel.

Comparing the displacement ductilities of walls W1 having 0.23% vertical steel with wall W7 having 0.44% vertical steel clearly indicates that the lower the percentage of steel the higher the displacement ductility. This is consistent with the fact that the lower the percentage of steel the higher the curvature ductility and consequently the member displacement ductility. It is to be noted that moderate percentage of steel (in the neighborhood of 0.2%) would result in a displacement

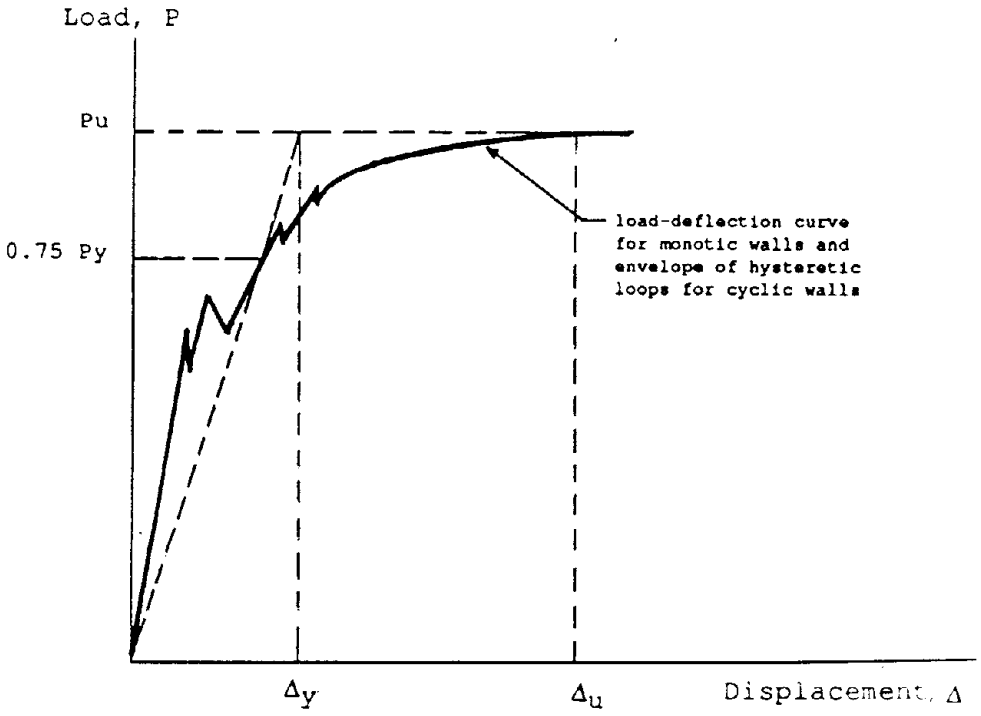

Py is the theoretical yield load

Pu is the maximum load (experimental)

Displacement ductility $\mu = \Delta_u/\Delta_y$

Figure 4.34 Definition of Displacement Ductility

Table 4.3 Experimental Results - Wall Displacements and Ductility

Wall No.	Δ_{cr}[a]	Δ_y[b]	Δ_u[c]	$\mu_e = \Delta_u/\Delta_y$
W1	0.275	0.90	4.90	5.44
W2	0.190	0.93	5.65[d]	6.08
W3	0.190	1.00	3.87[d]	3.87
W4	0.226	0.19	1.80	9.47
W5	0.280	0.27	7.94[d]	29.4
W6	0.189	1.73	3.10	1.79
W7	0.105	1.53	3.16	2.07
W8	0.170	1.28	4.64	3.63
W9	0.255	1.00	3.80	3.80
W10	0.090	1.95	5.24	2.69
W11	0.090	1.87	6.18[d]	3.33
W12	0.176	0.25	4.00	16.00
W13	0.150	1.73	8.35[d]	4.83
W14	0.304	0.50	3.93	7.80

a- Mid-Span Deflection at first crack.

b- Mid-Span Deflection at yield load as calculated from the load-deflection curve using equivalent elasto-plastic response (see Fig.4.34).

c- Deflection atmaximum load.

d- Walls were pushed monotonically after cyclic loading to attain displacement at maximum load.

e- Displacement ductility

ductility capacity greater than 4 which provides adequate energy absorption capability required in high seismic areas.

Comparing the displacement ductilities of the partially grouted walls W10 and W11 with similar fully grouted walls W1 and W2 indicates that partial grouting results in higher displacement ductilities mainly because yielding of reinforcing bars occurred at lower displacements.

Comparing the displacement ductility of wall W2 tested under cyclic pattern C1 and the displacement ductility of wall W3 tested under cyclic pattern C2 clearly indicates that the pattern of cyclic loading has an effect on wall ductility. Cyclic pattern C2 (Figure 3.8-b) representing an earthquake with large initial peak resulted in a lower displacement at maximum capacity compared to cyclic pattern C1 with a gradually increasing load history which consequently resulted in a lower displacement ductility.

5. CONCLUSIONS

Based on the experimental results and the analysis performed on the fourteen wall panels, the following conclusions are drawn:

1. The common mode of failure of the wall panels under out-of-plane flexure is a separation of the masonry units at the bed joints on the tension face and spalling of the mortar and faceshells on the compression face. Averted splitting of the faceshell occurred at the location of the vertical steel near ultimate load indicating a localized bond failure. The number of cracks generated at the bed joints on the tension face is a function of the amount of reinforcement and grouting.

2. The increase in the percentage of vertical reinforcement has no significant effect on the load at first crack, while extent of grouting dramatically affect the cracking moment and consequently the maximum extreme fiber tensile stress.

3. The percentage of vertical reinforcement significantly increased the ultimate load capacity of the wall panels. Extent of grouting has no significant effect on the wall flexural strength.

4. The Bond Wrench test technique provides an adequate estimate of wall cracking moment required for calculation of wall deflections. The maximum flexural tensile stress obtained

from the Bond Wrench test agrees very well with the values of maximum tensile stress at first crack obtained from the wall panel test results.

5. The shape of the load-deflection curve of the wall panels is influenced by the percentage of the vertical reinforcement. The strain beyond the maximum load deceased with the increase of the percentage of reinforcement. Grouting of the cells has no significant effect on the shape of the load-deflection curve.

6. The cyclic test results revealed a ductile behavior of the walls with a unique "pinched" shape of the loops for centrally reinforced walls, which departs considerably from the elasto-plastic curves commonly used for ductile materials.

7. The hysteresis loops of the wall with the staggered reinforcement did not show the pinching phenomenon and, therefore, a higher energy absorption capacity was achieved.

8. Displacement ductility ratios ranging from 1.79 for the wall with 0.44 percent of vertical steel to 29.4 for the wall with 0.15 percent of vertical steel. Percentage of vertical steel significantly affected the ductility ratio.A steel percentage less than or equal to 0.2 percent would result in a ductility ratio greater than 4 which is adequate for energy absorption in seismic areas. Staggering the reinforcement resulted in higher displacement ductility.

9. Cyclic displacement pattern affected the wall ductility. The pattern representing an earthquake with an initial high peak resulted in a lower displacement ductility than TCCMAR sequential

phase loading which has a gradually increasing load history.

10. extent of grouting had a considerable effect on wall ductility. Partially grouted walls exhibited higher displacement ductility than fully grouted walls.

11. The specified value of the modulus of rupture in the UBC-88 code agrees with that obtained from the partially grouted wall test results, while the code underestimates the modulus of rupture for fully grouted walls. It appears that code values are reasonable only for partially grouted walls.

12. The theoretical analysis based on the Whitney stress block method, suggested in the UBC-88 code estimating the maximum moment capacity of the wall panels.

REFERENCES

1. Abboud, B. E., "The Use Of Small Direct Models For Concrete Block Masonry Assemblages And Slender Reinforced Walls Under Out-Of-Plane Loads" thesis presented to Drexel University, philadelphia, Pennsylvania, in June 1987, in partial fulfillment of the requirements for the degree of Doctor of Philosophy.

2. Adham, S., Avanessian, V. and Traina, I.," Out-of-Plane Dynamic Testing of Concrete Masonry Walls,"Proceedings of the Fourth Meeting of the Joint Technical Coordinating Committee on Masonry Research, San Diego, California, October 1988.

3. American Concrete Institute/ American Society of Civil Engineers, " Building Code Requirements for Concrete Masonry Structures," ACI/ASCE Standard 530-88, 1988.

4. American Society for Testing and Materials 1984 Annual Standards, Section 1, Vol. 01.04, Philadelphia, PA., 1984.

5. American Society for Testing and Materials 1984 Annual Standards, Section 4, Vol. 04.05, Philadelphia, PA.,1984.

6. Andersen, D.L., Nathan, N.D., Cherry, S. and Cajer, R.B., "Seismic Design of Reinforced Concrete Masonry Walls," Proceedings of the Second Canadian Masonry Symposium, Ottawa, Canada, June 1980.

7. Annonymous, "Test Report on Slender Walls," Report of the Task Committee on Slender Walls, Edited by J.W. Athey, ACI,

Southern California Chapter, and the Structural Engineers Association of Southern California, Feb. 1980-Sept. 1982, Los Angeles, CA.

8. Blume, J., Newmark, N. and Corning,L.,Design of Multistory Reinforced Concrete Buildings for Earthquake Motions, Portland cement ssociation, Skokie, Illinios, 1961

9. Cajdert, A. and Losberg, A., " Laterally Loaded Light Expanded Clay Block Masonry - The Effect of Reinforcement in Horizontal Joints," The 3rd International Brick Masonry Conference, Essen,April 1973.

10. Cajdert, A., "Laterally Loaded Masonry Walls," Ph.D. Thesis, Chalmers University of Technology, Goteborg, Sweden, 1980.

11. Catherine Chia, "Flexural Behavior of Joint Reinforcement Block Masonry Walls," Thesis presented to Drexel University, Philadelphia, Pennsylvania, in June 1987, in partial fulfillment of the requirements for the degree of the Master of Science in Civil Engineering.

12. Cranston, W.B. and Roberts, J.J., "The Structural Behavior of Concrete Masonry- Reinforced and Unreinforced," Proceedings of the Journal of the Structural Engineer, No. 11, Volume 54,London, England, Nov. 1976, PP. 423-436

13. Dickey, W.L. and Mackintosh, A., "Results of Variation of "b" or Effective Width In Flexural Concrete Block Panels," Masonry Institute of America, L.A., 1971.

14. Fereig S. M., Hamid A. A., "Flexural Strength of Reinforced Block Masonry Walls", Proceedings of the Fouth North

American Masonry Conference, California, August 1987.

15. Hamid, A., Assis, G. and Harris G. " Material Properties of Grouted Block Masonry Under Compression " , Proceedings of the Third Meeting of Joint Technical Coordinating Committee for Masonry Research, Tomamu, Japan, Oct. 15-17, 1987.

16. Hamid, A. A., and Drysdale, R. G., "Flexural Tensile Strength of Concrete Block Masonry", Journal of Structural Engineering, ASCE, New York, Vol. 114, No. 1, January 1988.

17. International Conference of Building Officials, "Masonry Code and Specifications," Uniform Building Code, Chapter 24, Whittier, California, 1988.

18. Newmark, N.M.," Current Trends in the Seismic Analysis and Design of High-Rise Structures," Chapter 16, Earthquake Engineering, Edited by R.L. Wiegel, McGraw-Hill, 1970

19. Noland J. L., "U.S.- Japan Coordinated Program for Masonry Building Research," Proceedings of the 4th Canadian Masonry Syposium, 1986, Vol. 2, Fredericton, N.B.

20. Omote, Y., Mayes, R., Chen, S. and Clough, R., "A Literature Survey Transverse Strength of Masonry Walls", EERC Report No. UCB/EERC-77/07, College of Engineering, University of California, Berkeley, California, March, 1977.

21. Priestley, M.J.N. and Park, R., "Strength and Ductility of Concrete Bridge Columns Under Seismic Loading," Structural Journal, ACI, Vol. 84, No. 1, January-February 1987, pp. 61-76.

APPENDIX A

SAMPLE FLEXURAL STRENGTH CALCULATIONS

The theoretical analysis of the wall panels based on Whitney Stress Block method, developed for reinforced concrete flexural members, suggested in the UBC code for reinforced masonry walls spanning vertically are presented in this Appendix. The analysis is also made based on strain compatibility and assuming a triangular stress distribution. The analysis for the wall panels was also determined based on the actual stress-strain curves of the masonry and steel and on strain compatibility.

WALL W1 6PLFG5M

Data:

-Masonry Properties:
  f'm =2,050 psi
  Em = 1,944,000 psi
-Steel Properties
  Es = 25,217,000 psi
  fy = 66,800 psi
  es = fy/Es =0.00265
  As = 2# 5 = 0.62 in^2
-Wall Dimension (Measured)
  b=47.438 in
  t= 5.625 in
  d= 2.930 in

Yield Load Calculation

f'm = 2,050 psi
Em = 1,944,000 psi
fy = 66,800 psi
As = 0.62 in^2

22. Amrhein, J., Reinforced Masonry Engineering Handbook, , 4th edition, Masonry Institute of America, Los Angeles, California, 1988

23. Scrivener, J.C., "Reinforced Masonry- Seismic Behavior and Design," Bulletin of the New Zealand Society for Earthquake Engineering, Vol.5, December 1972.

24. Schneider, R.R. and Dickey, W.L., Reinforced Masonry Design, Prentice-Hall, Inc, Englewood Cliffs, N.J., 1980.

25. Sveinsson, B., Kelly, T., Mayes,R. and Jones, L., " Out-of-Plane Response of Masonry Walls to Seismic Loads," Proceedings of the Fourth North American Masonry Conference, University of California, Los Angeles, August 1987.

26. Tadros, M.," Flexural Behavior of Reinforced Concrete Masonry Members," Proceedings of the Third North American Masonry Conference, University of California, Los Angeles, June 1985

27. Turkstra, C., Ojinaga, J. and Shyu, E., " Development of a Limit State Masonry Code," Proceedings of the Third Canadian Masonry Symposium, Edmonton, Alberta, June 1983.

b = 47.438 in
d = 2.930 in

From strain compatibility and equilibrium :

$k = \sqrt{(p\ n)^2 + (2\ p\ n)} - p\ n = 0.286$
Where p = As/bd = 0.00446
n = Es / Em = 13
J = 1 - (k/3) = 0.905
My = As fy (Jd) = 109,688 lb-in
Py = My / 42.75 = 2,566 lb

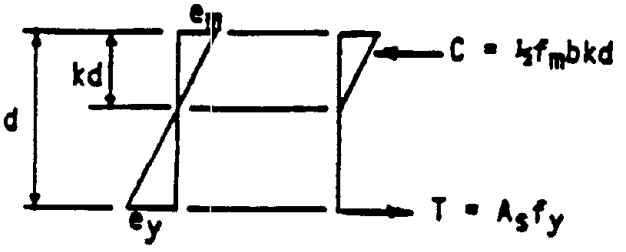

Ultimate Load Calculation (based on Whitney block approach)

C = T ----> 0.85 f'm b a = As fy
a = As fy / 0.85 f'm b = 0.501 in
Mu = As fy (d-a/2) = 110,939 lb-in
Pu = Mu / 42.75 = 2,595 lb

Ulimate Load Calculation (based on trianglar stress distribution and strain compatibility.

f'm= 2,050 psi
Em =1,944,000 psi
fy = 66,800 psi
ey = 0.00265
As = 0.620 in^2
b =47.438 in
d = 2.930 in

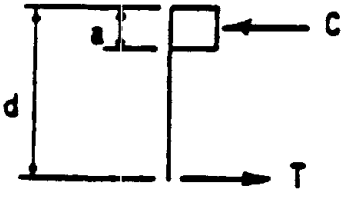

Equilibrium : C = T
0.5 f'm b (kd) = As fy
kd = As fy / 0.5 f'm b
kd = 0.851
Mu = As fy (d - kd/3) = 109,558 lb-in
Pu = Mu / 42.75 =2,563 lb

Strain compatibility: ey / (d-kd) = em / kd
em = ey (kd) / (d-kd)
= 0.00108 in/in < 0.003 in/in

Analysis based on the actual stress-strain curve

Calculation of the yielding moment

assume em = 0.0020
kd/d-kd = em/es
---->kd = 1.26 in.

Compression forces :
C2 = (2x 2050/3) 1.26 x 47.438 = 81688 lb

Tension forces :
T = As fy = 0.62x66800 = 41416 lb << C

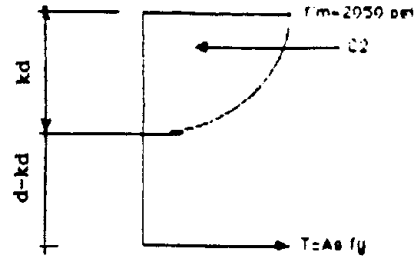

by iteration we obtain em = 0.0011
----> kd = 0.859 in.
fm = 1520 psi
C = 41300 lb = T

The yielding moment :
My = T (jd)
= 41416 (2.61) = 108008 lb-in.
Py = 108008/42.75 = 2526 lb

Calculation of the Ultimate Moment

assume es = 0.0035 > ey

kd/d-kd = 0.0030/0.0035
----> kd = 1.35 in.
e_2 =2 kd /3= 0.90 in.
e_1 = kd-e2 = 0.45 in.

compression forces:
C1 = (2050+1640)x0.5x0.45x47.438 = 39385 lb
C2 = (2x2050/3)x0.90x47.438 = 58349 lb
C =C1+C2 = 97734 lb > T

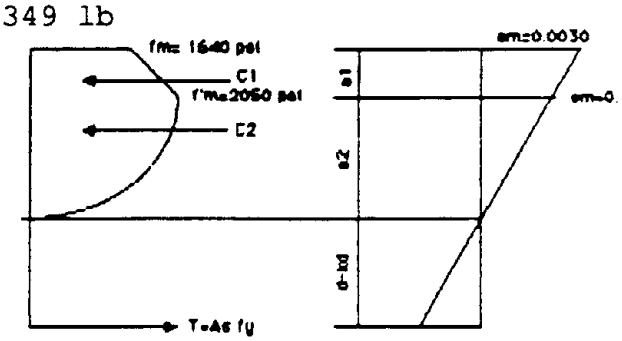

By iteration we obtain es = 0.0125
kd = 0.567 in.
e_2 = 0.377 in.
e_1 = 0.190 in.
C1 = 16629 lb
C2 = 24441 lb
C = 41070 lb = T (O.K)

Mu = C1 (0.467) + C2 (0.237) + T (2.363)
= 16629(0.467) + 24441 (0.237) + 41070 (2.363)
= 110607 lb
Pu = 110607/ 42.75 = 2587 lb

WALL W4 6PLFG4M

Data:

-Masonry Properties:
f'm =2,050 psi
Em =948 f'm = 1,944,000 psi
-Steel Properties
Es = 26,190,000 psi
fy = 55,000 psi
es = fy/Es =0.0021 in/in
As = 2#4 = 0.40 in^2
-Wall Dimension (Measured)
b=47.75 in
t= 5.67 in
d= 2.83 in

Yield Load Calculation

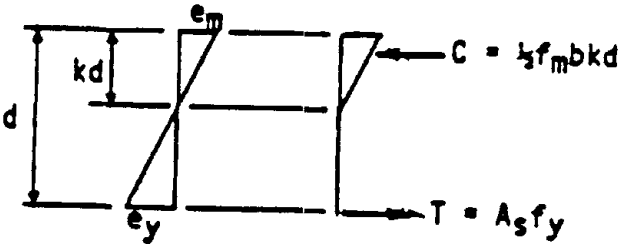

f'm = 2,050 psi
Em = 1,944,000 psi
fy = 55,000 psi
As = 0.40 in^2
b = 47.75 in
d = 2.830 in

From strain compatibility and equilibrium :

$k = \sqrt{(p\,n)^2 + (2\,p\,n)} - p\,n = 0.247$
Where p = As/bd = 0.0030
n = Es / Em = 13.5
J = 1 - (k/3) = 0.918
My = As fy (Jd) = 53,153 lb-in
Py = My / 42.75 = 1,337 lb

Ultimate Load Calculation (based on Whitney block approach)

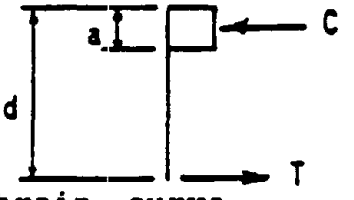

C = T ----> 0.85 f'm b a = As fy
a = As fy / 0.85 f'm b = 0.266 in
Mu = As fy (d-a/2) = 59,333 lb-in
Pu = Mu / 42.75 = 1,388 lb

Analysis based on the actual stress-strain curve

Calculation of the yielding moment

assume em = 0.0017
kd/d-kd = em/es
---->kd = 1.27 in.

At strain of 0.0017 , fm = 1890 psi

Compression forces :

C2 = (2x 1890/3) 1.27 x 47.75 = 76416 lb

Tension forces :

T = As fy = 0.40x55000 = 22000 lb << C2

by iteration we obtain em = 0.0006

----> kd = 0.629 in.

fm = 1123 psi

C = 22483 lb = T

The yielding moment :

My = T (jd)

= 22000 (2.59) = 57070 lb-in.

Py = 57070/42.75 = 1335 lb

Calculation of the Ultimate Moment :

assume es = 0.0050> ey

kd/d-kd = 0.0030/0.0050

----> kd = 1.06 in.

e_2 =2 kd /3= 0.71 in.

e_1 = kd-e2 = 0.35 in.

compression forces:

C1 = (2050+1640)x0.5x0.35x47.75 = 30834 lb

C2 = (2x2050/3)x0.71x47.75 = 46333 lb

C =C1+C2 = 77168 lb > T

By iteration we obtain es = 0.0250

kd = 0.30 in.

e_2 = 0.20 in.

e_1 = 0.10 in.

C1 = 8810 lb

C2 = 13051 lb

C = 21860 lb = T (O.K)

Mu = C1 (0.248) + C2 (0.125) + T (2.53)

= 8810(0.248) + 13051 (0.125) + 22000 (2.53)

= 59476 lb

Pu = 59476/ 42.75 = 1391 lb

WALL W6 6PLFG7M

Data:

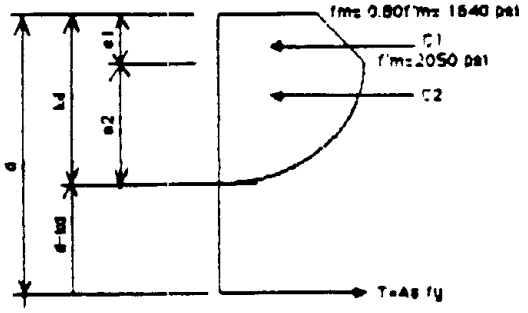

-Masonry Properties:
- f'm =2,050 psi
- Em =948 f'm = 1,944,000 psi

-Steel Properties
- Es = 27,478,000 psi
- fy = 63,200 psi
- es = fy/Es =0.00230
- As = 2#7 = 1.20 in^2

-Wall Dimension (Measured)
- b= 47.625 in
- t= 5.625 in
- d= 2.840 in

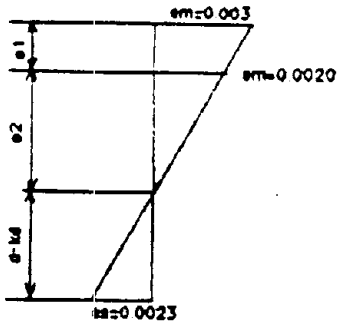

Balanced Condition

kd/d-kd = em/ey
kd/2.84-kd = 0.0030/0.0023
----> kd = 1.61 in.
e_2 = 0.0020x1.61/0.0030 = 1.07 in.
e_1 = 1.61-1.07 = 0.54 in.

The compression forces :
C1 = 0.5 (1640 + 2050) 0.54 x 47.625 = 47450 lb
C2 = (2x 2050/3) 1.07 x 47.625 = 69645 lb
C = C1 + C2 = 47450 + 69645 = 117095 lb

From equilibrium :
C = T = As fy
117095 = As (63200) ----> As = 1.85 in^2
----> P_b = As/ bd
= 1.85 / 47.625 x 2.84 = 0.0137
P = 1.2/ 47.625 x 2.84 = 0.0089 < P_b
this means that the steel will reach its yield stress before the masonry reachs its ultimate stress.

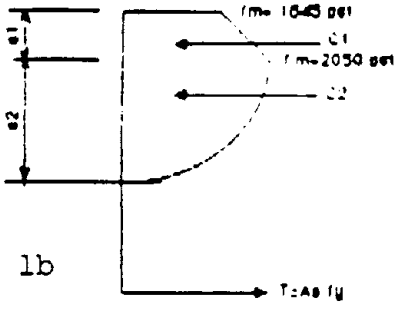

- Calculation of the yielding moment
assume em = 0.0025
----> kd = 1.48 in.
e_2 = 1.18 in.
e_1 = 0.30 in.

Compression forces :
C1 = 0.5 (1845 + 2050) 0.30 x 47.625 = 27825 lb
C2 = (2x 2050/3) 1.18 x 47.625 = 76800 lb
C = 27825 + 76800 = 104625 lb

Tension forces :
T = As fy = 1.2 x 63200 = 75840 lb < C (not O.K)

by iteration we obtain em = 0.00175
----> kd = 1.23 in.
e_2 = 1.23 in.
e_1 = 0.00 in.

the masonry stress at strain 0.00175 is fm = 1917 psi
C2 = (2 x 1917 / 3) 1.23 x 47.625 = 74864 lb = T (O.K)

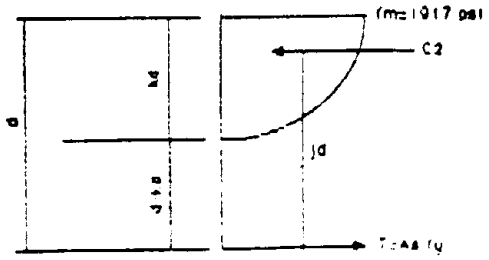

Calculation of yielding moment

My = T (jd)
= 75840 (2.38) = 180500 lb-in.
Py = 180500/42.75 = 4220 lb

Calculation of Ultimate Moment

assume es = 0.0025 > ey
kd = 1.55 in.
e_2 = 1.03 in.
e_1 = 0.52 in.
C1 = 45691 lb
C2 = 67040 lb
C = 112731 lb > T = 75840 lb

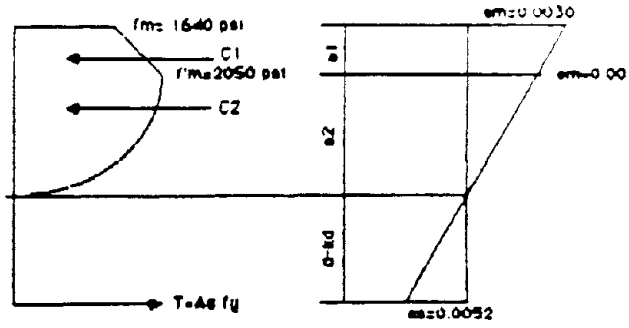

By iteration we obtain es = 0.0052
kd = 1.04 in.
e_2 = 0.69 in.
e_1 = 0.36 in.
C1 = 30754 lb
C2 = 44910 lb
C = 75664 lb = T (O.K)

Mu = C1 (0.87) + C2 (0.43) + T (1.8)
= 30754 (0.87) + 44910 (0.43) + 75840 (1.8)
= 182600 lb
Pu = 182600/ 42.75 = 4270 lb

APPENDIX B

TESTS OF REINFORCED MASONRY WALLS BUILT WITH MASONRY CEMENT MORTAR

B.1. Introduction

Masonry cement has been used for loadbearing masonry construction. Masonry cements are marketed to provide a general purpose mortar containing everything but sand and water in one bag. Therefore, fewer materials are handled and mixing is more convenient. The choice of masonry cement in place of a Portland cement and lime combination is mainly dependent on economy and conveniency at the job site.

Masonry cements usually have more air content than Portland cement and lime mortars which may result in lower bond strength. The ACI 530-88/ASCE 5-88 masonry code (3) reduces the allowable flexural tension by one-quarter when using masonry cement mortars in place of conventional Portland cement and lime mortars, regardless of type of construction (ungrouted or grouted). It is documented in the literature (1,14,16) that grouting the cores of hollow units reduces the significance of the mortar type in affecting the flexural strength of masonry.

B.2. Objective and Scope

It is the objective of the follow-up study presented herein, which is partially supported by the Portland Cement Association, to experimentally investigate the effect of mortar type on the behavior of vertically spanned reinforced block masonry walls.

Two walls built with Type S masonry cement were tested under monotonic and cyclic loading. The results are compared with those from similar walls built with Portland cement-lime mortar and tested under monotonic and cyclic loadings(walls W1 and W2, Table 3.1). This direct comparison provides the basis for assessing whether of not the use of masonry cement mortar in place of Portland cement-lime mortar would have an adverse effect on wall behavior, mainly; cracking pattern, cracking load (modulus of rupture), deflection under service load, flexural strength and ductility.

B.3. Experimental Program

B.3.1. Materials

Blocks - 6" nominal, grade N, concrete blocks used in the construction of the two walls are the same blocks used in the construction of TCCMAR walls. The concrete blocks used in the construction of the test panels are manufactured by Blocklite, California. The physical and mechanical properties of the blocks are presented in Table 2.1.

Mortar - Type S masonry cement mortar was used for the construction of the two walls. The composition of the masonry cement as provided by the manufacturer is:

Type I clinker	76.0%
Limestone	20.0%
Gypsum	3.7%
Admixture*	0.3%
	100 %

* Combination of air-entraining agent, water repellent and broad life extender.

The air content of masonry cement used in this program was 16 percent as given by the manufacturer. The procedure and control specimens are similar to those adopted for Portland cement-lime mortars (see Section 2.3). The average compressive strength of masonry cement cylinders was 2150 psi which is considerably less than that for Portland cement-lime mortar(4780 psi for mortar used to build partially grouted walls W10 and W11).

Grout - the two walls were built and grouted with other TCCMAR walls (phase II). The proportions and properties are presented in Section 2.4.

Reinforcement - two No. 5 bars, Grade 60 steel, were used in the construction of TCCMAR walls. The properties are presented in Section 2.5.

Masonry Prisms - Six prisms were built with masonry cement mortar. Three of the six prisms were grouted with the same grout used in the wall panels. The prisms were tested under axial compression at the same time as the wall panels to determine compressive strength.The average compressive strength of the hollow prism was 1310 psi based on gross area compared to 1560 psi for Portland cement-lime prisms which amounts to 16 percent reduction in strength. The average compressive strength of the grouted prisms was 1910 psi compared to 2050 psi for Portland cement-lime prisms which amounts to only 6.8 percent reduction. This is consistent with the fact that grouting reduces the significance of the strength of the mortar joints on prism strength.

B.3.2. Test Specimens

The two walls built with masonry cement mortar were identical in geometry and construction details to TCCMAR wall W1 (Table 3.1). They were built by the same mason. The walls were partially grouted only in the cells which contained the steel rebars. For details, see Section 3.3.

B.3.3. Test Setup, Equipment and Instrumentation

The same test setup and instrumentation adopted for TCCMAR walls were used to test the masonry cement walls. The details are presented in Sections 3.4, 3.5 and 3.7 of this report.

B.3.4. Loading

One wall was tested under monotonic loading similar to that used in testing the walls in the TCCMAR program. The other wall was tested under cyclic loading using sequential phase cyclic loading (Pattern C1, Figure 3.7) as recommended by TCCMAR for cyclic testing of masonry walls.

B.4 Experimental Results and Discussion

B.4.1 General

The test results for the two masonry cement walls are presented along with the results of the similar two walls built with Portland cement-lime mortar to facilitate direct comparison of the effect of mortar type on wall behavior.

B.4.2 Crack Patterns and Mode of Failure

The crack patterns of the two masonry cement walls under monotonic and cyclic loadings are presented in Figures B.1 and B.2, respectively along with the similar two Portland cement-lime mortar. As can be seen, cracks were developed at the mortar joints in the pure bending zone due to mortar debonding. Walls tested under monotonic load exhibited mortar and faceshell spalling at ultimate.

Comparing the crack patterns of the masonry cement walls with those of the Portland cement-lime walls indicates that the type of mortar has no significant effect on crack patterns.

B.4.3 Cracking Moment

Cracking moments are calculated from the loads at first crack using net sectional properties. Cracking moments and corresponding maximum fiber tensile stress for the two masonry cement walls are presented in Table B.1 along with the results from Portland cement-lime walls for comparison purposes.

The results show that using masonry cement mortar instead of Portland cement-lime mortar did not result in a reduction of the value of the maximum fiber tensile stress at first crack. Grouting the walls reduced the significance of the mortar joints in influencing the cracking moment because of the large tensile strength of grout in relation to the relatively weaker mortar bond strength.

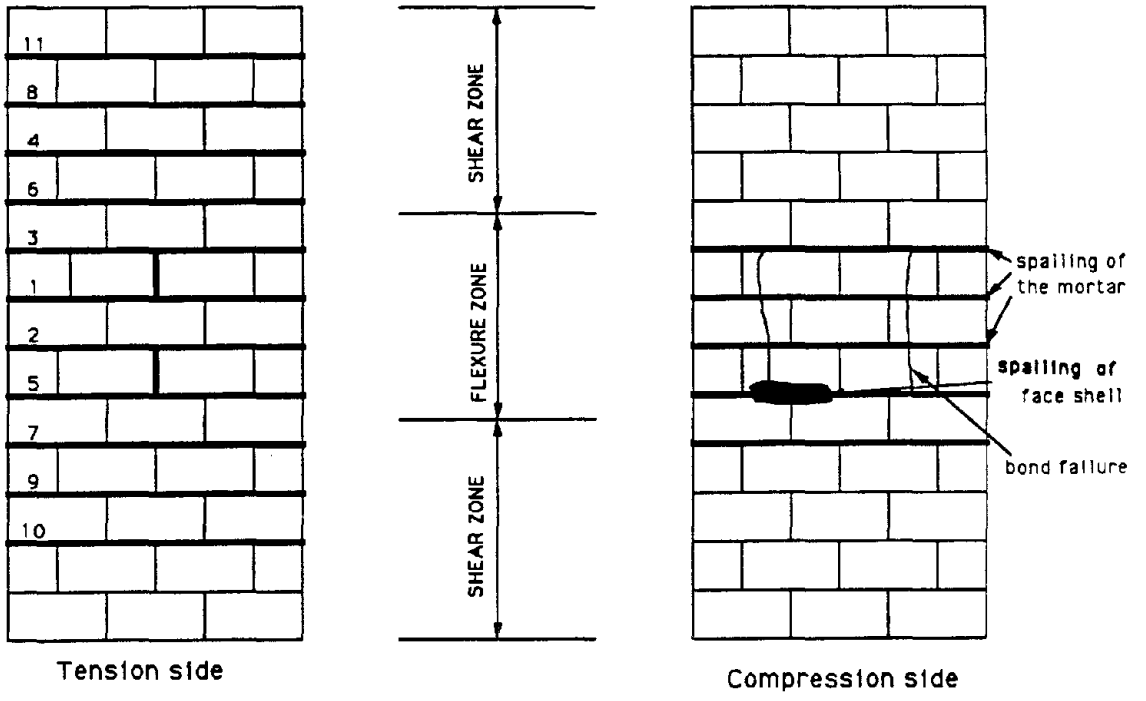

a) Masonry Cement Wall

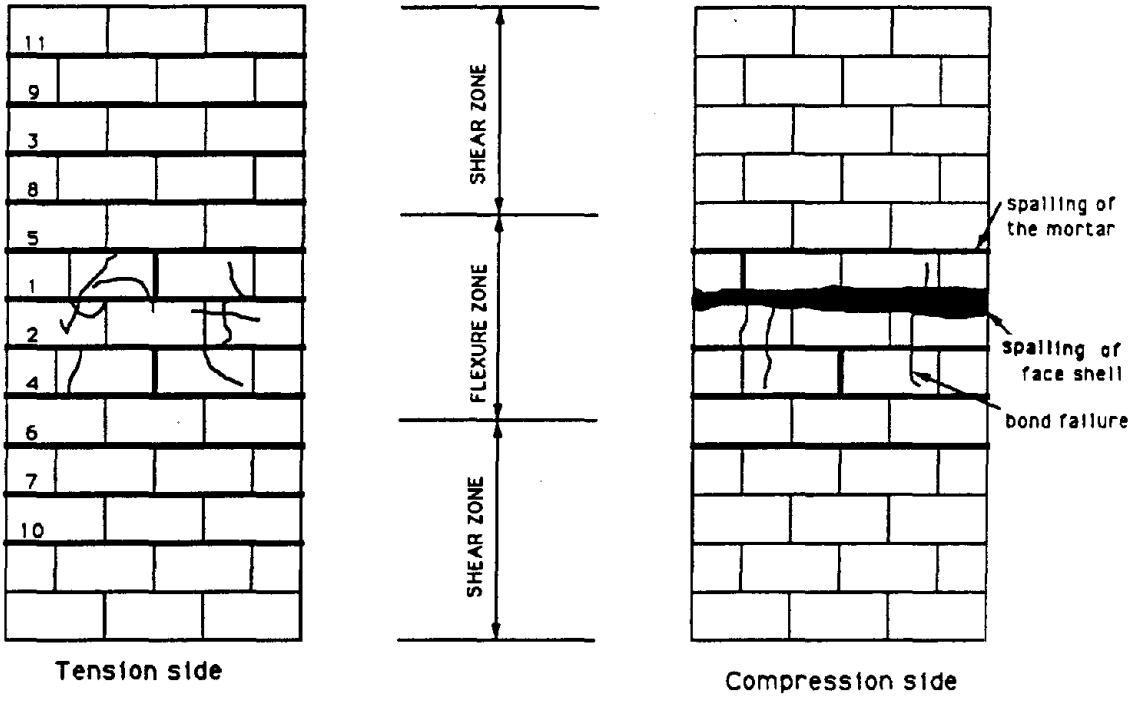

b) Portland Cement-Lime Wall

Figure B.1 Crack Patterns for Monotonically Loaded Walls

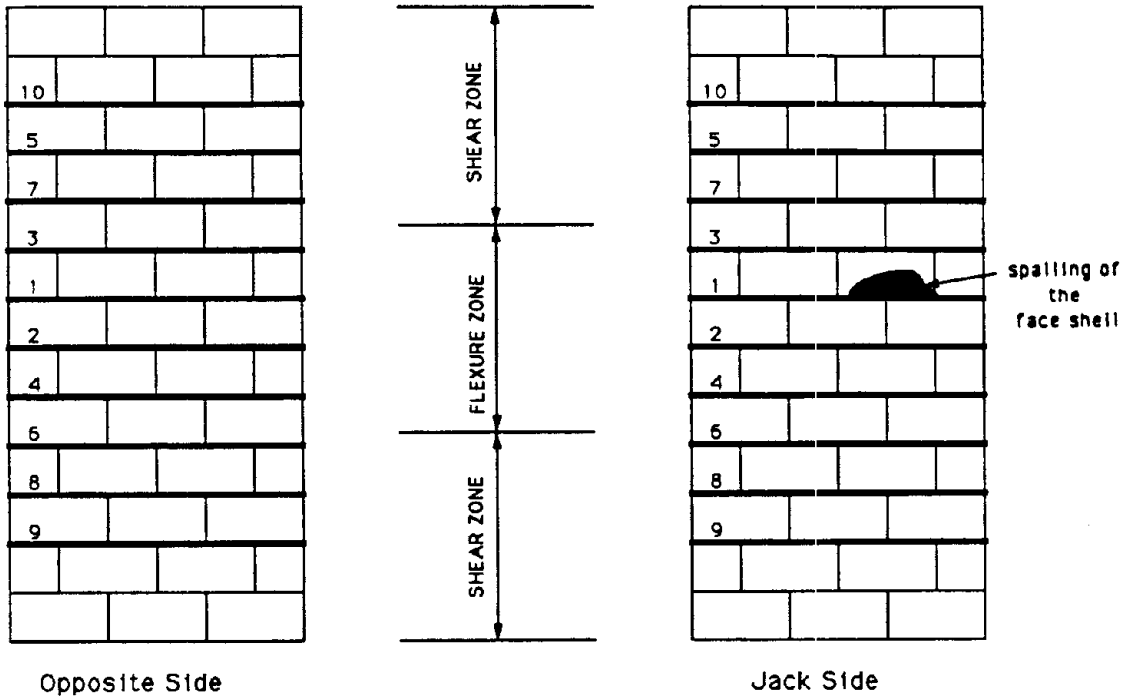

a) Masonry Cement Wall

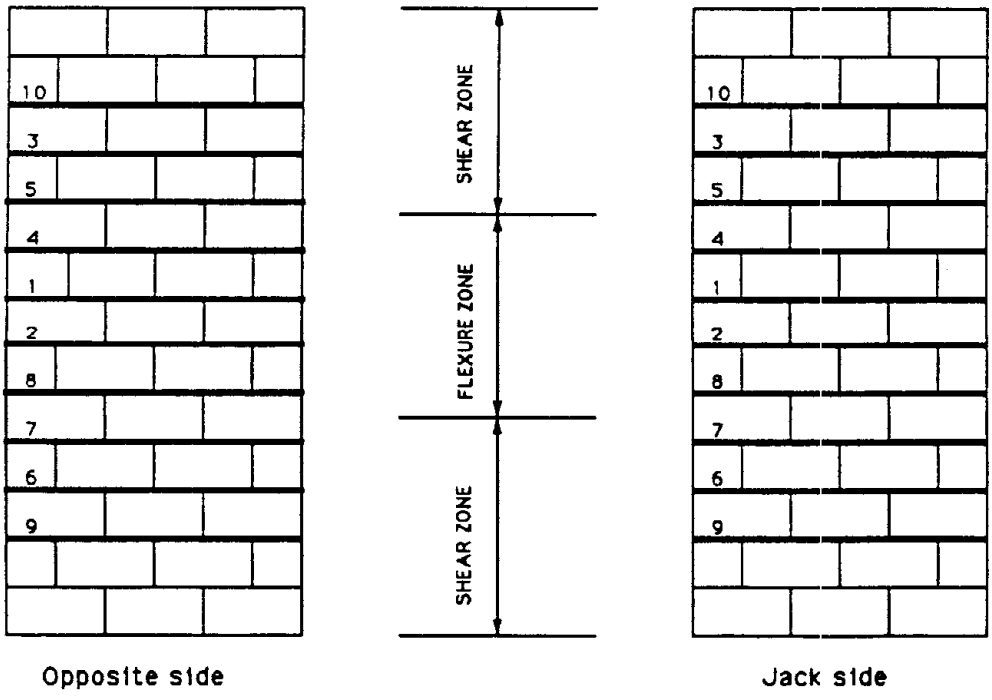

b) Portland Cement-Lime Wall

Figure B.2 Crack Pattern For Cyclically Loaded Walls

Table B.1 Test Results

Wall	M_{cr} (K-in.)	f'_t[a] (psi)	M_u (K-in.)	Δy[b] (in)	Δu[c] (in)	μ[d]
MC - Monotonic	27.7	136	118.3	2.00	9.80	4.90
PL - Monotonic	28.7	141	116.5	0.90	4.90	5.44
MC - Cyclic	26.9	132	106.0	1.70	9.50	5.60
PL - Cyclic	25.7	127	123.6	0.93	5.65	6.08

a- Maximum flexural tensile stress (Modulus of rupture)based on net area of cross section.

b- Displacement at yield load, see Figure 4.34

c- Displacement at maximum attained load.

c- Displacement ductility = $\Delta u/\Delta y$

It is to be noted that the cyclic loading resulted in a small reduction in maximum tensile stress at first crack for both masonry cement and Portland cement-lime walls.

B.4.4 Load-Deflection Relationships

The load-deflection curves are presented in Figures B.3 and B.4 for the monotonically loaded and cyclically loaded masonry cement walls, respectively. The load-deflection curves for the Portland cement-lime walls are also presented in the figures for comparison. For cyclic loading, the walls were pushed monotonically to ultimate after reaching the maximum actuator displacement limit ($\pm$ 5 inches). As can be seen from the curves, linear elastic response up to the cracking load was observed , followed by a reduction in stiffness due to cracking. Large inelastic deformations after yielding was evident. Comparing the curves of monotonically loaded walls and the envelope of the hysteresis loops for cyclically loaded walls indicate a similar behavior of masonry cement and Portland cement-lime walls.

B.4.5 Flexural Strength

The ultimate moment carrying capacity of the walls are presented in Table B.1. Under monotonic loading, the two types of walls (masonry cement and Portland cement-lime) had comparable flexural strength. This is to be expected because the small reduction in compressive strength (6.8 %) when using masonry cement mortar would not have a significant effect on ultimate moment of under-reinforced sections. Under cyclic loading, however, a reduction of 14 % was obtained for the masonry cement wall compared to Portland cement-lime wall. This

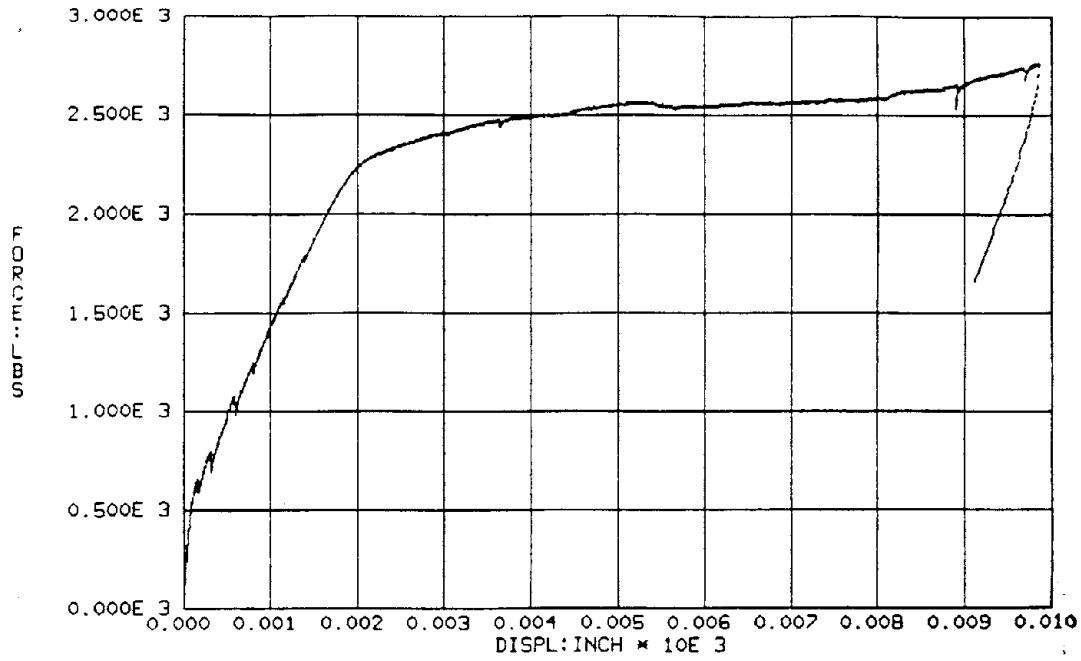

a) Masonry Cement Wall

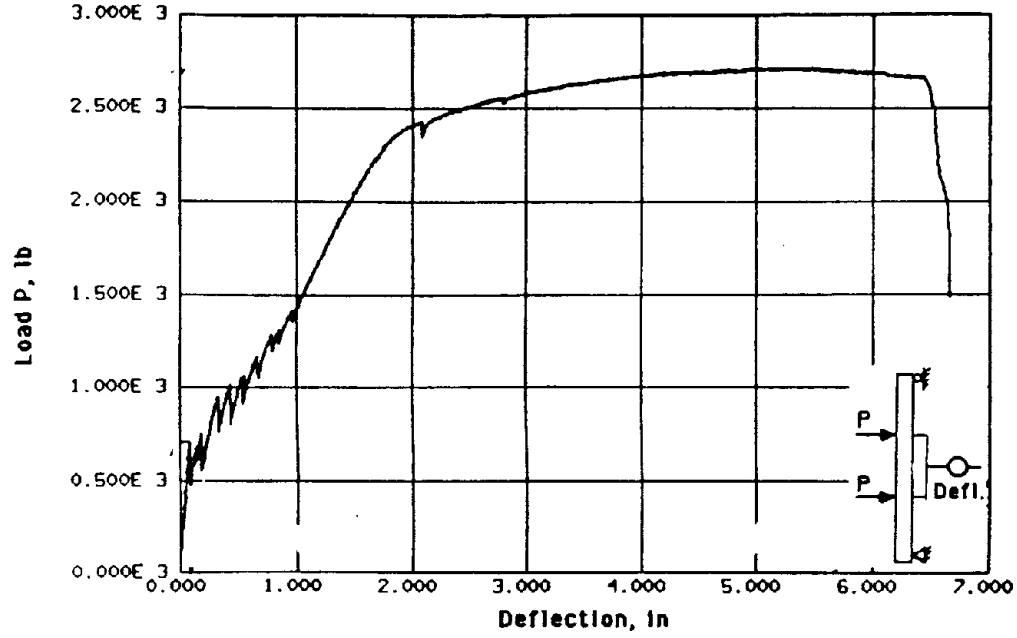

b) Portland Cement-Lime Wall

Figure B.3 Load-Deflection Curves for Walls Tested under Monotonic Loads

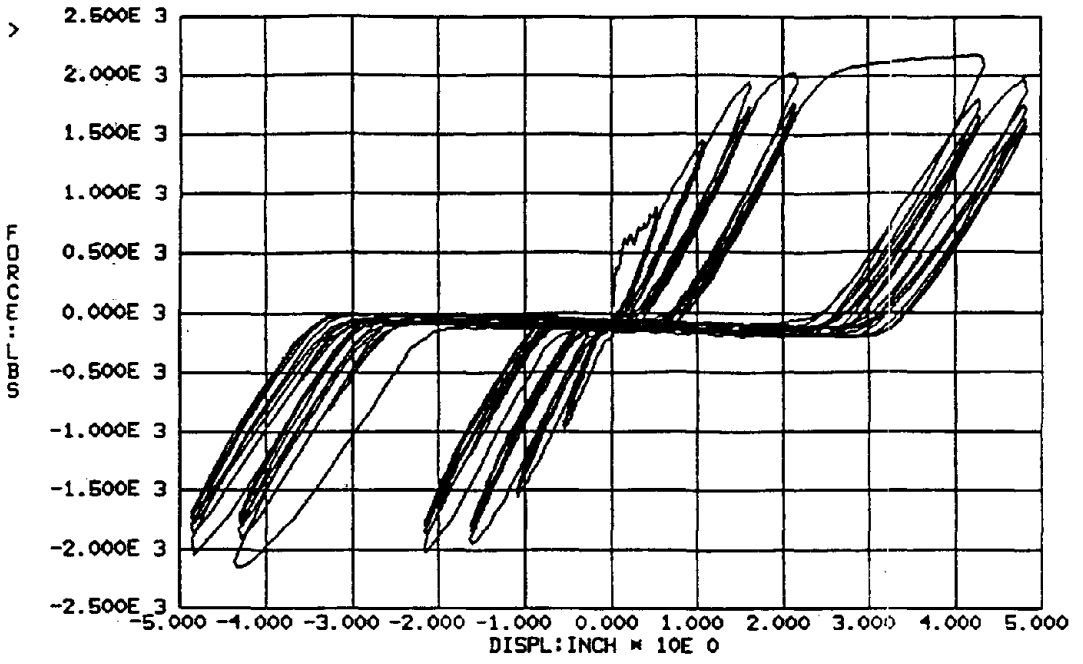

a) Masonry Cement Wall

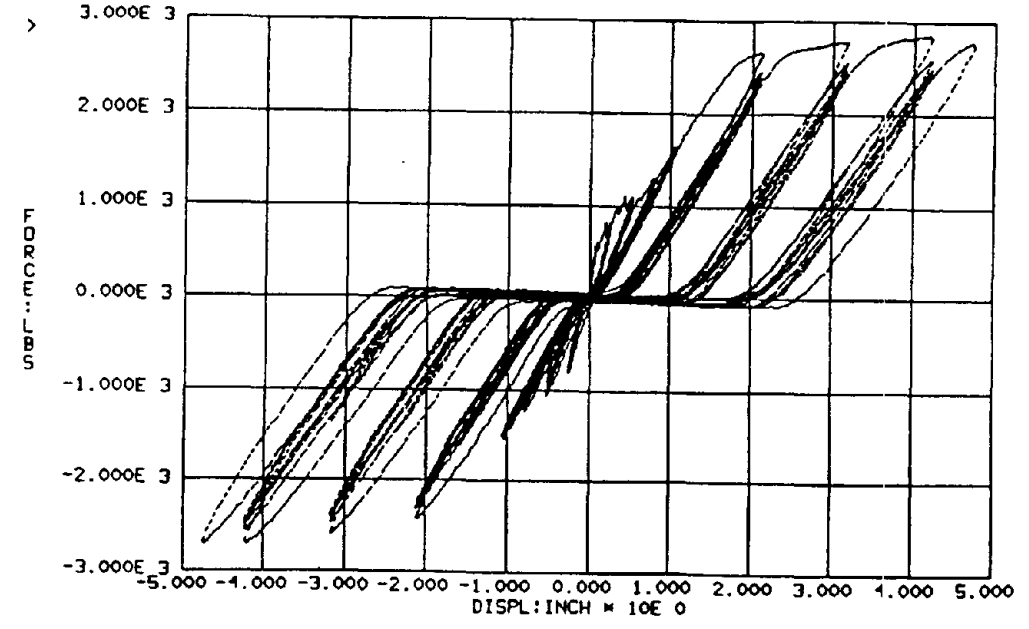

b) Portland Cement-Lime Wall

Figure B.4 Load- Deflection Curves for Walls Tested Under Cyclic Loads

could be attributed to material variability and variation in the location of vertical rebars.

B.4.6 Displacement Ductility

The displacement ductilities of the masonry cement walls are presented in Table B.1 along with companion Portland cement-lime walls. As can be seen from the table, the displacement ductilities of masonry cement walls are comparable with those for Portland cement - lime walls.